UdS Service des bibliothèques et archives

Savoirs UdeS
DÉPÔT INSTITUTIONNEL

Z-Scores for pediatric echocardiography dimensions adjusted for body size, BMI and age

Jonathan Lauzon-Schnittka
Virginie Plante
Nagib Dahdah
Steven C. Greenway
Christian Drolet
Kenny Wong
Andrew S. Mackie
Luc Mertens
Tiscar Cavallé-Garrido
Joshua Penslar
Derek Wong
Luis Martín Garrido-García
Frédéric Dallaire

Conditions d'utilisation/Terms of Use:
Ceci est le manuscrit final de l'article suivant / This is an Accepted Manuscript version of the following article : Lauzon-Schnittka, J., Plante, V., Dahdah, N., Greenway, S. C., Drolet, C., Wong, K., Mackie, A. S., Mertens, L., Cavallé-Garrido, T., Penslar, J., Wong, D., Garrido-García, L. M., Dallaire, F., et on behalf of the Canadian Congenital and Pediatric Cardiology Research Network. (2025). Z Scores for Pediatric Echocardiography Dimensions Adjusted for Body Size, BMI, and Age. Circulation. Cardiovascular Imaging, e017944. https://doi.org/10.1161/CIRCIMAGING.124.017944



Cet article a été téléchargé à partir du dépôt institutionnel *Savoirs UdeS* de l'Université de Sherbrooke.

Z-Scores for Pediatric Echocardiography Dimensions Adjusted for Body Size, BMI and Age

Running title: The CCPCRN Pediatric Echocardiography Z-Scores

Authors

Jonathan Lauzon-Schnittka[1], Virginie Plante[1] MD MSc, Nagib Dahdah[2] MD, Steven C. Greenway[3] MD MSc MBA, Christian Drolet[4] MD BSc, Kenny Wong[5] MD, Andrew S. Mackie[6] MD SM, Luc Mertens[7] MD PhD, Tiscar Cavallé-Garrido[8] MD, Joshua Penslar[9] MD, Derek Wong[10] MD, Luis Martín Garrido-García[11] MD MSc and Frédéric Dallaire[1] MD PhD, on behalf of the Canadian Congenital and Pediatric Cardiology Research Network.

Affiliations

1. Université de Sherbrooke and Centre de recherche du Centre hospitalier universitaire de Sherbrooke, Sherbrooke, Canada

2. Division of Pediatric Cardiology, CHU Ste-Justine, Université de Montréal, Montréal, Québec, Canada

3. Departments of Cardiac Sciences and Pediatrics, Libin Cardiovascular Institute and Alberta Children's Hospital Research Institute, Cumming School of Medicine, University of Calgary, Calgary, Alberta, Canada

4. Division of Pediatric Cardiology, Centre Hospitalier Universitaire de Québec, Québec City, Québec, Canada

5. Pediatric Cardiology, IWK Health Centre, Dalhousie University, Halifax, Nova Scotia, Canada

6. Department of Pediatrics, University of Alberta, 11405-87 Avenue, Edmonton, Alberta, Canada

7. Division of Cardiology, The Hospital for Sick Children, Department of Paediatrics, University of Toronto, Ontario, Canada

8. Department of Pediatrics, Division of Cardiology, Montreal Children's Hospital, McGill University, Montréal, Canada

9. Department of Pediatrics, Kingston Health Sciences Center, Queen's University, Kingston, Ontario, Canada

10. Department of Pediatric Cardiology, Children's Hospital of Eastern Ontario, University of Ottawa, Ottawa, Ontario, Canada

11. Pediatric Cardiology Department, Hospital Angeles Lomas. Huixquilucan, Mexico

Corresponding author

Frédéric Dallaire, Université de Sherbrooke, 3001, 12e Avenue Nord, Sherbrooke, Quebec, Canada, J1H 5N4, phone: 819-346-1110, ext. 74634, email address: frederic.a.dallaire@usherbrooke.ca.

Journal Subject Terms: Echocardiography, Pediatrics, Obesity

Abstract

BACKGROUND: Cardiovascular dimensions measured during pediatric echocardiograms must be normalized for body size. However, other variables may confound their interpretation, such as age and abnormal body habitus. This retrospective cross-sectional study of the Canadian Congenital and Pediatric Cardiology Research Network aimed to create Z-score equations for commonly measured dimensions in pediatric 2D echocardiography that were free of residual confounding effects of body size, body-mass index (BMI) and age.

METHODS: The reference sample consisted of >20,000 children without heart disease from 9 institutions who underwent clinical echocardiography that was reported as normal. A Generalised Additive Model for Location, Scale and Shape (GAMLSS) was used to model the expected distributions of measurements as a function of sex, height, weight, BMI and age.

RESULTS: Compared to a model that only considered body surface area, the proposed Z-scores demonstrated less bias in subgroups of overweight, very young, and early school-aged children.

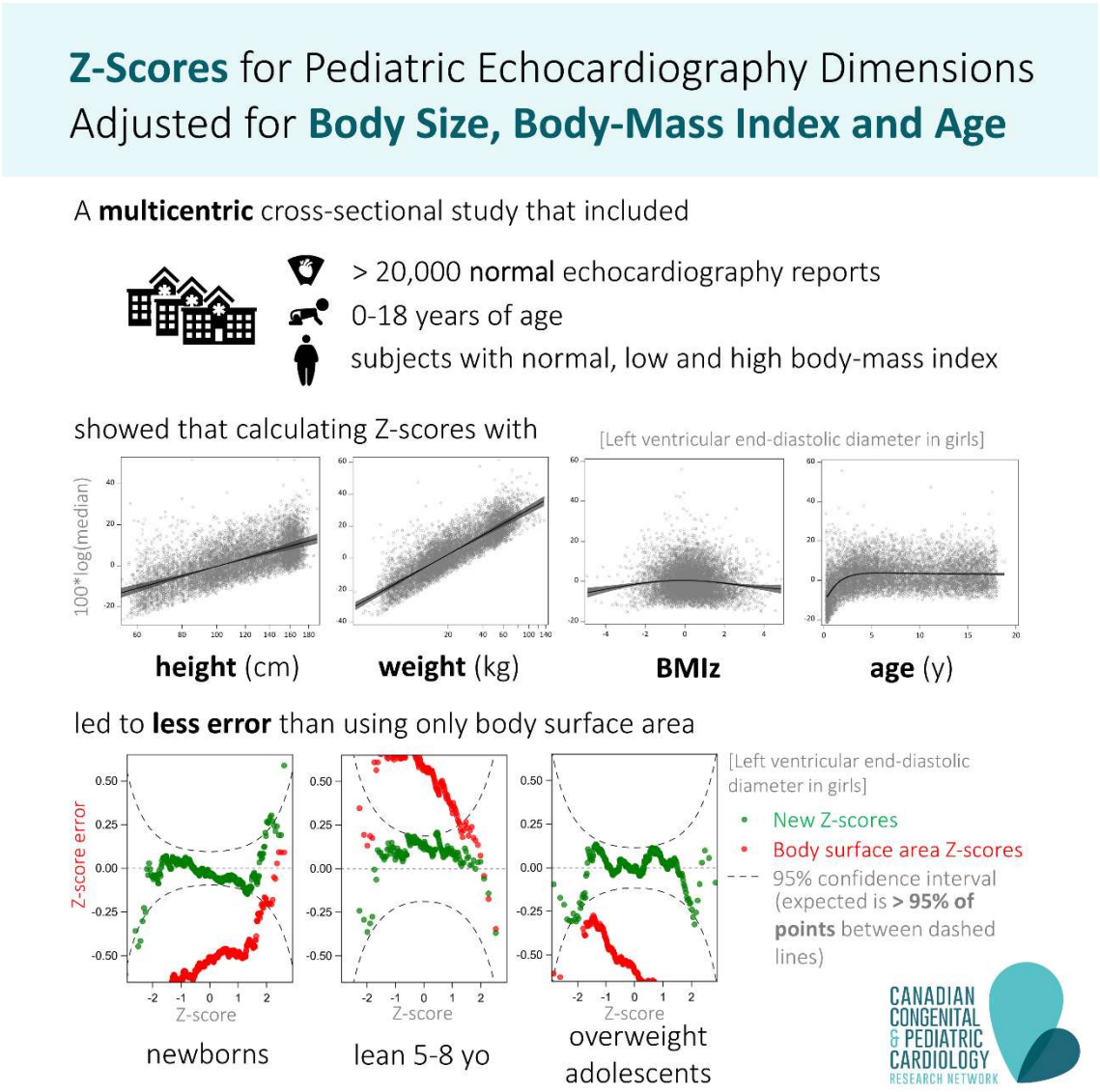
CONCLUSION: The proposed Z-score equations may improve diagnostic and therapeutic accuracy by ensuring that body size, BMI and age do not confound the interpretation of measurements.

KEY WORDS: Echocardiography, Pediatrics, Reference Values, Obesity

Clinical perspective

Z-scores for pediatric echocardiography allow to distinguish pathological variations of heart dimensions from the physiological changes that accompany body growth. Currently available Z-score equations often normalize heart dimensions to body surface area (BSA) and do not consider other confounding variables, such as body habitus and age. In this multicentric cross-sectional study of more than 20,000 healthy children, it is found that Z-scores calculated with only BSA show errors on the order of one full Z-score in some groups, notably newborns, lean school-aged children and overweight adolescents. Using Generalized Additive Model for Location, Scale and Shape (GAMLSS) enabled the proposition of a new Z-score set that correct these errors by considering height, weight, body mass index and age. For example, an obese 15-and-a-half-year-old female (172 cm and 94.5 kg) being evaluated for aortic regurgitation would see an erroneous underestimation of her left-ventricular end-diastolic diameter (LVEDD) Z score with a model based on BSA: a Z-score of 0.7 would be obtained when only BSA is considered and could suggest the absence of left ventricle dilatation. When normalized for height, weight, BMIz and age, the Z-score is calculated at 2.2, which may warrant closer follow-up. The proposed GAMLSS Z scores offer a more accurate description of the expected cardiac diameters according to body size, which therefore enable a more accurate assessment of the impact of diseases on cardiac dimensions.

Graphical abstract



Background

Quantitative measurements of cardiac dimensions obtained by echocardiography are routinely used to assist in the diagnosis of cardiac diseases and to inform clinical decisions. For these measurements to help distinguish pathology from health, clinicians need an accurate description of the expected cardiac dimensions in healthy patients. High quality, non-biased reference values for echocardiography are therefore a prerequisite for a trustworthy interpretation of any measurements. In pediatric cardiology, Z-scores are often used to compare measurements against a set of reference values, because they are simple to use and allow the quantification of the deviation from the normal [1,2].

Reference values that are biased or unvalidated in some population may lead to diagnostic and therapeutic errors in patients of that population. Many studies proposing Z-scores have excluded overweight and obese patients from their reference population, arguing that they are not strictly healthy [2–5]. Consequently, few valid reference values exist for patients with body mass index Z scores (BMIz) outside what is considered "healthy." Furthermore, many sets of Z-scores normalize cardiac dimensions to a single body size measurement, most often body surface area (BSA) [2]. It has been shown that BSA-based Z-scores may be insufficient for the adequate modelling of the whole range of BMIz seen in pediatric patients [3,6–9]. This study aimed to solve these issues by creating minimally biased Z-scores for a variety of echocardiography measurements with a large sample of children without heart disease and a wide range of BMI.

Methods

Data availability statement

This was a study from the Canadian Congenital and Pediatric Cardiology Research Network (CCPCRN). A subset of the data used in this study is available for secondary use upon request to the corresponding author, in accordance with the CCPCRN policies.

Study design and study sample

This cross-sectional study used the echocardiography reference data bank of the CCPCRN [6,10]. This data bank includes over 20,000 normal echocardiograms performed from 2001 to 2021 on patients ≤ 18 years for murmur, chest pain, palpitations, near-syncope or syncope. The 8 participating centers identified potential participants from local databases and submitted their data through REDCap [11]. Additional measurements for coronary artery diameters were obtained through a collaboration with Angeles Lomas Hospital in Mexico.

From the echocardiography reports, information regarding the indication for the study and its results were used to determine eligibility of participants. Only echocardiograms that were read as "normal" by the attending pediatric cardiologist and that were accompanied by an unremarkable physical examination (except for a benign physiological murmur) and medical history were included. Patients were excluded if they were subjected to a condition that could influence cardiac dimensions, including, but not limited to, genetic anomalies, myopathies, chronic hypertension, chronic anemia, pulmonary hypertension, chronic renal disease and prior exposure to chemotherapy. Patients with extreme BMIz (< -5 or > 5) were excluded because insufficient sample sizes precluded reasonable modelling in these groups. When multiple echocardiography reports were available for a single patient, only the first was included. Participants were not excluded on the basis of Z-scores or cardiac dimensions found in the echocardiography reports. Nor inpatients nor outpatients were excluded. Premature infants were not excluded but special care was used to determine the validity of the reference values in very small infants. Each center obtained the approval of its respective research ethics board. As this was a retrospective study of de-identified data, the ethics boards waived the need for informed consent.

Data collection

We collected weight, height, and age at the time of the echocardiogram. BMIz was calculated with the World Health Organization's standard values [12]. BSA was calculated using the formula published by Haycock et al [13]. Visually obvious outliers likely attributable to data entry errors were excluded if their removal improved convergence of the models. Biological sex at birth was collected and females and males were analyzed separately.

Cardiac measurement data were extracted directly from the echocardiography reports. We only included in our analysis diameters that were routinely measured in all echocardiograms in a given participating institution, and we excluded diameters not measured in >75% of patients in a given institution for any given year. All measurements were performed in recognized health institutions by qualified personnel, according to the recommendations for echocardiography quantification of the American Society for Echocardiography [1]. Left ventricular mass was estimated with the Devereux equation [14].

Normalization methods

We used a Generalized Additive Model for Location, Scale and Shape (GAMLSS) to predict the distribution of cardiac dimensions from height, weight, BMIz and age [15]. GAMLSS models are a multivariable generalization of the lambda-mu-sigma (LMS) method, a well-accepted method to create reference values [16,17]. The Box-Cox exponential distribution was used as described by Stasinopoulos and Rigby [18]. Four parameters define this distribution and allow to model the median, the coefficient of

variation, the skewness, and the kurtosis. Predictive functions based on one or more explanatory variables are then created to predict these parameters. Modelling the coefficient of variation allowed to model any heteroscedasticity. Modelling the skewness and kurtosis relaxed the assumption of normality that is otherwise made about the data. If no skewness or no kurtosis is detected, the Box-Cox Power exponential distribution may reduce to the normal distribution.

To predict the median of the distribution, a multiplicative function of height, weight, BMIz and age was considered. Height and weight were normalized with a linear function in the logarithmic space. This is a form of allometry and is the most physiologically plausible effect for such body size variables [17,19,20]. The effects of BMIz and age were modelled with smoothing splines, as no reasonable assumption can be made regarding the shape of their effects. The coefficient of variation, the skewness and the kurtosis were modelled with a function of age.

BSA was not directly used because it is a parameter that is never actually measured in the clinic. It is instead estimated with a multiplicative equation based on height and weight. This means that using BSA instead of height and weight themselves would be the same as the proposed model, with the added constraint that the relative effects of height and weight are fixed to some predetermined ratio. This constraint has no advantages for statistical modelling.

Model fitting involved determining if each variable was necessary and optimizing the complexity of the smoothing splines, with the objective to find the simplest model that could create unbiased Z-scores. For this, we initially used an automatic procedure to optimize the Schwartz-Bayesian criterion (SBC), a goodness of ft statistic that penalizes increasing complexity if it does not lead to sufficient improvements in the predictions. As some authors have reported this criterion to sometimes favor models that were more parsimonious than they should, the Generalized Akaike Information criterion with penalty k = 3 (GAIC3) was also used to compare the results [21,22].

From the results of this automatic optimization procedure, worm plots were used to identify any residual misfits and adjust the model complexity accordingly. Worm plots are a visual diagnostic tool that allows to finely detect misfits in the location, the dispersion, and the normality of Z-scores [23]. They have been used, notably, by the World Health Organization for the development of the growth standards that are used today [22].

Comparison with a BSA-allometric model

We compared the proposed GAMLSS model to a BSA-allometric model ($y/BSA^{\alpha} \sim N[\mu, \sigma]$), because the latter has often been used in to produce echocardiography Z-scores in children [2]. For the regression of this BSA-allometric model, the optimal allometric exponent alpha was computed as the slope of the linear relationship between y and BSA in the log-log space. All measurements were then indexed to the alpha power of BSA. The

mean and standard deviation of this index were computed to create BSA-based Z-score equations. The performance of this model can reasonably be expected to reflect the performance of currently available BSA-based Z-score equations because these generally use very similar modelling techniques. Direct comparison to published Z-score equations was not performed because it would unfairly favor the models obtained from the current dataset.

Empirical validation

As described above, the SBC and worm plots were the main diagnostic tools used to assess model fit. To synthesize these results, the mean Z-score in select subpopulations was calculated to directly evaluate the average error in these populations. The mean Z-score in underweight (BMIz < -2) and obese (BMIz > 2) subjects was calculated, as was the mean Z-score in different strata of age.

In the Results, we show figures with two variables that are used as examples: the aortic valve diameter in males and the left ventricle end-diastolic diameter in males. All relevant figures are presented for all included measurements in both sexes in Supplementary Figures S1-S46.

Results

Study sample

Information on a total of 22,188 subjects were available in our database. Of these, 111 had no data about the echocardiographic variables of interest to this study, 439 were excluded because of missing or aberrant anthropometric data and 8 were excluded because their age was above 18 years. After exclusions, 21,630 subjects were included in the study cohort. Table 1 shows how many studies were available for each echocardiographic measurement for females and males respectively. The sex, age and BMIz distribution of the study cohort is presented in Figure 1. The height and weight distributions are available in Supplementary Table S1.

Hyperparameter selection

The hyperparameters selected by the automatic search and the final hyperparameters are shown in Supplementary Table S2. As expected, the GAIC3 favored models that were more complex in comparison to those favored by the SBC. In general, some residual misfits were apparent in the worm plots produced by the model favored by the SBC. However, the predictive curves in the models selected by the GAIC3 sometimes appeared overfitted. The model hyperparameters were therefore adjusted to maximize data fit while avoiding to model unnecessarily complex associations. For all variables, the SBC favored the chosen model to the BSA-based allometric model.

Fitted associations

Figure 2 shows the predictive curves for the median for each included explanatory variable. In these graphs, the Y-axis is scaled such that the difference between two points may be interpreted as the percentage difference between the predictions at those points [24]. For example, it can be seen in the lower-right plot in Figure 2 that age contributes to a 10% increase in the predicted median of the left-ventricular end-systolic diameter in females in the first two years of life.

A detailed description of the fitted associations can be found in the Supplementary Results. Importantly, it was found that the independent modelling of height and weight, as well as the inclusion of BMIz as a predictor, distinguish the proposed model from the BSA-based model by allowing the predicted median to more closely follow the different distributions that are found in different BMIz strata. Figure 3 illustrates this finding: in these scatter plots of heart dimensions for BSA, a BSA-based model can only fit a single line across the data, even though it shown that lean patients and overweight patients of similar BSA are distinct from one another, and that the predicted median of the proposed model better follows the different distributions.

For some echocardiographic measurements that were not measured routinely by all centers, fewer than one thousand data points were available for each sex (see Table 1). Because of the smaller sample size available for these measurements, we were wary of modelling complex nonlinear effects in age or BMIz, because of the increased risk of overfitting. Therefore, only allometric effects of height and weight were modelled for the median of these measurements.

The modelled associations for the coefficient of variation, skewness and kurtosis are also described in the Supplementary Materials. It should be noted that because no significant kurtosis was detected and because modelling kurtosis complexifies the Z-score calculation, the final Z-scores for all measurements do not consider kurtosis and thus reduce to the usual LMS transformation.

Validation

The final worm plots showed minimal misfits for the GAMLSS model. However, they revealed clear misfits for the BSA-allometric model. Figure 4 shows an example of a worm plot for the Z-scores of the aortic valve diameter in obese males. The X-axis represents the expected Z-score of each measure given its quantile in the subgroup. The Y-axis represents the difference between the calculated Z-score and this expected Z-score. Conceptually, the Y-axis therefore represents the “error” in Z-score. Therefore, a model with no error should show points on the $y = 0$ dashed line, and the more distance between the points and the $Z=0$ horizontal line, the greater the error. Because of expected random noise, deviations from the $y = 0$ line are tolerated within the expectation that more than 95% of the subgroup should remain between the dashed 95% confidence interval. The single worm plot in figure

4 is accompanied by a histogram that was generated with the same data, which illustrates that, conceptually, shifts in the distribution lead to errors that appear as a shifted worm plot. Figure 5 shows worm plots in different strata of age and BMIz. Worm plots stratified by age and by BMIz are presented for all measurements in Supplementary Figures S1-S46 A and B.

We synthesized the results of all worm plots through heatmaps of the mean Z-scores in chosen strata of the sample (Figures 6 and 7), in which green represents the expected mean Z score of 0, and red represents a greater deviation from the expected mean Z score of 0. Conceptually, this value quantifies the shift in the distribution compared to the theoretical Z-score distribution which is represented by the length of the blue line in Figure 4. Figure 6 shows the mean Z-scores in lean (BMIz < -1) and obese (BMIz > 2) patients from both the proposed GAMLSS model and BSA allometry. This figure illustrates that deviations from the expected mean of zero were seen in the BSA-allometric model, especially in obese subjects, which suggests that this model failed to fully normalize for the effects of BMIz. While this effect was not as large across all echocardiographic measurements, it generally remained present. These errors were mostly improved in the GAMLSS multivariable model. For some measurements however, some residual errors were apparent, especially when effects of age and BMIz were not modelled, such as for the coronary arteries. However, their importance was variable, which is why effects to correct them were not modelled as this could have led to overfitting.

Similarly, we show in Figure 7 the mean Z-scores in different strata of age. It shows that the BSA-allometric model failed to normalize for effects of age in most variables, with errors especially seen in newborns, in patients around 5 to 7 years of age, and in older adolescents. In the currently proposed GAMLSS Z-scores, these errors were minimized.

Finally, an additional repeat cross-validation analysis was performed (Supplementary Table S3) and confirmed that for all variables where BMIz and age were included in the model, the chosen model led to lower deviance than the BSA-based model when regressed and tested on distinct samples. This suggests that the improvements in data fit were not due to overfitting. Furthermore, the analysis in Figures 6 and 7 were replicated under cross-validation, which revealed similar results (Supplementary Figures S47 and S48).

<u>For whom are these reference values different from BSA-based reference values?</u>

For all patients, we calculated the difference between the Z-scores produced by the BSA-based model and the proposed GAMLSS model. We plotted these differences as a function of BMIz and age in a colored scatter plot shown in Figure 8, which illustrates which patient groups saw an important change in their Z-score. These graphs revealed that, for most patients, there were small differences in Z-scores. However, depending on a patient's BMIz and age, differences upwards of two full Z-score were observed. The differences in Z-scores were especially great in newborns, and when the direction of the effects of BMIz

and age were concordant, such as in lean patients of 5 to 7 years of age and overweight adolescents.

It has been suggested that the clinical relevance of differences in model predictions should be evaluated by observing the relative difference in predicted means. An analysis of this type is presented in the Supplementary Results and reveals differences in predictions upwards of 10 percent depending on the age and BMIz of patients (Supplementary Figures S1-46 H).

Sensitivity analyses

To address reservations regarding the inclusion of overweight subjects in the reference population, we tested whether the inclusion of subjects with «abnormal» BMIz could have biased the results for those with BMIz in the normal range. When very lean and overweight patients were excluded from the prediction models, Z scores for subjects with normal BMIz were not significantly affected (see the Supplementary Results for details). Similarly, the exclusion of very small infants did not affect the Z-score significantly, which suggests that the decision not to exclude premature infants did not affect the reference values.

Finally, the institution from which the measurements were obtained influenced the distribution of the Z-scores, with mean Z-scores deviating from 0 by more than half a Z-score in certain centres and certain measurements (detailed results in Supplementary Table 4).

Implementing the Z-scores

Because smoothing splines were used, the generated Z-score equations require computations that can only be comfortably performed by automatic calculators. Instructions for their implementation are provided in the supplementary materials. We also provide an example Excel calculator, a SAS macro and an R function that can calculate the Z-scores. Finally, Z scores can be calculated easily using an online calculator available at https://www.rchsd.org/zscore/.

Discussion

The scarcity of validated reference values for pediatric echocardiography in the overweight population is what motivated this study. Nevertheless, our overarching objective was to provide a complete set of minimally biased reference values that could be applied to infants and children of all body sizes and ages. Our results show that our approach provided predicted values with adequate fit and distribution, and with less systematic errors compared to reference values based on BSA. In this discussion, we address three main potential sources of bias, namely the sampling method, the measurement methods, and the normalization methods.

Sampling methods

In the current study, as with almost all recently published reference values for echocardiography [2,25], data were sampled from echocardiograms routinely performed in pediatric cardiology clinics. This ensures that the sample is representative of the patients that are seen in these clinics, but it implies that the patients included in the study had a clinical indication for receiving an echocardiogram. It is therefore possible that subjects with heart diseases were evaluated as normal by the attending cardiologist and were therefore included in the study sample. Nonetheless, even if such abnormal patients were mistakenly included in the study, they probably did not represent an important proportion of the sample because only echocardiograms performed for signs or symptoms frequent in patients without cardiac disease were included.

Many studies have excluded patients with abnormally high BMIz, arguing that they are not strictly "healthy" and may therefore bias reference values because their cardiac dimensions are not normal [2–5]. Overweight may indeed be associated with pathological cardiac dimensions, principally because of its association with hypertension. However, even in the absence of pathology such as hypertension, it is probable that patients with higher BMIz have physiologically different cardiac dimensions from patients with BMIz in the normal range. Excluding patients with an abnormal BMIz may therefore create reference values that are unrepresentative of this population. We have indeed previously shown that reference values that were created with samples that excluded overweight patients are biased when used in an obese population [6]. This has driven our decision to include overweight and underweight patients in the current study.

In should be however noted that while patients with a diagnosis of hypertension were excluded from the study, the presence of subclinical or undiagnosed hypertension could have altered the cardiac dimensions in overweight patients. Validation of these Z-scores with obese subjects with known normal ambulatory blood pressure would be needed to completely rule out this possibility. This was not done in the current study, however the sensitivity analyses suggested that the Z-scores of patients with normal BMIz were not affected by the presence of overweight subjects.

This study used data mainly from Canadian centres. It is likely that white children were overrepresented. The proposed Z-scores should therefore be used with caution in populations that have a different ethnic composition, though reported effects of race and ethnicity are small and possibly insignificant [5]. Finally, it should be noted that while subjects were not excluded on the basis of gestational age, no specific validation has been performed for premature infants in the current study, because this data was not available. Validation of these ranges in premature infants would be necessary before their use in this population.

Measurement methods

To minimize potential bias, the measurement methods in a study aiming to establish reference values should reflect the measurement practices that will be used in the clinic. In this study, data were extracted directly from routine echocardiography reports and should therefore be expected to reflect the measurement practices of the echocardiography laboratories of the included institutions. However, even between different institutions included in this study, some differences in the distributions of the measurements were observed. To address this, some authors have used a core laboratory and remeasured dimensions from the source images [3,5]. The use of a core laboratory has many benefits in intervention studies, as it decreases variability by lowering inter- and intra-reader variability. However, for reference values, it may artificially decrease the normal variation observed in routine clinic settings. Furthermore, systematic biases by a single reader in a core laboratory is possible. These biases will cancel out in intervention studies (both groups are read by the same observer) but will bias prediction models if this systematic bias differs from what is routinely measured by a vast range of readers in clinics. Because our measurements were taken from multiple centers with multiple readers, it is expected that systemic biases by readers will distribute randomly, which will increase accuracy of the predicted mean, but could increases the variance, which in turn would produce less "stringent" Z scores.

Normalization methods

Body size normalization with BSA is frequent in the medical reference values literature [26]. This widespread practice has roots in early physiological studies that noted that metabolic demands are linearly related to BSA [27,28]. This association underpins the assumptions that are made when the pure BSA-allometric model is used to normalize heart dimensions, namely that 1) BSA predicts metabolic demands, and 2) body size influences cardiac dimensions only through changing metabolic demands. Both assumptions are probably imperfect.

Though BSA is certainly associated with metabolic demands, contemporary studies have suggested that fat-free mass is the most important determinant of resting metabolic rate, with fat mass being a secondary determinant [29,30]. This suggests that both increased lean mass and adipose mass lead to increased cardiac dimensions, but to different degrees. BSA, as it is presently estimated with equations based on height and weight, cannot differentiate between lean and adipose tissues. As shown in Figure 3, the independent modelling of height and weight and the inclusion of BMIz in the proposed model allowed to lower the predictions in patients with higher BMIz, an effect which is consistent with the physiological expectation that leaner mass has a greater effect on cardiac dimensions than more adipose mass. However, of course, BMIz is only a proxy for adiposity. It is likely that patients with a high BMIz but low true adiposity – the so called "muscular" patients – are

not ideally modelled with BMIz. Nonetheless, BMIz remains the best proxy of adiposity readily accessible in the clinic [31,32].

The assumption that body size influences cardiac dimensions only through changing metabolic demands is difficult to reconcile with the finding that height empirically appears to show a great effect on cardiac dimensions. Indeed, if metabolic demands were the only link between body size and heart dimensions, we would expect that weight and BMIz would be favored as explanatory variables. We therefore speculate that there also exists a "constitutional" size for cardiac structures, around which the heart adapts to varying metabolic demands. These constitutional dimensions may be expected to be closely linked to height, and the variations around these dimensions may be explained by the variations in metabolic demands linked to body weight and BMIz. If one accepts that different cardiac structures respond differently to variations in metabolic demands, this speculative framework also explains the finding that height and weight were found to have different relative importance for different cardiac dimensions. For example, left ventricular wall thicknesses, as well as coronary artery diameters, variables which should be expected to be particularly responsive to variations in metabolic demands, were found to be more strongly associated with weight than other cardiac dimensions.

Finally, beyond the effects of body size, an independent effect of age was considered in the current study. Growth and aging are of course co-occurring phenomena in children, and therefore any effect of general body growth on cardiac dimensions is likely to be adequately normalized simply with anthropometric variables. However, it is possible that specific effects of tissue maturation and hormonal changes lead to differences between the growth patterns of heart structures and of overall anthropometric measures. For example, the weaning from the fetal circulation is likely to require complex cardiovascular adaptation patterns in the first weeks of life. These considerations give theoretical grounds for the independent effects of age that were modelled.

In recent years, the main argument for the use of BSA in echocardiography reference values has been that it is more predictive of cardiac dimensions than either height or weight alone [1,20,25]. This is a compelling argument when multivariable models are not considered. However, as shown in the current and previous studies [5,6], a combination of explanatory variables improves the fit to the data when compared to models based on a single explanatory variable. In the current study, the improvements in the SBC and the repeat cross-validation analysis were objective demonstrations of these improvements. Beyond these general measures of data fit, the worm plot analysis and heat maps allowed to identify which groups most benefited from the use of supplementary normalizing variables, namely the patients at the extremes of the BMIz spectrum, as well as newborns, children of 5-7 years of age, and adolescents. It should be noted that while the results suggest that the proposed reference values better described the distribution of heart dimensions in normal patients, further studies are needed to evaluate whether they would improve the predictive value of Z score for specific cardiac diseases.

The clinical importance of adequate normalization

The objective of measurement normalization is to eliminate physiological effects that may confound measurement interpretation. Insufficient measurement normalization may affect clinical care in two ways, relating on one hand to the cross-sectional evaluation of patients, and, on the other hand, to their longitudinal evaluation.

The former possible consequence relates to the first echocardiogram performed in each patient. Insufficiently normalized reference values would signify that the expectations of the clinician about the distribution of Z-scores do not match the true distribution of Z-scores seen in comparable healthy individuals. Clinicians expect Z-scores to follow a standard normal distribution, and so that about 95% of healthy patients will have a Z-score between -2 and 2. However, if the true distribution is shifted in some populations because physiological effects have not been fully taken into consideration, this range will be incorrect. For example, when using a BSA-allometry, we find that the empirical 95% expected range for the Z-scores of the Sinus of Valsalva diameter in an obese 16-year-old male was closer to -2.5 to 1.5. These distributional shifts may lead clinicians to have the wrong sense that a measurement is beyond expectations while in fact it is not, or vice versa.

The cross-sectional implications of inadequate normalization are in fact the same implications of any type of bias, such as bias from sampling methods and measurement methods. However, these latter types of biases are less important when a patient is evaluated longitudinally: after a "baseline" Z-score has been established for the patient, subsequent evaluations can be made by comparing the dimensions to those previously measured. However, inadequate normalization can bias this longitudinal evaluation. Clinicians expect that the Z-score of a cardiac dimension across time reflect the stability or progression of a patient's clinical status. However, if cardiac dimensions are physiologically changing due to some effect that is not fully considered by the Z-score equations, the Z-scores may change because of this imperfect normalization, despite no change in clinical status.

For example, we find that, when using BSA-allometry, the Z-scores for the left-ventricular end-diastolic diameter in females are expected to fall by 0.8 Z-scores between 5 and 14 years of age. If, in the same period, the patient gains weight and sees their BMIz increase from 0 to 2, a further decrease of 0.45 Z-scores is expected under BSA allometry. If this patient is followed for left ventricular dilatation, this artificial 1.25 Z score unit decrease caused by BSA-allometry could mask progression of the disease.

The inclusion of BMIz and age as explanatory variables in the reference values complexifies Z-score calculation to some degree, as the use of smoothing splines entails the need for reference tables. Nonetheless, because of the clinical implications of inadequate normalization, we argue that the advantages of the inclusion of these effects are sufficient to overcome their disadvantages. In our opinion, the complexification of the Z-

score calculation is no reason to tolerate biases in reference values that may impact patient care, especially seeing as Z-scores are usually obtained from automatic calculators that can easily handle table-based multivariable prediction equations.

Conclusions

New pediatric echocardiography reference values are presented from a large clinical sample without the exclusion of overweight patients. An empirically driven yet physiologically plausible model was used to normalize the measurements for body size, BMIz and age. The more accurate fit between predicted and observed values and the reduction of residual biases compared to BSA-based allometric models could improve diagnostic accuracy and avoid misdiagnosis in growing patients and in patients with abnormal body habitus.

Acknowledgments

The authors acknowledge all the skillful and dedicated echocardiography technicians who contributed to acquiring the images and measurements used in this study.

Funding sources

This project was partly funded by the Fondation de la Recherche Pédiatrique (Montréal, Canada). Jonathan Lauzon-Schnittka was supported by a scholarship from the Canadian Institutes of Health Research (Ottawa, Canada) and the Fonds de Recherche du Québec (Québec, Canada). Dr Dallaire received salary support from the Fonds de Recherche du Québec. As a requirement for the support from the Fonds de Recherche du Québec, a Creative Common CC-BY-NC-ND copyright licence as been applied to the author accepted manuscript version of this text. The funders had no role in the design and conduct of the study; collection, management, analysis, and interpretation of the data; preparation, review, or approval of the manuscript; and decision to submit the manuscript for publication.

Disclosures

The authors have nothing to disclose.

Supplementary Material

Supplementary Results

Tables S1-S4

Figures S1-S48

Calculating Z-Scores (.zip file)

Patient consent statement

This work complies with the Canadian Tri-Council Policy Statement on Ethical Conduct for Research Involving Humans. The authors confirm that informed patient consent was waived by the relevant institutional research ethics boards

References

1. Lopez L, Colan SD, Frommelt PC, Ensing GJ, Kendall K, Younoszai AK, Lai WW, Geva T. Recommendations for Quantification Methods During the Performance of a Pediatric Echocardiogram: A Report From the Pediatric Measurements Writing Group of the American Society of Echocardiography Pediatric and Congenital Heart Disease Council. J Am Soc Echocardiog. 2010;23:465–95.

2. Mawad W, Drolet C, Dahdah N, Dallaire F. A review and critique of the statistical methods used to generate reference values in pediatric echocardiography. J Am Soc Echocardiogr. 2013;26:29–37.

3. Foster BJ, Khoury PR, Kimball TR, Mackie AS, Mitsnefes M. New Reference Centiles for Left Ventricular Mass Relative to Lean Body Mass in Children. J Am Soc Echocardiogr. 2016;29:441-447.e2.

4. Cantinotti M, Giordano R, Scalese M, Murzi B, Assanta N, Spadoni I, Maura C, Marco M, Molinaro S, Kutty S, et al. Nomograms for two-dimensional echocardiography derived valvular and arterial dimensions in Caucasian children. J Cardiol. 2017;69:208–15.

5. Lopez L, Colan S, Stylianou M, Granger S, Trachtenberg F, Frommelt P, Pearson G, Camarda J, Cnota J, Cohen M, et al. Relationship of Echocardiographic Z Scores Adjusted for Body Surface Area to Age, Sex, Race, and Ethnicity: The Pediatric Heart Network Normal Echocardiogram Database. Circ Cardiovasc Imaging. 2017;10:e006979.

6. Plante V, Gobeil L, Xiong WT, Touré M, Dahdah N, Greenway SC, Drolet C, Wong KK, Mackie AS, Bradley TJ, et al. Alternative to Body Surface Area as a Solution to Correct Systematic Bias in Pediatric Echocardiography z Scores. Can J Cardiol. 2021;37:1790–7.

7. Cardinal MP, Blais S, Dumas A, Hamilton V, Larose E, LeBlanc S, Déry J, Grotenhuis H, Leiner T, Mawad W, et al. Novel Z Scores to Correct Biases Due to Ventricular Volume Indexing to Body Surface Area in Adolescents and Young Adults. Can J Cardiol. 2021;37:417–24.

8. Dallaire F, Bigras JL, Prsa M, Dahdah N. Bias related to body mass index in pediatric echocardiographic Z scores. Pediatr Cardiol. 2015;36:667–76.

9. Dewey FE, Rosenthal D, Jr DJM, Froelicher VF, Ashley EA. Does Size Matter? Circulation. 2008;117:2279–87.

10. Dallaire F, Battista MC, Greenway SC, Harris K, Jean-St-Michel E, Mackie AS, members of the CPCRN. The Canadian Pediatric Cardiology Research Network: A Model National Data-Sharing Organization to Facilitate the Study of Pediatric Heart Diseases. Cjc Open. 2021;3:510–5.

11. Harris PA, Taylor R, Thielke R, Payne J, Gonzalez N, Conde JG. Research electronic data capture (REDCap)—A metadata-driven methodology and workflow process for providing translational research informatics support. J Biomed Inform. 2009;42:377–81.

12. Onis M de, Onyango AW, Borghi E, Siyam A, Nishida C, Siekmann J. Development of a WHO growth reference for school-aged children and adolescents. B World Health Organ. 2007;85:660–7.

13. Haycock GB, Schwartz GJ, Wisotsky DH. Geometric method for measuring body surface area: A height-weight formula validated in infants, children, and adults. J Pediatrics. 1978;93:62–6.

14. Devereux, Reichek. Echocardiographic determination of left ventricular mass in man. Anatomic validation of the method. Circulation. 1977; 55:613-8.

15. Rigby RA, Stasinopoulos DM. Generalized additive models for location, scale and shape. J Royal Statistical Soc Ser C Appl Statistics. 2005;54:507–54.

16. Cole TJ, Green PJ. Smoothing reference centile curves: The lms method and penalized likelihood. Statist Med. 1992;11:1305–19.

17. Cole TJ, Stanojevic S, Stocks J, Coates AL, Hankinson JL, Wade AM. Age- and size-related reference ranges: A case study of spirometry through childhood and adulthood. Stat Med. 2009;28:880–98.

18. Rigby RA, Stasinopoulos DM. Smooth centile curves for skew and kurtotic data modelled using the Box–Cox power exponential distribution. Stat Med. 2004;23:3053–76.

19. Jolicoeur P. 193. Note: The Multivariate Generalization of the Allometry Equation. Biometrics. 1963;19:497.

20. Sluysmans T, Colan SD. Theoretical and empirical derivation of cardiovascular allometric relationships in children. J Appl Physiol (1985). 2005;99:445–57.

21. Stasinopoulos M, Rigby R, Heller G, Vloudouris V, Bastian F de. Flexible regression and smoothing : using GAMLSS in R. In: LLC CP, editor. 2017. p. 379.

22. Onis M de, Onyango AW. WHO child growth standards. Lancet. 2008;371:204.

23. Buuren S van, Fredriks M. Worm plot: a simple diagnostic device for modelling growth reference curves. Stat Med. 2001;20:1259–77.

24. Cole TJ. Sympercents: symmetric percentage differences on the 100 loge scale simplify the presentation of log transformed data. Stat Med. 2000;19:3109–25.

25. Cantinotti M, Scalese M, Molinaro S, Murzi B, Passino C. Limitations of current echocardiographic nomograms for left ventricular, valvular, and arterial dimensions in children: a critical review. J Am Soc Echocardiogr. 2012;25:142–52.

26. Heaf JG. The origin of the 1·73-m2 body surface area normalization: problems and implications. Clin Physiol Funct Imaging. 2007;27:135–7.

27. Kleiber M. Body Size and Metabolic Rate. Physiological Review. 1947; 27:511-41

28. Gutgesell HP, Rembold CM. Growth of the human heart relative to body surface area. Am J Cardiol. 1990;65:662–8.

29. Sabounchi NS, Rahmandad H, Ammerman A. Best-fitting prediction equations for basal metabolic rate: informing obesity interventions in diverse populations. Int J Obes. 2013;37:1364–70.

30. Löffler MC, Betz MJ, Blondin DP, Augustin R, Sharma AK, Tseng YH, Scheele C, Zimdahl H, Mark M, Hennige AM, et al. Challenges in tackling energy expenditure as obesity therapy: From preclinical models to clinical application. Mol Metab. 2021;51:101237.

31. Boeke CE, Oken E, Kleinman KP, Rifas-Shiman SL, Taveras EM, Gillman MW. Correlations among adiposity measures in school-aged children. BMC Pediatr. 2013;13:99.

32. Cole TJ, Faith MS, Pietrobelli A, Heo M. What is the best measure of adiposity change in growing children: BMI, BMI %, BMI z-score or BMI centile? Eur J Clin Nutr. 2005;59:419–25.

TABLES

Table 1. Number of studies for each echocardiographic measurement for females and males.

Measurement*	Number of studies	
	Males	Females
Left-ventricular end-diastolic diameter	11222	9534
Left-ventricular end-systolic diameter	11211	9532
Left-ventricular posterior wall thickness	11189	9503
Left-ventricular septal wall thickness	11189	9503
Left-ventricular mass	11180	9493
Mitral valve annulus in apical view	3091	2594
Aortic valve annulus	10806	9173
Sinus of Valsalva	9932	8365
Sinotubular junction	414	307
Ascending aorta	7681	6481
Proximal arch of aorta	395	338
Distal arch of aorta	244	226
Aortic isthmus	477	453
Tricuspid valve annulus in apical view	3085	2567
Pulmonary valve annulus	5076	4249
Left pulmonary artery	4742	4006
Right pulmonary artery	4815	4060
Left main coronary artery	1010	846
Left anterior descending artery	920	801
Left circumflex artery	763	612
Right coronary artery (proximal)	980	844
Right coronary artery (medium)	722	562
Right coronary artery (distal)	702	548

*Echocardiographic measurements are based on the diameter of the various cardiac dimensions, unless otherwise specified.

FIGURES

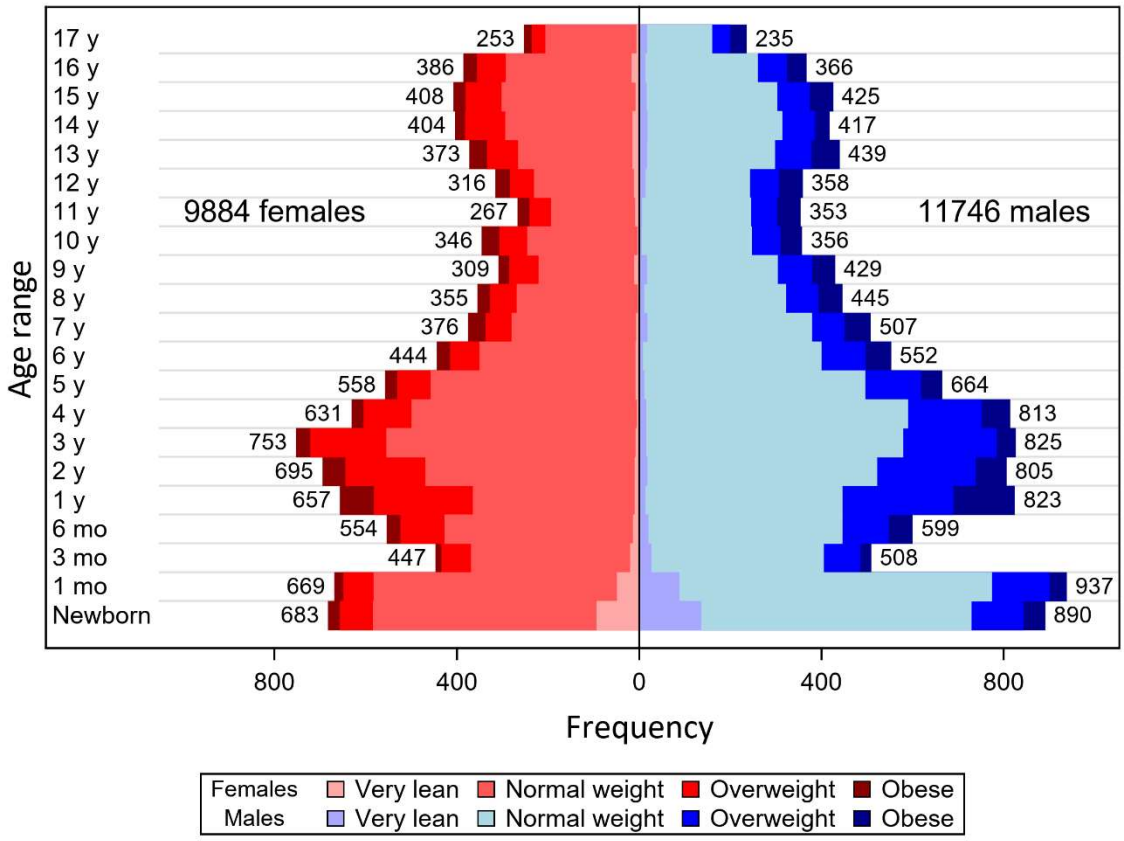


Figure 1. Number of subjects by sex, age and BMIz category. Very lean: BMIz < -2; Overweight: 1 < BMIz < 2; Obese: BMIz > 2

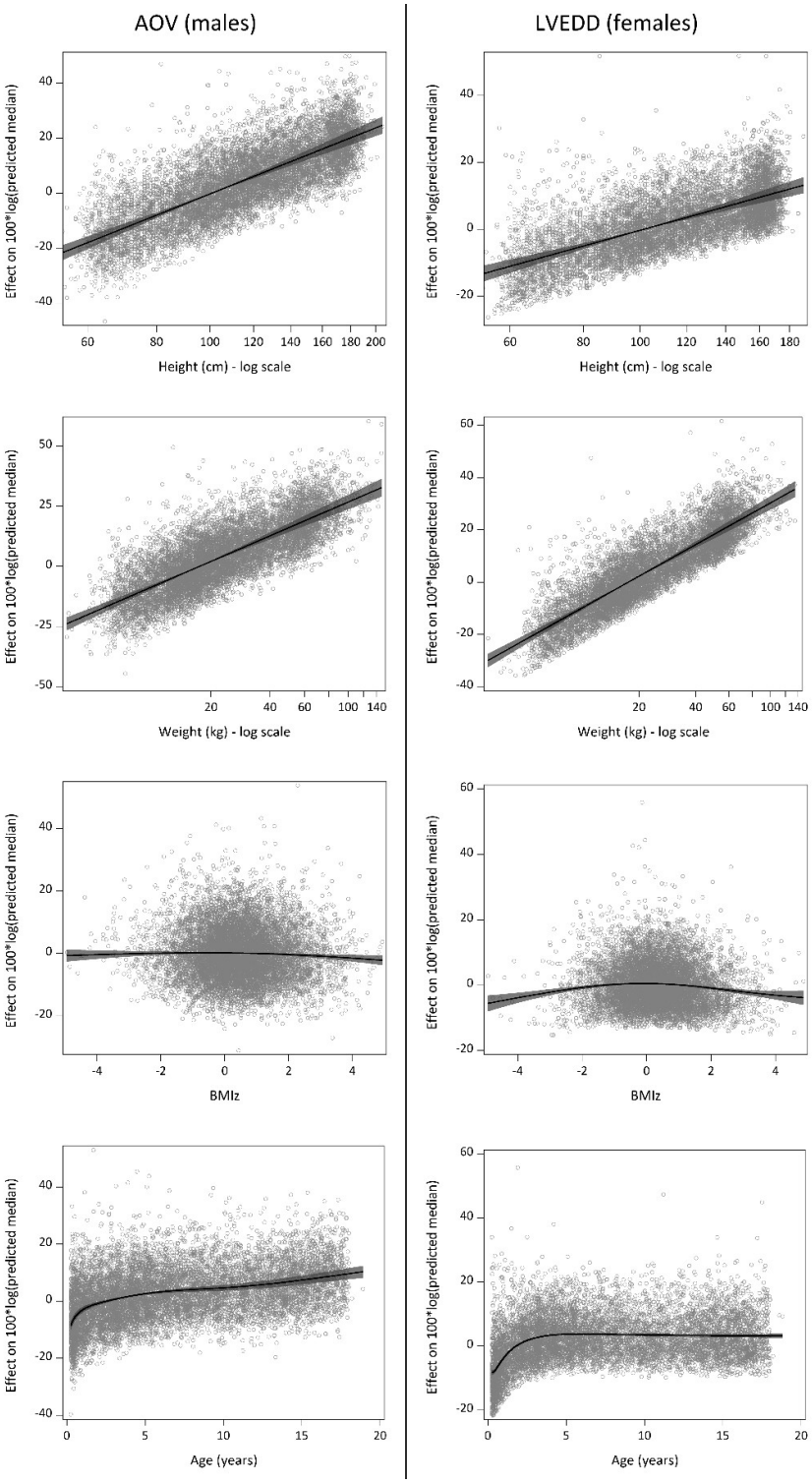


Figure 2. Predictive curves for the median. The Y-difference between two points equals the percentage difference between the predictions at those points. AOV: aortic valve diameter; LVEDD: left ventricle end-diastolic diameter.

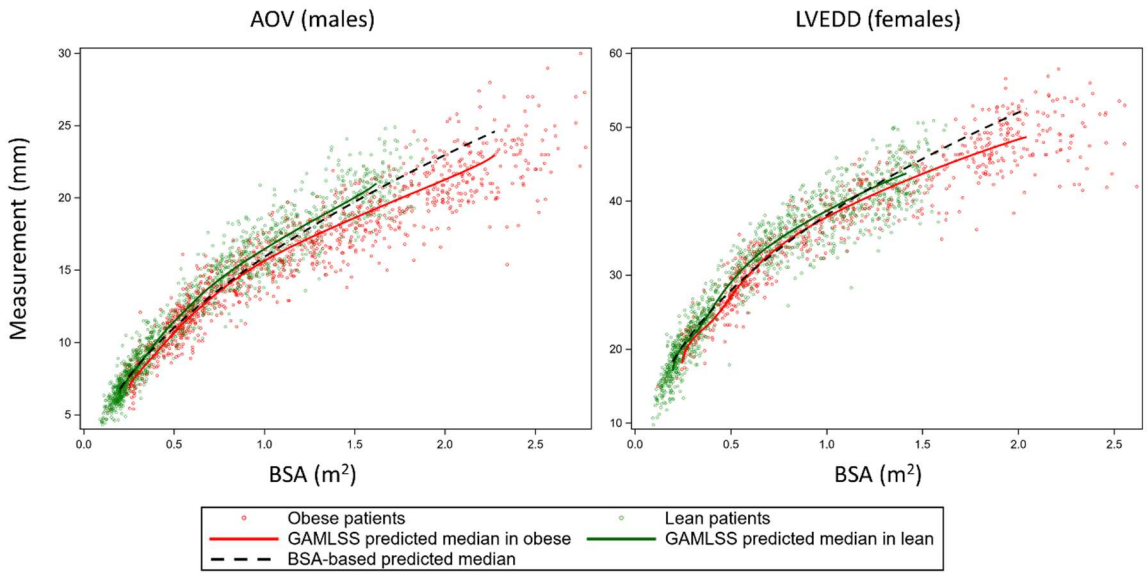


Figure 3. Scatter plot of heart dimension as a function of BSA in lean (BMIz < -1) and obese (BMIz > 2) patients, with predicted median from both models. AOV: aortic valve diameter; BSA: body surface area; LVEDD: left ventricle end-diastolic diameter.

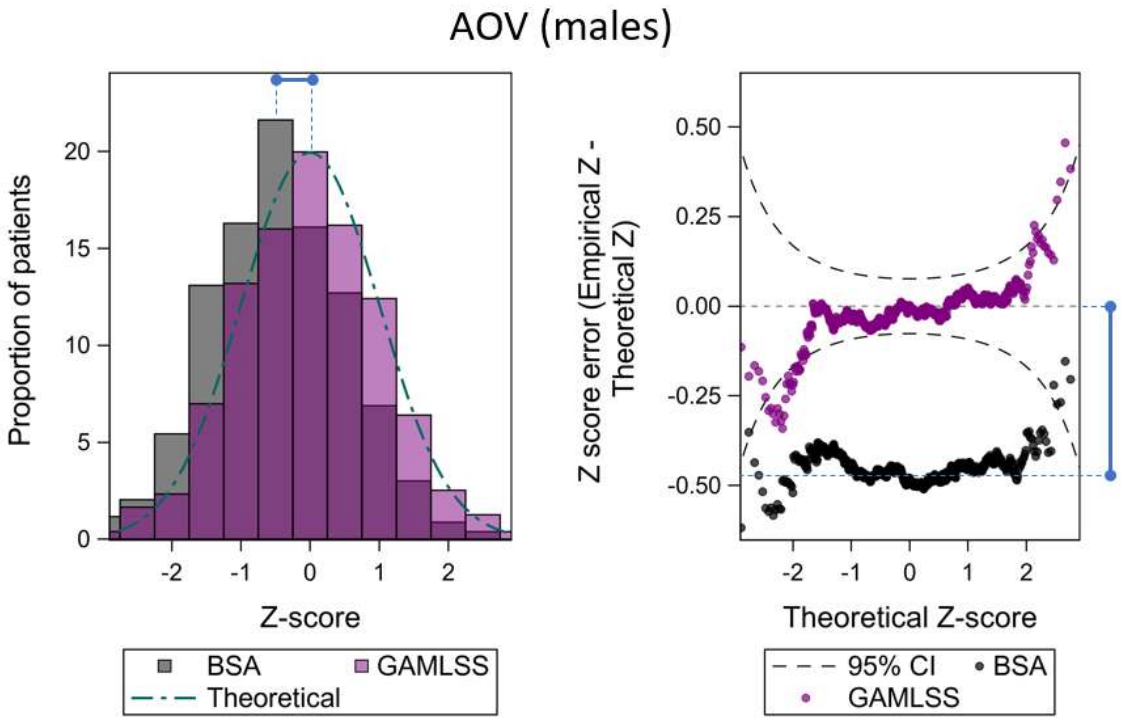


Figure 4. Aortic valve diameter Z-scores in the GAMLSS model and the BSA allometric model in obese (BMIz > 2) males. Left: histogram; Right: worm plot. Blue line: conceptually, shifts in the distribution (mean error) lead to shifts in the worm plots. In the worm plot, the expectation is that 95% of points should lie between the dashed lines. Deviations from this expectation suggests misfits. AOV: aortic valve diameter; LVEDD: left ventricle end-diastolic diameter.

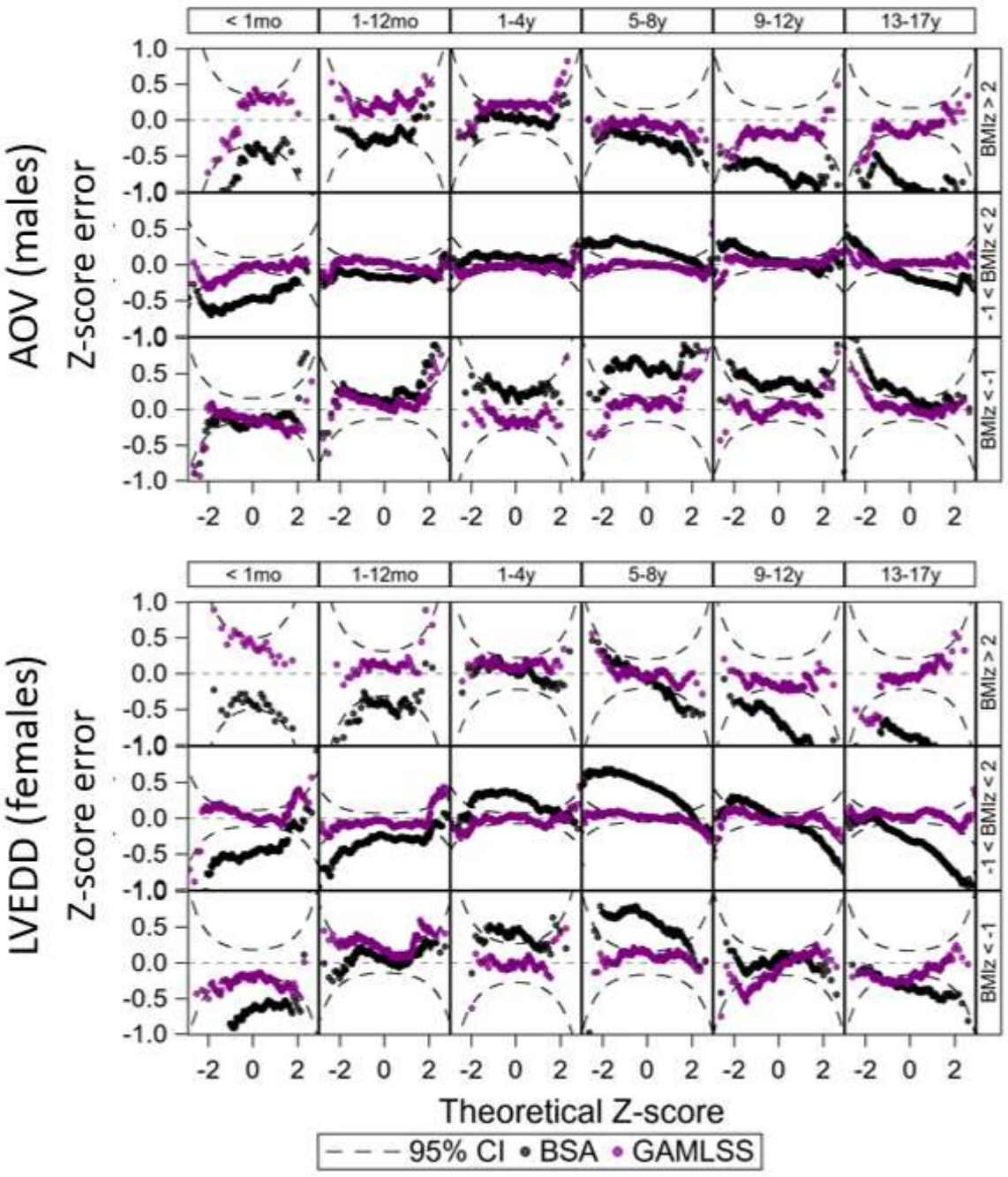


Figure 5. Worm plots by age and BMIz of the Z-scores in the GAMLSS model and the BSA-allometric model. Expected: 95% of points between the dashed lines in all panels. Deviations from this expectation suggests misfits. AOV: aortic valve diameter; LVEDD: left ventricle end-diastolic diameter.

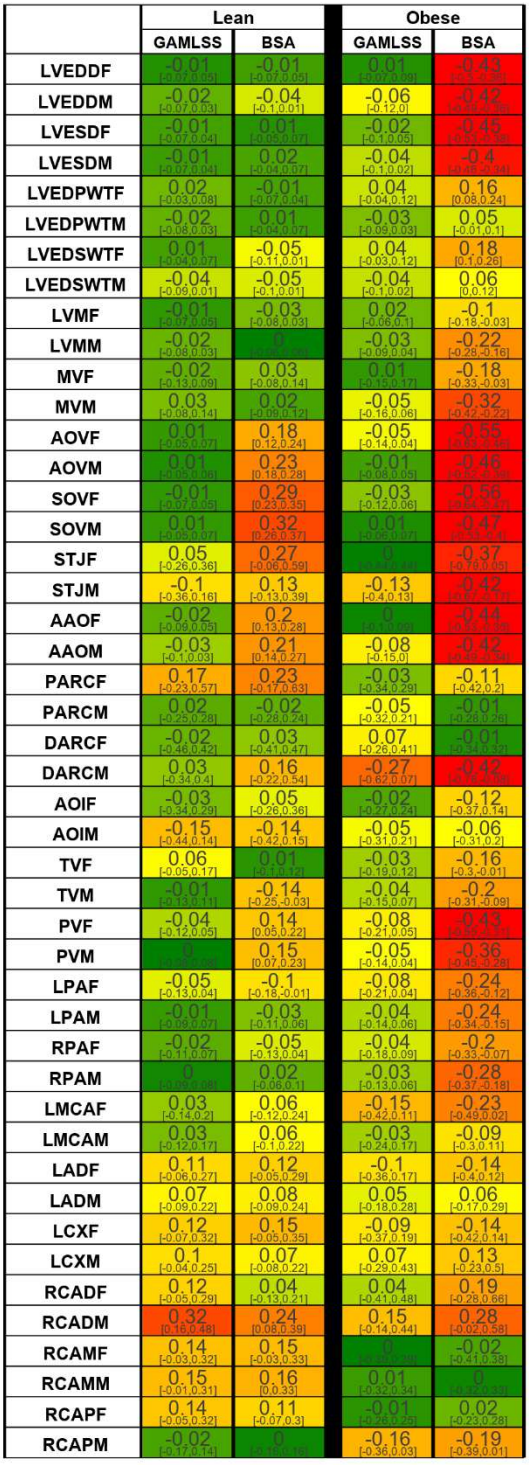


Figure 6. Heatmap of the mean Z-score in lean and obese patients in the GAMLSS model and the BSA-allometric model. Each cell provides the mean Z-score [95% CI]. Expected mean in all strata is 0, deviations from 0 suggest systematic error. Colors are calculated using the absolute value of the mean. Lean: BMIz < -1. Obese: BMIz > 2. GAMLSS:

Generalized Additive Model for Location, Scale and Shape. BSA: allometric model with body surface area. LVEDDF: left-ventricular end-diastolic diameter in females; LVEDDM: left-ventricular end-diastolic diameter in males; LVESDF: left-ventricular end-systolic diameter in females; LVESDM: left-ventricular end-systolic diameter in males; LVEDPWTF: left-ventricular posterior wall thickness in females; LVEDPWTM: left-ventricular posterior wall thickness in males; LVEDSWTF: left-ventricular septal wall thickness in females; LVEDSWTM: left-ventricular septal wall thickness in males; LVMF: left-ventricular mass in females; LVMM: left-ventricular mass in males; MVF: mitral valve diameter in apical view in females; MVM: mitral valve diameter in apical view in males; AOVF: aortic valve diameter in females; AOVM: aortic valve diameter in males; SOVF: Sinus of Valsalva diameter in females; SOVM: Sinus of Valsalva diameter in males; STJF: sinotubular junction diameter in females; STJM: sinotubular junction diameter in males; AAOF: ascending aorta diameter in females; AAOM: ascending aorta diameter in males; PARCF: proximal arch diameter of aorta in females; PARCM: proximal arch diameter of aorta in males; DARCF: distal arch diameter of aorta in females; DARCM: distal arch diameter of aorta in males; AOIF: aortic isthmus diameter in females; AOIM: aortic isthmus diameter in males; TVF: tricuspid valve diameter in apical view in females; TVM: tricuspid valve diameter in apical view in males; PVF: pulmonary valve diameter in females; PVM: pulmonary valve diameter in males; LPAF: left pulmonary artery diameter in females; LPAM: left pulmonary artery diameter in males; RPAF: right pulmonary artery diameter in females; RPAM: right pulmonary artery diameter in males; LMCAF: left main coronary artery diameter in females; LMCAM: left main coronary artery diameter in males; LADF: left anterior descending artery diameter in females; LADM: left anterior descending artery diameter in males; LCXF: left circumflex artery diameter in females; LCXM: left circumflex artery diameter in males; RCADF: right coronary artery in distal segment in females; RCADM: right coronary artery in distal segment in males; RCAMF: right coronary artery in medium segment in females; RCAMM: right coronary artery in medium segment in males; RCAPF: right coronary artery diameter in proximal segment in females; RCAPM: right coronary artery diameter in proximal segment in males.

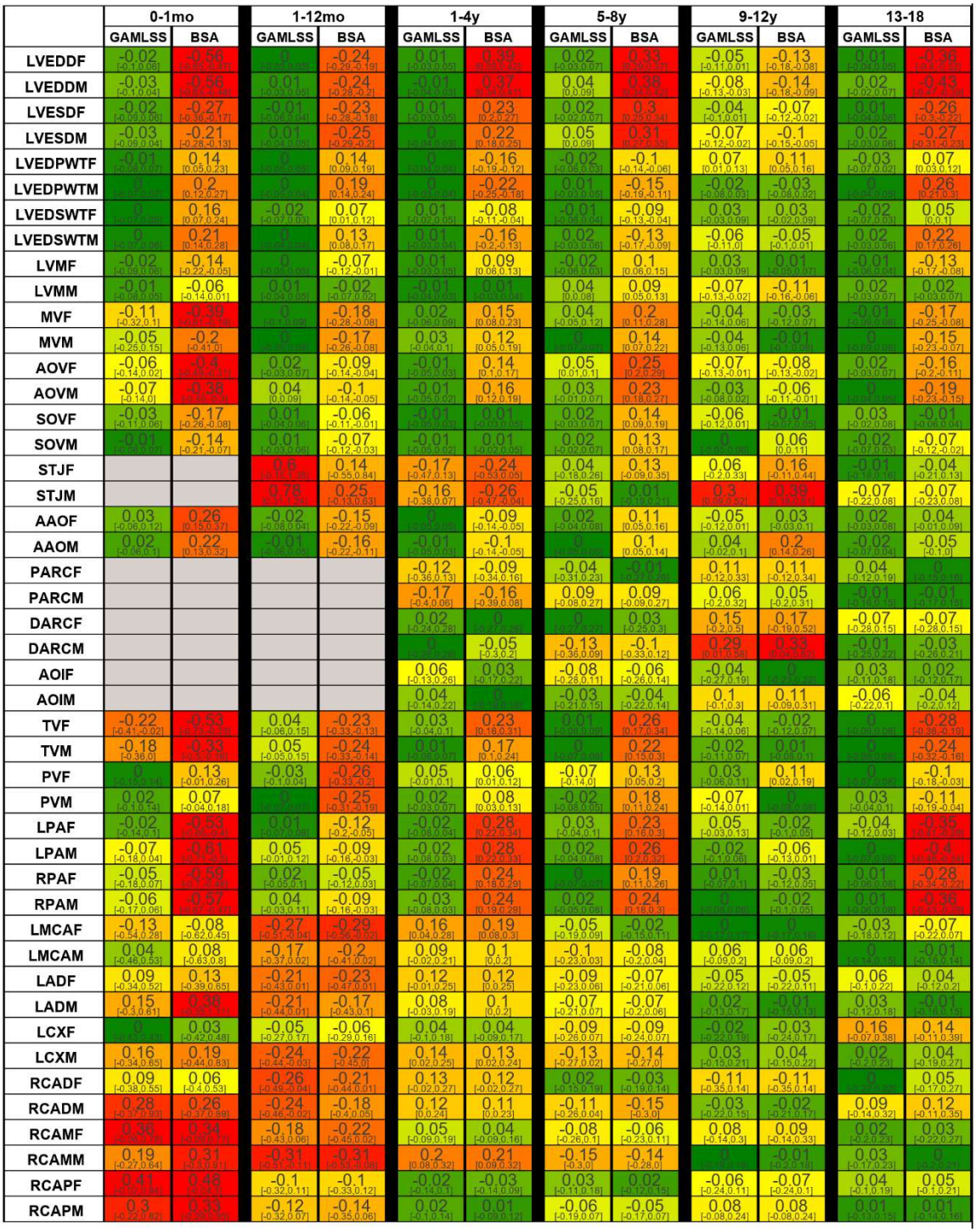


Figure 7. Heatmap of the mean Z-score in different strata of age (< 1 year) for the GAMLSS model and the BSA-allometric model. Each cell provides the mean Z-score [95% CI]. Expected mean in all strata is 0, deviations from 0 suggest systematic error. Colors are calculated using the absolute value of the mean. See Figure 6 for acronyms.

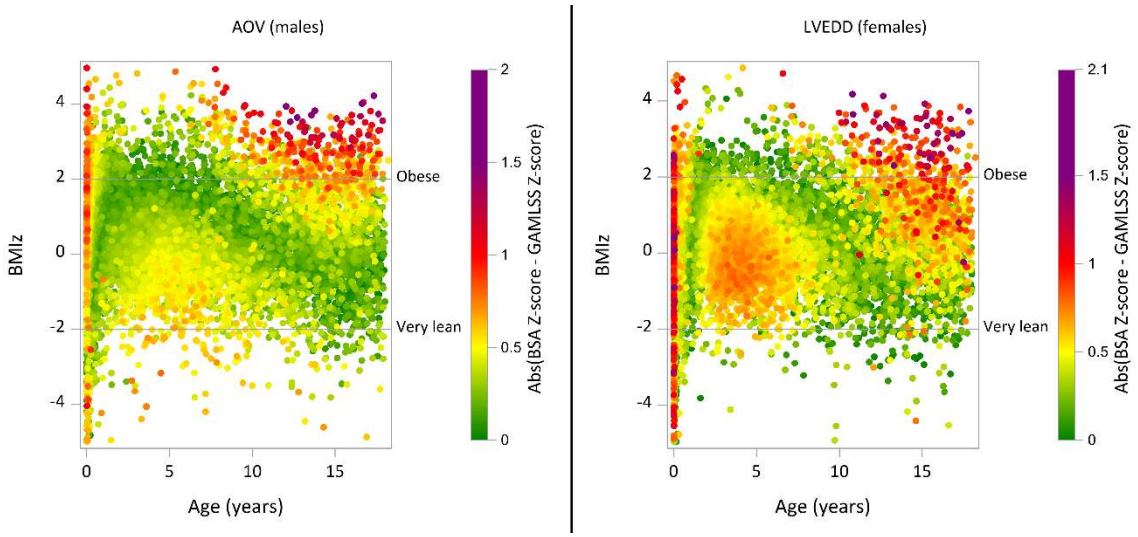


Figure 8. Difference between Z-score obtained with the multivariable model and the BSA-allometric model as a function of age and BMIz. AOV: aortic valve diameter; LVEDD: left ventricle end-diastolic diameter.

Supplementary Materials

Z-Scores for Pediatric Echocardiography Dimensions Adjusted for Body Size, Body-Mass Index and Age

Contents

Supplementary Results

- Section 1. Description of the fitted associations (p. 2)
- Section 2. Sensitivity analyses (p. 5)

Supplementary Tables

- Table S1. Height and weight distributions of the sample (p. 6)
- Table S2. Results of the hyperparameter search (p. 7)
- Methods for Table S2 (p. 12)
- Table S3. Results of the repeat cross-validation analysis (p. 12)
- Table S4. Mean Z-score by institution (p. 14)

Supplementary Figures S1-48

- Description of figures S1-46 (p. 18)
- Figures S1-S46 (p. 21)
- Methods for Figures S47 and S48 (p. 67)
- Figure S47. Heatmap of mean Z-scores in strata of age under cross validation (p. 68)
- Figure S48. Heatmap of mean Z-scores in strata of BMIz under cross-validation (p. 71)

Supplementary Results

Section 1. Description of the fitted associations

Median

Height was found to be a strong predictor of most cardiac dimensions. Beyond this effect of height, an effect of weight was found in all echocardiographic measurements. However, in many cases, the effect of weight was indirectly obtained through an effect of BMIz. Indeed, for many echocardiographic measurements, the SBC favored a model with height and BMIz as explanatory variables, but no direct effect of weight. In these cases, the effect of BMIz was generally positive, which reflects the positive relationship between weight and BMIz at a fixed height. Indeed, after height normalization, any increase in weight yields an increase in BMIz. This implies that if BMIz is included without weight, BMIz serves as a surrogate to weight normalization. This was explicitly tested by adding weight to the models where BMIz was used alone, which did not improve data fit (data not shown). Furthermore, using weight but not BMIz led to worse data fit in the extremes of BMIz, but similar data fit in different strata of weight (data not shown).

To further examine the effect of weight and BMIz on the predicted median and better illustrate the behavior described above, we simulated patients of varying body weight, but constant height and age. We then plotted the predicted median as a function of weight. Examples of this are shown in Supplementary Figure S0 (next page). It shows a finding that is consistent across almost all echocardiographic measurements for which an effect of BMIz was modelled: the predicted median always increases with increasing weight, but the rate of increase was higher in patients with a low BMIz than in those with a high BMIz.

In contrast, a BSA-allometric model supposes constant increases in cardiac dimensions with any increase of weight. A notable exception for this finding were the left-ventricular wall thickness variables, for which even when BMIz was included in the model, a relatively constant increase in measurements was observed, even in patients with higher BMIz.

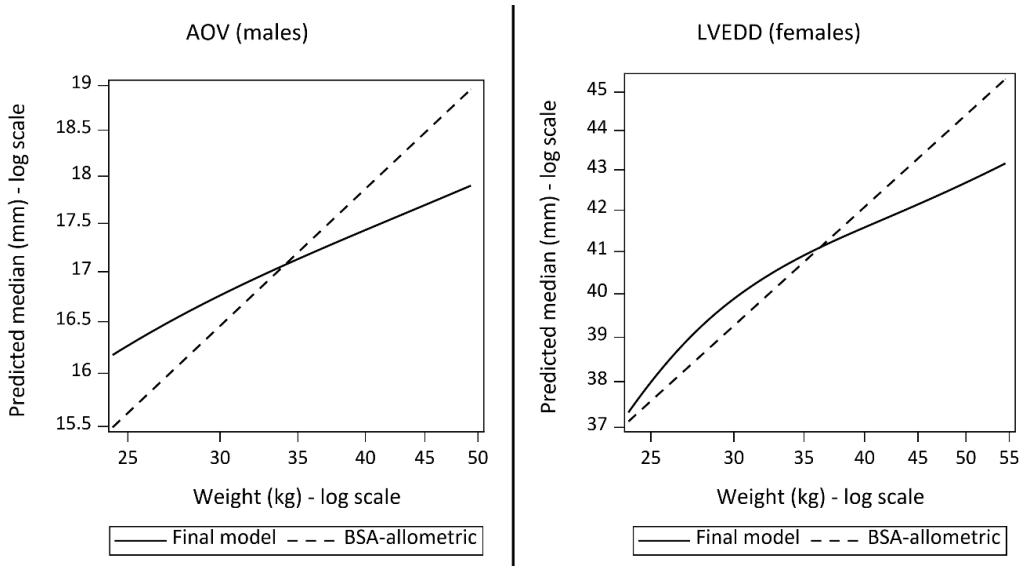


Figure S0. Predicted median as a function of weight. AOV: aortic valve diameter; LVEDD: left ventricular end-diastolic diameter; BSA: body surface area

Height and weight (directly or indirectly through BMIz) affected the predicted median with different magnitudes in different measurements. For some measurements, such as valve diameters, height showed a greater effect than weight, whereas in other measurements variables, such as the left ventricular wall thicknesses, weight appeared to be the dominant explanatory variable.

A nonlinear effect of age was modelled for most echocardiographic measurements. This effect was generally not as large as the effect of body size but was often important in children under one year of age. These sometimes complex nonlinear effects were generally

similar in females and males for a given measurement, which suggest they are not an artefact of overfitting and that they are indeed necessary to model cardiac dimensions in the younger ages.

Coefficient of variation

For most variables, an effect of age on the coefficient of variation was necessary to eliminate all apparent heteroscedasticity. The coefficient of variation was generally found to decrease with increasing age in the first years of life and then increase steadily into adolescence. These patterns may arise from variations in measurement precision throughout age, or from true change in the dispersion of cardiac dimensions.

Skewness

Modelling skewness improved data fit for most variables. The skewness parameter ranged from around 0-0.4 (relatively significant positive skewness) in variables such as the pulmonary valve diameter and pulmonary artery diameters to around 2-3 (relatively significant negative skewness) in variables such as the left-ventricular diameters. Most variables, however, tended to show slight positive skewness with a parameter around 0.7. Some variables, such as the diameter of the ascending aorta, showed essentially no skewness.

Kurtosis

For most variables, the SBC favored models that did not model kurtosis. For some variables, such as, modelling the kurtosis with a constant was favored by the SBC. In these variables, the value for the kurtosis parameter ranged from 1.50 to 1.85, which represents slight positive kurtosis. However, modelling kurtosis significantly increases Z-score

calculation complexity, and because the modelled kurtosis was small, it was decided to not model this parameter. Therefore, for all echocardiographic measurements, the model reduced to the standard LMS transformation.

Section 2. Sensitivity analyses

We tested the sensitivity of the reference values to the overweight patients. We created Z-scores equations excluding overweight patients and calculated the new Z-scores in the remaining population. For non-overweight subjects, the median of the absolute differences between these Z-scores and the proposed ones ranged from 0.02 to 0.04 depending on the measurement, and the 95th percentile of these differences ranged from 0.04 to 0.13.

It appeared that more lean subjects existed in patients younger than 3 months than in the rest of the sample (Figure 1 in main article). We therefore also tested the sensitivity of the reference values to this subgroup. Removing lean patients of less than 3 months from the reference population had little effect on the Z-scores of remaining patients. Notably, the median absolute differences in Z-scores ranged from 0.003 to 0.05 in patients under 3 months of age and from 0.001 to 0.06 in lean patients, depending on the measurement.

Table S1. Height and weight distributions of the sample

Age group	Sex	Height				Weight			
		Mean	Standard deviation	Min	Max	Mean	Standard deviation	Min	Max
0-3 months	males	53.4	5.3	31.0	99.60	4.3	1.3	0.9	15.3
	females	52.5	4.9	28.5	66.00	4.0	1.1	0.9	8.5
3-12 months	males	67.9	5.4	40.0	83.00	8.1	1.6	2.9	13.7
	females	66.4	5.0	42.0	80.50	7.5	1.4	3.1	12.4
1-4 years	males	93.9	10.7	65.0	152.40	14.7	3.2	6.4	37.0
	females	92.8	10.4	67.0	132.20	14.1	3.1	5.9	31.7
5-8 years	males	121.0	9.0	97.0	150.00	24.3	6.0	13.6	60.0
	females	120.2	9.3	95.0	159.00	23.7	5.9	13.6	54.4
9-12 years	males	144.6	10.4	116.5	180.20	39.4	12.1	17.9	128.6
	females	145.8	10.8	101.0	174.00	40.5	12.9	17.0	134.8
13-17 years	males	170.4	10.5	105.0	205.50	63.7	17.3	22.0	167.0
	females	161.9	7.5	117.0	190.00	57.5	13.4	26.7	135.0

Table S2. Results of the hyperparameter selection

Variable	Criterion	Selected hyperparameters							
		Height	Weight	P	Age	BMIz	Sigma	Lambda	Tau
LVEDDM	SBC	I	I	0.1	7	2	4	3	N
	GAIC3	I	I	0.1	8	3	5	4	N
	manual	I	I	0.1	7	2	4	3	N
LVEDDF	SBC	I	I	0	7	3	3	C	1
	GAIC3	I	I	0	8	4	4	C	2
	manual	I	I	0	7	3	3	C	N
LVESDM	SBC	I	I	0.1	7	2	3	C	N
	GAIC3	I	I	0.1	8	3	4	1	N
	manual	I	I	0.1	7	3	3	C	N
LVESDF	SBC	I	I	0	7	3	3	C	N
	GAIC3	I	I	0	8	3	4	C	2
	manual	I	I	0	7	3	3	C	N
LVEDPWTM	SBC	N	I	0.1	4	N	1	C	N
	GAIC3	I	I	0.2	7	3	3	C	1
	manual	I	I	0.2	7	N	1	C	N
LVEDPWTF	SBC	N	I	0.1	4	N	1	C	C
	GAIC3	N	I	0.3	8	1	3	C	C
	manual	I	I	0.1	7	N	1	C	N
LVEDSWTM	SBC	N	I	0.1	5	N	2	C	N
	GAIC3	I	I	0.2	7	N	4	C	N
	manual	I	I	0.1	5	N	2	C	N
LVEDSWTF	SBC	N	I	0	4	N	1	1	C
	GAIC3	N	I	0.7	7	2	3	1	C
	manual	I	I	0	4	N	1	1	N
LVMM	SBC	I	I	0.1	8	2	3	2	C
	GAIC3	I	I	0.1	8	3	4	3	C
	manual	I	I	0.1	8	3	3	2	N
LVMF	SBC	N	I	0	7	2	3	2	1
	GAIC3	N	I	0	8	3	4	4	1
	manual	I	I	0	7	2	3	2	N
MVM	SBC	I	I	1	N	2	C	N	N
	GAIC3	I	I	0.1	1	2	1	C	N
	manual	I	I	0.3	2	2	1	C	N

Variable	Criterion	Selected hyperparameters							
		Height	Weight	P	Age	BMIz	Sigma	Lambda	Tau
	SBC	I	I	0.1	1	1	C	N	N
	GAIC3	I	I	0.1	1	1	2	1	N
MVF	manual	I	I	0.3	3	1	2	C	N
	SBC	I	I	0.4	5	N	2	2	C
	GAIC3	I	I	0.4	7	2	2	2	1
AOVM	manual	I	I	0.4	5	2	2	2	N
	SBC	I	I	0.1	1	N	1	N	C
	GAIC3	I	I	0	4	4	1	2	C
AOVF	manual	I	I	0.1	1	3	1	C	N
	SBC	I	N	0.3	6	1	1	C	C
	GAIC3	I	N	0.2	8	2	1	C	1
SOVM	manual	I	N	0.3	6	1	1	C	N
	SBC	I	N	0.3	5	1	1	C	C
	GAIC3	I	N	0.4	6	3	2	3	C
SOVF	manual	I	N	0.3	5	1	1	C	N
	SBC	I	I	1	N	N	C	N	N
	GAIC3	I	I	1	N	N	C	N	N
STJM	manual	I	I	1	N	N	C	N	N
	SBC	I	I	1	N	N	C	N	N
	GAIC3	I	N	1	1	1	C	N	N
STJF	manual	I	I	1	N	N	C	N	N
	SBC	I	N	0.1	6	1	1	N	N
	GAIC3	I	N	0.1	8	4	1	C	N
AAOM	manual	I	N	0.1	6	1	1	N	N
	SBC	I	I	1	1	2	2	N	N
	GAIC3	I	N	0	7	3	2	N	N
AAOF	manual	I	N	0.1	6	2	1	N	N
	SBC	N	I	1	N	N	C	N	N
	GAIC3	N	I	1	1	N	C	N	N
PARCM	manual	I	I	1	N	N	C	N	N
	SBC	N	I	1	1	N	C	N	N
	GAIC3	N	I	1	4	N	1	N	N
PARCF	manual	I	I	1	N	N	C	N	N
	SBC	I	I	1	N	N	C	N	N
DARCM	GAIC3	I	N	0	3	1	C	1	4

Variable	Criterion	Selected hyperparameters							
		Height	Weight	P	Age	BMIz	Sigma	Lambda	Tau
	manual	I	I	1	N	N	C	N	N
	SBC	N	I	1	N	N	C	N	N
	GAIC3	N	I	0.1	1	N	C	N	1
DARCF	manual	I	I	1	N	N	C	N	N
	SBC	N	I	1	N	N	C	N	N
	GAIC3	I	I	1	N	N	C	N	3
AOIM	manual	I	I	1	N	N	C	N	N
	SBC	N	I	1	N	1	C	N	N
	GAIC3	N	I	0	7	1	C	N	N
AOIF	manual	I	I	1	N	N	C	N	N
	SBC	I	N	0	1	1	C	N	N
	GAIC3	I	I	0.1	1	2	C	C	C
TVM	manual	I	N	0.5	3	2	C	C	N
	SBC	I	N	0	1	1	C	C	N
	GAIC3	I	N	0	1	1	5	C	N
TVF	manual	I	N	0.4	3	1	2	C	N
	SBC	I	N	1	N	1	1	1	N
	GAIC3	I	N	0.4	2	2	2	1	N
PVM	manual	I	N	0.4	3	1	2	1	N
	SBC	I	N	1	1	1	1	C	N
	GAIC3	I	N	1	6	1	1	C	N
PVF	manual	I	N	0.2	3	1	1	C	N
	SBC	I	N	0	5	1	1	1	N
	GAIC3	I	N	0	6	1	1	1	N
LPAM	manual	I	N	0	5	1	1	1	N
	SBC	I	I	0	4	N	1	1	N
	GAIC3	I	I	0	5	3	1	2	N
LPAF	manual	I	I	0	4	2	1	1	N
	SBC	I	N	0	4	1	C	C	N
	GAIC3	I	N	0	5	2	1	C	2
RPAM	manual	I	N	0	5	1	C	C	N
	SBC	I	N	0	5	1	C	C	N
	GAIC3	I	N	0	5	1	1	3	C
RPAF	manual	I	N	0	5	1	C	C	N
LMCAM	SBC	I	I	1	N	N	2	N	N

Variable	Criterion	Selected hyperparameters							
		Height	Weight	P	Age	BMIz	Sigma	Lambda	Tau
	GAIC3	N	I	0	7	N	4	1	1
	manual	I	I	0.3	N	N	2	N	N
	SBC	N	I	0.2	1	N	2	N	N
	GAIC3	N	I	0.2	1	N	3	N	N
LMCAF	manual	I	I	0.5	N	N	2	N	N
	SBC	N	I	1	N	N	3	N	C
	GAIC3	N	I	0	6	N	4	C	3
LADM	manual	I	I	0.3	N	N	2	N	N
	SBC	N	I	1	N	1	C	N	C
	GAIC3	N	I	0.4	1	N	2	N	C
LADF	manual	I	I	0.5	N	N	2	N	N
	SBC	N	I	1	N	N	C	1	N
	GAIC3	I	I	0.3	8	1	2	1	C
LCXM	manual	I	I	0.4	N	N	2	N	N
	SBC	N	I	1	N	1	C	N	C
	GAIC3	N	I	1	N	1	C	C	C
LCXF	manual	I	I	0.8	N	N	2	N	N
	SBC	N	I	1	1	N	C	C	N
	GAIC3	N	I	0.5	1	N	2	1	N
RCAPM	manual	I	I	0.4	N	N	2	N	N
	SBC	N	I	1	N	N	C	N	N
	GAIC3	N	I	1	N	N	C	1	N
RCAPF	manual	I	I	0.3	N	N	2	N	N
	SBC	N	I	1	N	1	C	N	C
	GAIC3	N	I	0	7	N	3	N	4
RCAMM	manual	I	I	0.4	N	N	2	N	N
	SBC	N	I	1	N	N	C	N	N
	GAIC3	N	I	1	N	1	3	N	1
RCAMF	manual	I	I	0.5	N	N	2	N	N
	SBC	N	I	1	N	N	C	N	N
	GAIC3	I	I	0.1	4	1	C	N	N
RCADM	manual	N	I	1	N	N	C	N	N
	SBC	N	I	1	N	N	C	C	N
	GAIC3	N	I	1	N	N	C	C	N
RCADF	manual	N	I	1	N	N	C	N	N

Height column: whether height is included (I) or not (N)
Weight column: whether weight is included (I) or not (N)
P column: transformation parameter for age (age^p if $p \neq 0$, log(age) if $p = 0$)
Age column: complexity of age effect on median where N = age not included, 1 = linear, 2 = near quadratic, 3 = near cubic, etc.
BMIz column: complexity of BMIz effect on median where N = BMIz not included, 1 = linear, 2 = near quadratic, 3 = near cubic, etc.
Sigma, lambda and tau columns: how these parameters are modelled. N = not modelled, C = modelled as a constant, 1 = linear effect of age, 2 = near quadratic effect of age, 3 = near cubic effect of age, etc.
SBC: Schwartz-Bayesian Criterion.
GAIC3: Generalized Akaike information criterion with penalty k = 3.
Manual: final manually selected hyperparameters.
LVEDDF: left-ventricular end-diastolic diameter in females; LVEDDM: left-ventricular end-diastolic diameter in males; LVESDF: left-ventricular end-systolic diameter in females; LVESDM: left-ventricular end-systolic diameter in males; LVEDPWTF: left-ventricular posterior wall thickness in females; LVEDPWTM: left-ventricular posterior wall thickness in males; LVEDSWTF: left-ventricular septal wall thickness in females; LVEDSWTM: left-ventricular septal wall thickness in males; LVMF: left-ventricular mass in females; LVMM: left-ventricular mass in males; MVF: mitral valve diameter in apical view in females; MVM: mitral valve diameter in apical view in males; AOVF: aortic valve diameter in females; AOVM: aortic valve diameter in males; SOVF: Sinus of Valsalva diameter in females; SOVM: Sinus of Valsalva diameter in males; STJF: sinotubular junction diameter in females; STJM: sinotubular junction diameter in males; AAOF: ascending aorta diameter in females; AAOM: ascending aorta diameter in males; PARCF: proximal arch diameter of aorta in females; PARCM: proximal arch diameter of aorta in males; DARCF: distal arch diameter of aorta in females; DARCM: distal arch diameter of aorta in males; AOIF: aortic isthmus diameter in females; AOIM: aortic isthmus diameter in males; TVF: tricuspid valve diameter in apical view in females; TVM: tricuspid valve diameter in apical view in males; PVF: pulmonary valve diameter in females; PVM: pulmonary valve diameter in males; LPAF: left pulmonary artery diameter in females; LPAM: left pulmonary artery diameter in males; RPAF: right pulmonary artery diameter in females; RPAM: right pulmonary artery diameter in males; LMCAF: left main coronary artery diameter in females; LMCAM: left main coronary artery diameter in males; LADF: left anterior descending artery diameter in females; LADM: left anterior descending artery diameter in males; LCXF: left circumflex artery diameter in females; LCXM: left circumflex artery diameter in males; RCAPF: right coronary artery diameter in proximal segment in females; RCAPM: right coronary artery diameter in proximal segment in males; RCADF: right coronary artery in distal segment in females; RCADM: right coronary artery in distal segment in males; RCAMF: right coronary artery in medium segment in females; RCAMM: right coronary artery in medium segment in males.

Methods for Supplementary Table S3

To evaluate the general model fit while considering the risk of overfitting, we performed repeat cross-validation. For each variable, the study population was randomly split in a training subsample (70%) and a validation subsample (the remaining 30%). The training subsample was used for model regression with the chosen hyperparameters. The deviance (-2×log likelihood) was then calculated on the validation subsample. This process was repeated with fifty randomly selected validation and training subsamples for all variables, and the median deviance value of these repeated trials was calculated and is presented in Table S2. The results show that for all variables for which an effect of age or BMIz was included, the validation sample deviance was lower for the GAMLSS model than for the BSA-allometric model. This does not suggest that the improvements seen in the GAMLSS were due to overfitting.

Table S3. Repeat cross-validation results

Variable	Median deviance in validation sample of 50 trials of cross-validation			
	Males		Females	
	GAMLSS	BSA	GAMLSS	BSA
AOV	8561,3	9773,9	10177,2	11744,5
AAO	7175,9	7941,0	8536,1	9465,7
LPA	4253,0	4839,4	5060,8	5772,3
MV	3524,7	3723,7	4286,0	4507,4
PV	5741,0	6240,4	6903,1	7536,4
RPA	4290,2	4835,9	5109,1	5781,2
SOV	9319,3	10362,5	11366,9	12660,2
TV	3637,1	3843,7	4480,1	4694,2
STJ	371,2	362,2	507,1	490,9
AOI	514,9	499,0	586,6	569,1
DARC	269,7	265,0	285,1	280,6

PARC	443,3	430,3	523,5	503,8
MPA	192,8	194,2	238,7	240,5
LVEDD	13153,9	14651,5	15476,9	17404,0
LVEDPWT	6462,0	7450,8	7671,6	9035,9
LVEDSWT	6856,1	7717,2	8270,4	9463,8
LVESD	12239,1	13528,7	14575,4	16133,6
LVM	18758,4	21506,8	22530,9	25970,0
LMCA	205,7	260,8	286,3	343,4
LAD	176,3	222,0	185,9	236,9
LCX	134,9	197,8	154,4	222,7
RCAP	201,1	251,4	242,0	292,8
RCAM	118,3	172,2	152,7	219,1
RCAD	108,6	168,4	142,1	200,1

AOV: aortic valve diameter; AAO: ascending aorta diameter; LPA: left pulmonary artery diameter; MV: mitral valve diameter in apical view; PV: pulmonary valve diameter; RPA: right pulmonary artery diameter; SOV: Sinus of Valsalva diameter; TV: tricuspid valve diameter in apical view; STJ: sinotubular junction diameter; AOI: aortic isthmus diameter; DARC: distal arch diameter of aorta; PARC: proximal arch diameter of aorta; LVEDD: left-ventricular end-diastolic diameter; LVEDPWT: left-ventricular posterior wall thickness; LVEDSWT: left-ventricular septal wall thickness; LVESD: left-ventricular end-systolic diameter; LVM: left-ventricular mass; LMCA: left main coronary artery diameter; LAD: left anterior descending artery diameter; LCX: left circumflex artery diameter; RCAP: right coronary artery diameter in proximal segment; RCAM: right coronary artery in medium segment; RCAD: right coronary artery in distal segment.

Table S4. Mean Z-score by institution

Dimension	Institution							
	1	2	3	4	5	6	7	8
LVEDDM	0,16 (0,00, 0,32)	-0,01 (-0,03, 0,01)	0,25 (0,10, 0,41)	0,18 (-0,04, 0,40)	-0,59 (-1,25, 0,07)	-0,02 (-0,34, 0,30)	0,02 (-0,06, 0,09)	
LVEDDF	0,20 (0,04, 0,36)	-0,01 (-0,03, 0,01)	0,34 (0,17, 0,50)	0,05 (-0,16, 0,26)	-0,34 (-0,76, 0,08)	0,01 (-0,39, 0,42)	0,06 (-0,01, 0,13)	
LVESDM	0,65 (0,49, 0,80)	-0,01 (-0,03, 0,01)	0,07 (-0,09, 0,22)	0,14 (-0,11, 0,40)	0,02 (-0,64, 0,68)	-0,16 (-0,61, 0,29)	-0,10 (-0,17, -0,03)	
LVESDF	0,60 (0,45, 0,74)	0,00 (-0,02, 0,02)	0,14 (-0,02, 0,30)	-0,23 (-0,48, 0,02)	0,16 (-0,31, 0,64)	0,00 (-0,37, 0,37)	-0,11 (-0,18, -0,04)	
LVEDPWTM	-0,33 (-0,48, -0,17)	-0,06 (-0,08, -0,04)	-0,25 (-0,42, -0,09)	0,38 (0,10, 0,65)	-0,25 (-0,88, 0,38)	0,15 (-0,36, 0,66)	0,94 (0,87, 1,01)	
LVEDPWTF	-0,22 (-0,38, -0,06)	-0,07 (-0,09, -0,05)	-0,14 (-0,31, 0,03)	0,36 (0,15, 0,58)	-0,06 (-0,44, 0,31)	0,03 (-0,28, 0,33)	1,01 (0,95, 1,08)	
LVEDSWTM	-0,13 (-0,27, 0,01)	-0,09 (-0,11, -0,07)	0,58 (0,45, 0,71)	0,89 (0,60, 1,17)	-0,32 (-0,88, 0,25)	0,25 (-0,05, 0,55)	1,00 (0,93, 1,07)	
LVEDSWTF	-0,13 (-0,28, 0,02)	-0,08 (-0,10, -0,06)	0,60 (0,44, 0,76)	0,78 (0,53, 1,03)	-0,28 (-0,64, 0,08)	0,25 (-0,03, 0,52)	0,94 (0,87, 1,01)	
LVMM	-0,12 (-0,28, 0,03)	-0,08 (-0,11, -0,06)	0,36 (0,21, 0,51)	0,80 (0,53, 1,07)	-0,71 (-1,28, -0,14)	0,21 (-0,23, 0,66)	1,01 (0,94, 1,07)	
LVMF	-0,07 (-0,22, 0,08)	-0,08 (-0,10, -0,06)	0,46 (0,30, 0,61)	0,64 (0,43, 0,85)	-0,35 (-0,68, -0,02)	0,13 (-0,29, 0,55)	1,04 (0,97, 1,11)	
MVM	0,00 (-0,24, 0,25)	0,00 (-0,04, 0,05)		-0,41 (-0,99, 0,17)	0,11 (-0,34, 0,56)		-0,01 (-0,10, 0,07)	
MVF	-0,10 (-0,29, 0,08)	0,01 (-0,03, 0,05)		-0,45 (-0,94, 0,04)	0,06 (-0,27, 0,39)		-0,02 (-0,10, 0,06)	
AOVM	0,40 (0,24, 0,57)	0,00 (-0,02, 0,03)	0,21 (0,05, 0,37)	0,16 (-0,16, 0,48)	0,34 (-0,09, 0,77)	-0,30 (-1,42, 0,82)	-0,21 (-0,28, -0,14)	
AOVF	0,30 (0,16, 0,43)	0,01 (-0,01, 0,03)	0,06 (-0,13, 0,25)	0,04 (-0,24, 0,33)	0,11 (-0,27, 0,49)	0,16 (-0,29, 0,61)	-0,22 (-0,28, -0,15)	
SOVM	-0,40 (-0,57, -0,22)	0,01 (-0,01, 0,03)	-0,27 (-0,43, -0,11)		-0,10 (-0,74, 0,55)		0,06 (-0,02, 0,14)	
SOVF	-0,47 (-0,62, -0,33)	0,01 (-0,01, 0,03)	-0,22 (-0,39, -0,05)		-0,48 (-0,82, -0,13)		0,05 (-0,03, 0,14)	
STJM	-0,92 (-1,19, -0,64)		0,01 (-0,15, 0,17)		0,26 (-0,35, 0,87)	0,36 (-0,55, 1,26)	0,31 (0,15, 0,48)	

STJF	-0,61 (-0,87, -0,36)		0,01 (-0,15, 0,18)		-0,26 (-0,57, 0,05)	0,54 (-0,16, 1,24)	0,28 (0,14, 0,41)	
AAOM	0,04 (-0,19, 0,28)	-0,01 (-0,03, 0,02)	-0,16 (-0,31, -0,01)	0,00 (-0,39, 0,38)	-0,07 (-0,89, 0,75)	-0,16 (-0,69, 0,36)	0,15 (0,06, 0,24)	
AAOF	-0,05 (-0,24, 0,14)	0,00 (-0,03, 0,02)	-0,21 (-0,39, -0,03)	0,12 (-0,22, 0,45)	-0,64 (-1,09, -0,19)	0,37 (0,02, 0,71)	0,12 (0,03, 0,20)	
PARCM	-0,01 (-0,20, 0,18)				0,28 (-0,13, 0,69)	0,35 (-1,67, 2,37)	-0,02 (-0,15, 0,12)	
PARCF	-0,01 (-0,17, 0,16)				0,60 (0,32, 0,88)	0,69 (-0,36, 1,74)	-0,09 (-0,23, 0,05)	
DARCM	-0,42 (-0,61, -0,22)				0,00 (-0,55, 0,55)		0,44 (0,28, 0,59)	
DARCF	-0,24 (-0,41, -0,07)				0,06 (-0,49, 0,62)		0,34 (0,15, 0,53)	
AOIM	-0,34 (-0,55, -0,13)				-0,46 (-1,01, 0,09)		0,13 (0,03, 0,23)	
AOIF	-0,43 (-0,60, -0,27)				-0,42 (-0,78, -0,06)	1,67 (-18,86, 22,21)	0,18 (0,08, 0,29)	
TVM	-0,43 (-0,69, -0,16)	0,02 (-0,03, 0,06)		-0,21 (-0,67, 0,26)	-0,32 (-0,89, 0,25)		0,03 (-0,05, 0,11)	
TVF	-0,56 (-0,76, -0,35)	0,03 (-0,01, 0,07)		0,01 (-0,57, 0,58)	-0,13 (-0,43, 0,18)		0,02 (-0,06, 0,10)	
PVM	-0,64 (-0,88, -0,39)	0,00 (-0,03, 0,03)		0,33 (-0,11, 0,77)	0,56 (0,07, 1,05)		0,06 (-0,01, 0,14)	
PVF	-0,69 (-0,90, -0,49)	0,01 (-0,02, 0,04)		-0,36 (-0,89, 0,17)	0,12 (-0,16, 0,40)		0,07 (0,00, 0,14)	
LPAM	-0,44 (-0,69, -0,18)	-0,01 (-0,05, 0,02)		-0,31 (-0,89, 0,27)	0,41 (-0,35, 1,16)	-0,46 (-1,40, 0,47)	0,18 (0,10, 0,27)	
LPAF	-0,47 (-0,70, -0,25)	-0,01 (-0,04, 0,02)		-0,03 (-0,57, 0,51)	-0,32 (-0,87, 0,23)	0,02 (-0,70, 0,74)	0,21 (0,13, 0,29)	
RPAM	-0,40 (-0,59, -0,20)	-0,01 (-0,05, 0,02)		-0,09 (-0,59, 0,41)	0,00 (-0,64, 0,63)	-0,98 (-1,37, -0,58)	0,22 (0,14, 0,30)	
RPAF	-0,46 (-0,63, -0,28)	-0,01 (-0,04, 0,02)		0,26 (-0,21, 0,73)	0,01 (-0,63, 0,64)	0,32 (-0,35, 0,99)	0,24 (0,16, 0,33)	
LMCAM	-0,44 (-2,80, 1,91)	-0,07 (-0,17, 0,03)			-0,77 (-2,00, 0,46)	0,09 (-1,57, 1,75)	0,28 (0,12, 0,45)	-0,03 (-0,13, 0,07)
LMCAF	0,48	-0,01			-0,84	-0,86	0,33	-0,08

	(0,20, 0,76)	(-0,11, 0,10)			(-1,24, -0,44)	(-1,88, 0,17)	(0,15, 0,51)	(-0,16, 0,00)
LADM	-0,71 (-1,27, -0,16)	-0,06 (-0,17, 0,05)			-0,40 (-1,03, 0,23)	-0,71 (-1,39, -0,03)	0,14 (-0,01, 0,30)	0,05 (-0,05, 0,14)
LADF	-0,59 (-1,90, 0,72)	-0,08 (-0,19, 0,03)			-0,98 (-1,69, -0,27)	-0,90 (-1,75, -0,05)	0,26 (0,10, 0,43)	0,01 (-0,07, 0,10)
LCXM		0,01 (-0,11, 0,12)				0,14 (-0,69, 0,98)		0,01 (-0,08, 0,10)
LCXF	-1,11 (-7,69, 5,47)	-0,07 (-0,19, 0,05)				-0,88 (-1,66, -0,10)		0,09 (0,01, 0,17)
RCAPM		-0,19 (-0,31, -0,07)						0,27 (0,17, 0,37)
RCAPF		-0,26 (-0,38, -0,14)						0,23 (0,15, 0,31)
RCAMM	-1,25 (-7,01, 4,51)	-0,11 (-0,23, 0,02)						0,17 (0,07, 0,26)
RCAMF	-0,78 (-1,69, 0,12)	-0,17 (-0,29, -0,04)				-0,40 (-12,36, 11,55)		0,16 (0,08, 0,24)
RCADM	-1,09 (-2,49, 0,31)	0,10 (-0,01, 0,20)			-0,18 (-1,21, 0,85)	-0,21 (-2,86, 2,44)	0,09 (-0,04, 0,22)	-0,21 (-0,31, -0,12)
RCADF	-0,27 (-1,80, 1,26)	0,22 (0,11, 0,33)			-0,81 (-1,10, -0,52)	-0,69 (-1,08, -0,30)	0,15 (0,01, 0,30)	-0,26 (-0,34, -0,18)

LVEDDF: left-ventricular end-diastolic diameter in females; LVEDDM: left-ventricular end-diastolic diameter in males; LVESDF: left-ventricular end-systolic diameter in females; LVESDM: left-ventricular end-systolic diameter in males; LVEDPWTF: left-ventricular posterior wall thickness in females; LVEDPWTM: left-ventricular posterior wall thickness in males; LVEDSWTF: left-ventricular septal wall thickness in females; LVEDSWTM: left-ventricular septal wall thickness in males; LVMF: left-ventricular mass in females; LVMM: left-ventricular mass in males; MVF: mitral valve diameter in apical view in females; MVM: mitral valve diameter in apical view in males; AOVF: aortic valve diameter in females; AOVM: aortic valve diameter in males; SOVF: Sinus of Valsalva diameter in females; SOVM: Sinus of Valsalva diameter in males; STJF: sinotubular junction diameter in females; STJM: sinotubular junction diameter in males; AAOF: ascending aorta diameter in females; AAOM: ascending aorta diameter in males; PARCF: proximal arch diameter of aorta in females; PARCM: proximal arch diameter of aorta in males; DARCF: distal arch diameter of aorta in females; DARCM: distal arch diameter of aorta in males; AOIF: aortic isthmus diameter in females; AOIM: aortic isthmus diameter in males; TVF: tricuspid valve diameter in apical view in females; TVM: tricuspid valve diameter in apical view in males; PVF: pulmonary valve diameter in females; PVM: pulmonary valve diameter in males; LPAF: left pulmonary artery diameter in females; LPAM: left pulmonary artery diameter in males; RPAF: right pulmonary artery diameter in females; RPAM: right pulmonary artery diameter in males; LMCAF: left main coronary artery diameter in females; LMCAM: left main coronary artery diameter in males; LADF: left anterior descending artery diameter in females; LADM: left anterior descending artery diameter in males; LCXF: left circumflex artery diameter in females; LCXM: left circumflex artery diameter in males; RCAPF: right coronary artery diameter in proximal segment in females; RCAPM: right coronary artery diameter in proximal segment in males; RCADF: right coronary artery in distal segment in females; RCADM: right coronary artery in distal segment in males;

RCAMF: right coronary artery in medium segment in females; RCAMM: right coronary artery in medium segment in males.

Supplementary Figures S1-46.

In the following pages, we show a set of Supplementary figures for every echocardiographic measurement included in the study. We show three types of figures: worm plots, which serve to evaluate data fit; partial residual graphs, which show the effect of the independent variables on the predicted median in the GAMLSS model; and two heatmaps that quantify the difference between the BSA-allometric model and the GAMLSS model.

Worm plots

We show in figures S1-46 A and B the worm plots of the final model in comparison to a pure BSA-allometry model for all measurements, with stratifications by age and BMIz.

As described in the paper, worm plots are stratified detrended Q-Q plots. Each panel in a worm plot represents a subgroup of the sample that has been stratified by some variable. In each panel, the X-axis represents the expected Z-score of the patient (given their quantile within the subgroup's echocardiographic measurement values). The Y-axis represents the difference between the empirical Z-score of some patient (given some model) and the expected Z-score. Conceptually, the Y-axis therefore represents the "error" in Z-score for any patient. Therefore, a model with no error should show points on the $y = 0$ line. Of course, random variation precludes this, therefore deviations from the $y = 0$ line are tolerated within the expectation that more than 95% of the subgroup should remain between the dashed 95% confidence interval.

Specific patterns in the worm plots suggest misfit in the distribution's median, its dispersion, its skewness or its kurtosis: a non-zero intercept in the trend suggests misfit in

the median; a non-zero linear slope suggests misfit in the dispersion; a non-zero quadratic shape (U or inverted U shape suggests misfits in the skewness; and a non-zero cubic shape (S shape) suggests misfits in the kurtosis. For a more detailed description of worm plots, we refer the reader to van Buuren and Fredriks [23].

Partial residuals

We show in Figures S1-46 C-F the partial residuals for the median of the distributions. As described in the main paper, the partial residual graphs show the effect of each independent variable on the log of the predicted median of the echocardiographic measurement. The slope of the trend at any point may be understood as the expected percentage change in cardiac dimension for every unit of change in the independent variable, all other things equal.

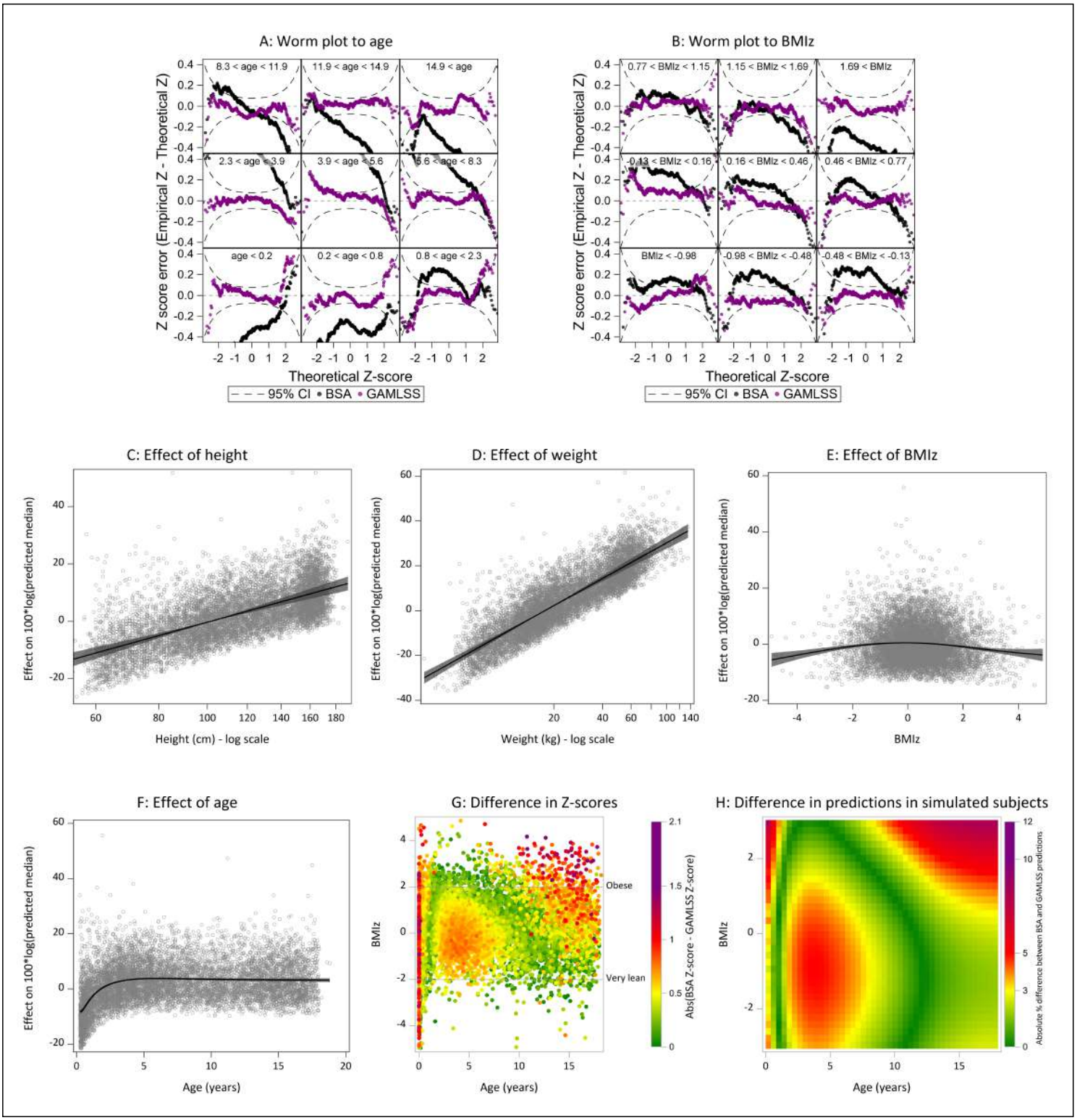
Heatmap of the difference between the final model and a pure BSA-allometric

We show in Figures S1-46 G and H two graphs that illustrate the differences between the GAMLSS model and a pure BSA allometric model. Figures S1-46 G are the same plots as Figure 8 in the main article and show a colored heatmap of the differences between the Z-scores obtained from both models as a function of age and BMIz.

Some authors suggest that the significance of the difference in between different models should be evaluated by observing the relative difference in predictions. We therefore show in Figures S1-46 H heatmaps of the percentage difference between the prediction for the median of the GAMLSS and BSA-allometric models, as a function of age and BMIz, in simulated patients. To generate these figures, simulated patients with incremental values of age and BMIz were generated. The height of the simulated patients was defined as the 50^{th}

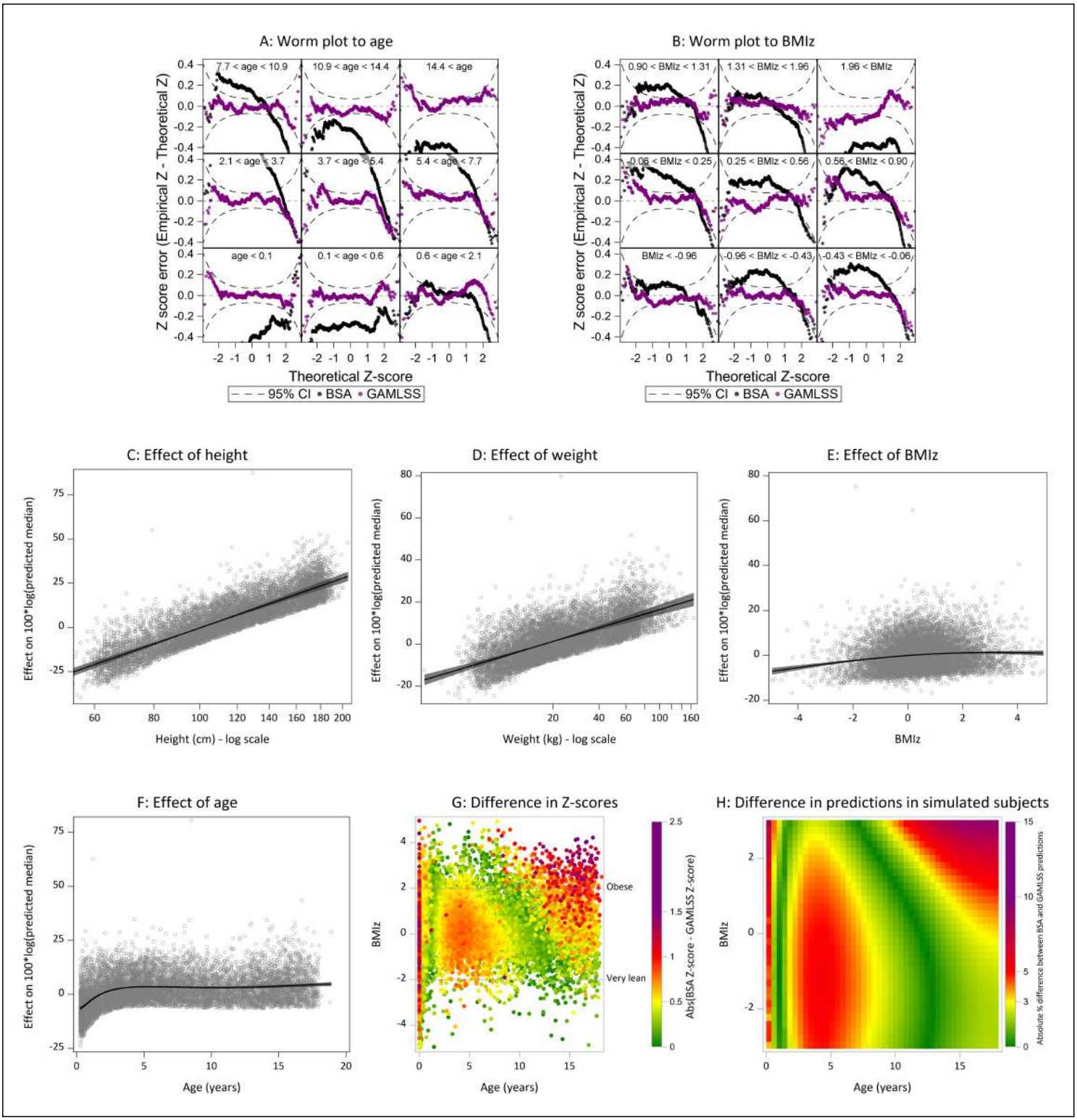
percentile of the height distribution according to their age by using the WHO growth standards [22]. The weight of the simulated patients was calculated with their BMI and height.

Predictions for the median of the distribution from both the final GAMLSS model and a pure BSA-allometric model were then calculated for all patients. The relative difference between these two predictions was then calculated [24]. The figure then shows this relative difference as function of age and BMIz in a colored map. Other authors have suggested a threshold of 5% for a difference in prediction that is clinically relevant.



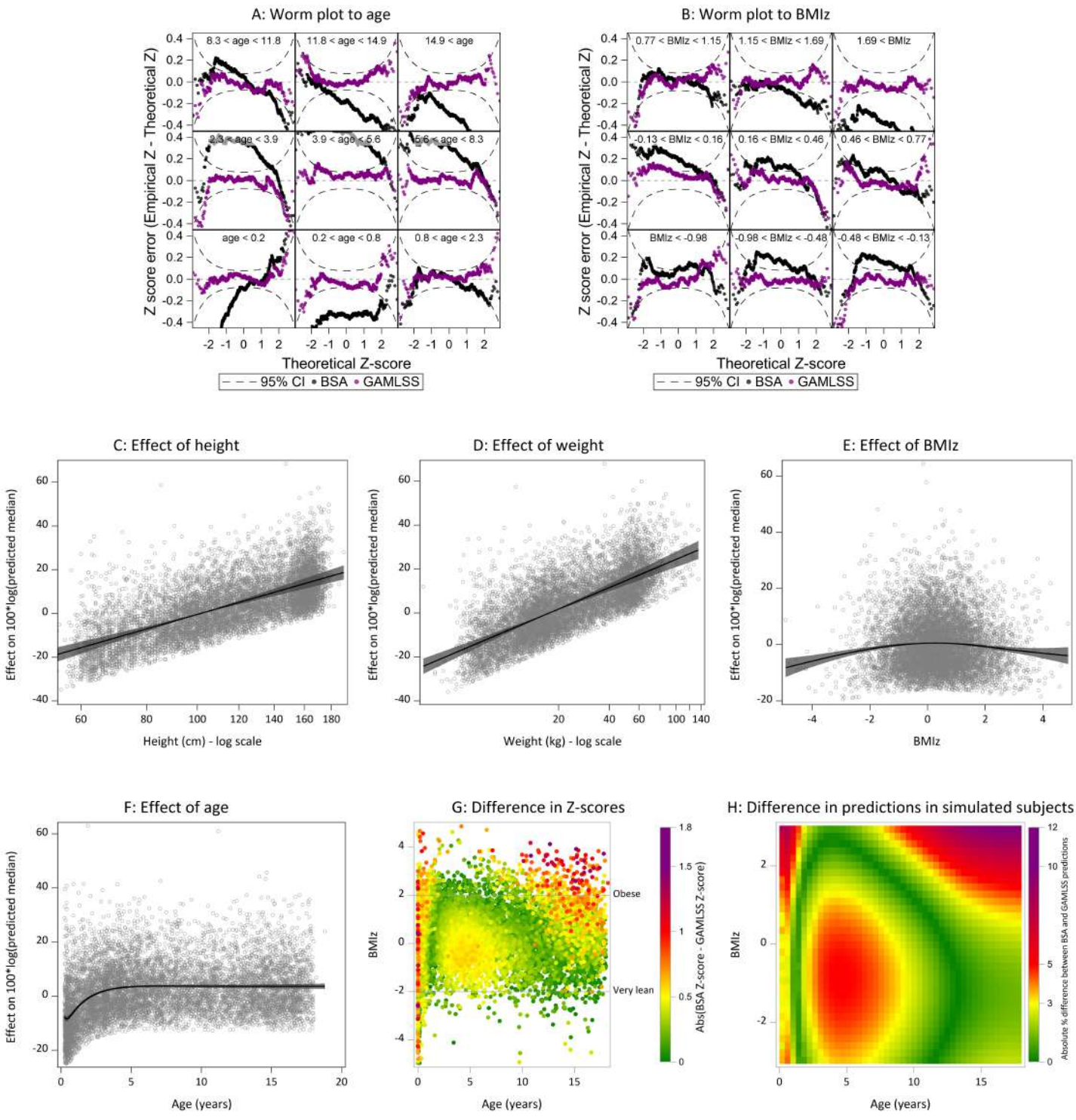
Supplementary figures S1 A-G: Left-ventricular end-diastolic diameter in females (LVEDDF)

A: Worm plot by age of the Z-scores of the GAMLSS model in comparison to the BSA-allometric model for LVEDDF. B: Worm plot by BMIz of the Z-scores of the GAMLSS model in comparison to the BSA-allometric model for LVEDDF. C: Effect of height on the log of the predicted median of the LVEDDF. D: Effect of weight on the log of the predicted median of LVEDDF. E: Effect of BMIz on the log of the predicted median of LVEDDF. F: Effect of age on the log of the predicted median of LVEDDF. G: Difference between Z-scores of the GAMLSS model and the BSA-allometric model for LVEDDF. H: Difference between predicted median of the GAMLSS model and the BSA-allometric model for LVEDDF in simulated subjects.



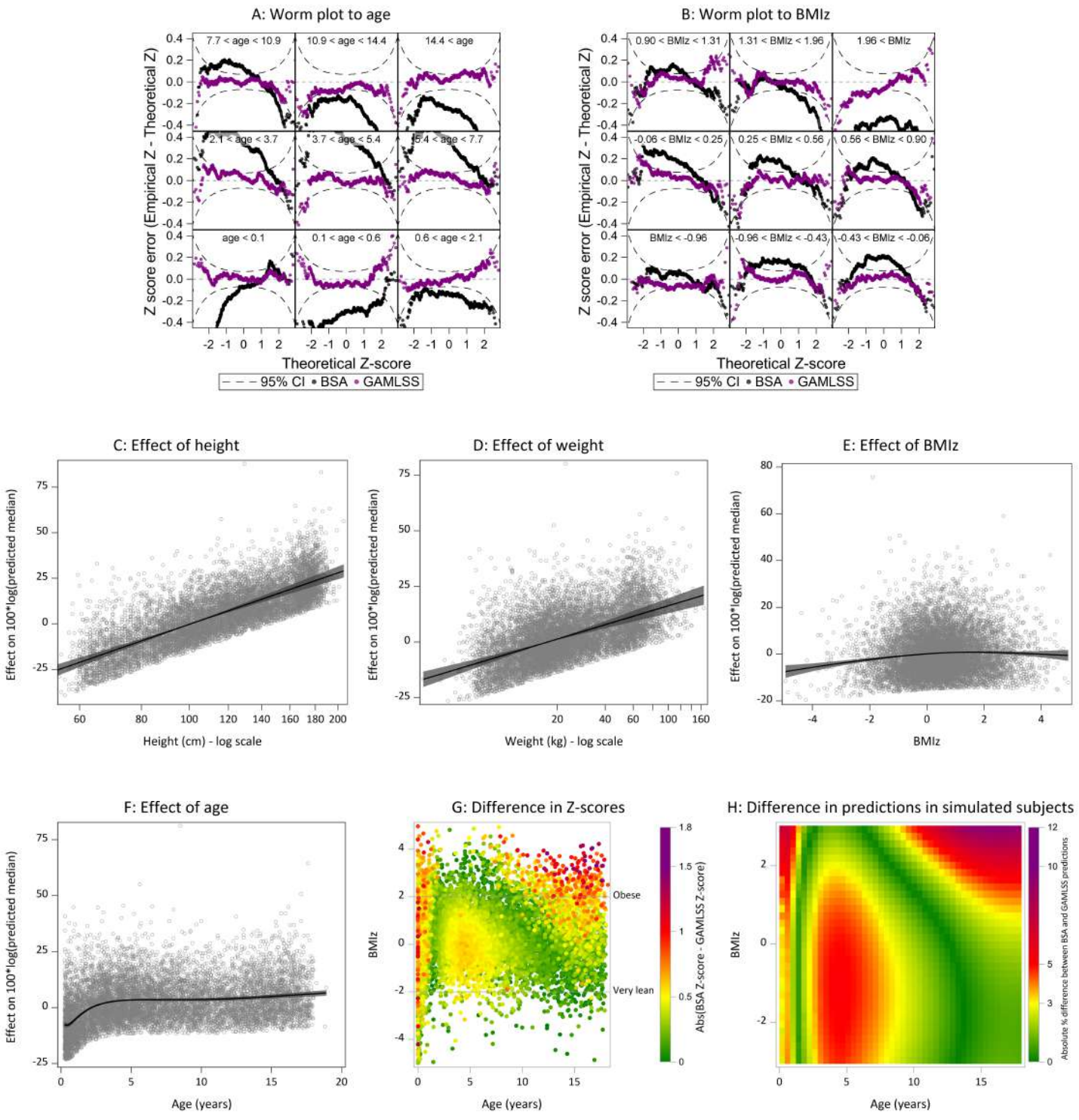
Supplementary figures S2 A-G: Left-ventricular end-diastolic diameter in males (LVEDDM)

A: Worm plot by age of the Z-scores of the GAMLSS model in comparison to the BSA-allometric model for LVEDDM. B: Worm plot by BMIz of the Z-scores of the GAMLSS model in comparison to the BSA-allometric model for LVEDDM. C: Effect of height on the log of the predicted median of the LVEDDM. D: Effect of weight on the log of the predicted median of LVEDDM. E: Effect of BMIz on the log of the predicted median of LVEDDM. F: Effect of age on the log of the predicted median of LVEDDM. G: Difference between Z-scores of the GAMLSS model and the BSA-allometric model for LVEDDM. H: Difference between predicted median of the GAMLSS model and the BSA-allometric model for LVEDDM in simulated subjects.



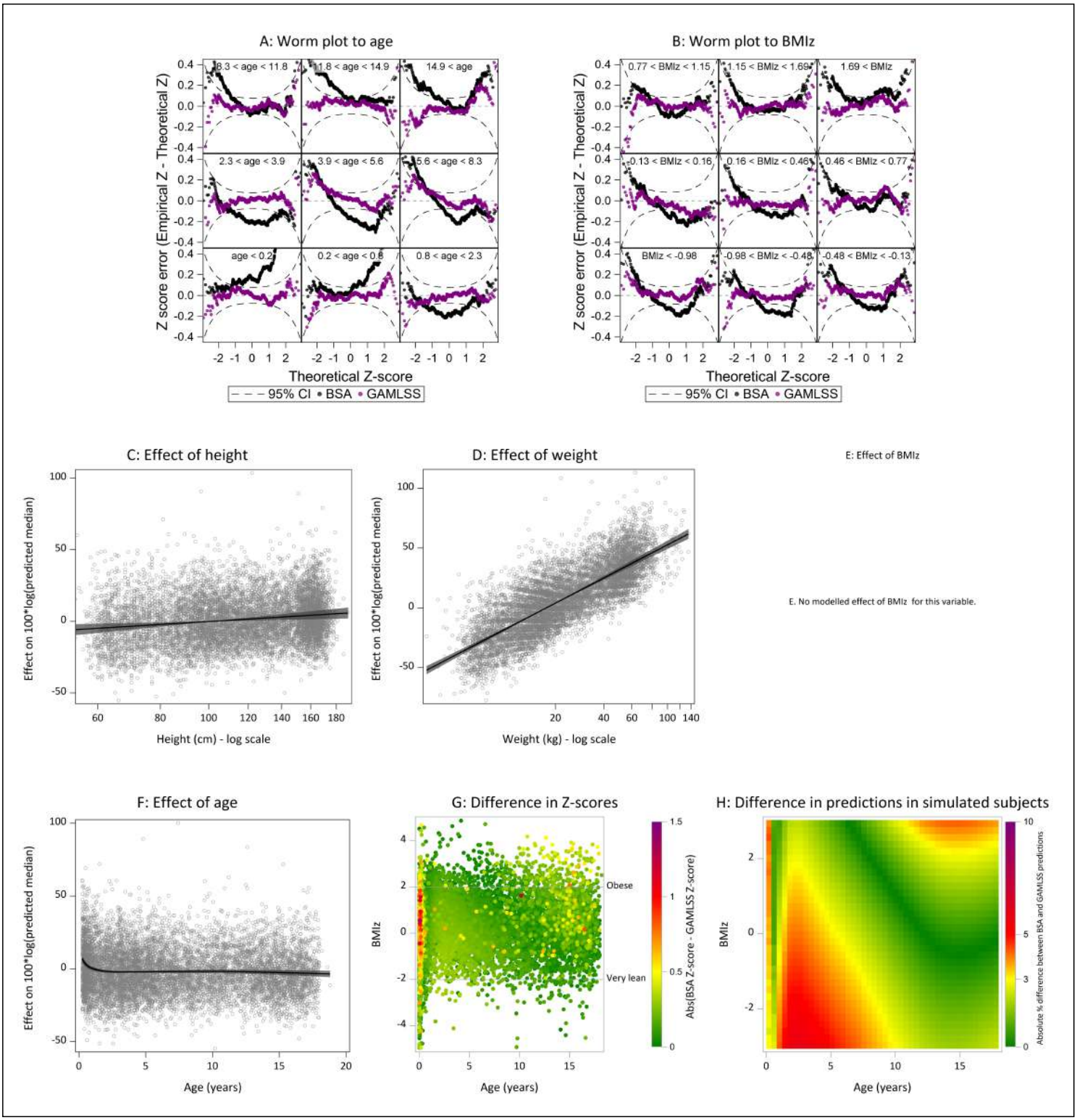
Supplementary figures S3 A-G: Left-ventricular end-systolic diameter in females (LVESDF)

A: Worm plot by age of the Z-scores of the GAMLSS model in comparison to the BSA-allometric model for LVESDF. B: Worm plot by BMIz of the Z-scores of the GAMLSS model in comparison to the BSA-allometric model for LVESDF. C: Effect of height on the log of the predicted median of the LVESDF. D: Effect of weight on the log of the predicted median of LVESDF. E: Effect of BMIz on the log of the predicted median of LVESDF. F: Effect of age on the log of the predicted median of LVESDF. G: Difference between Z-scores of the GAMLSS model and the BSA-allometric model for LVESDF. H: Difference between predicted median of the GAMLSS model and the BSA-allometric model for LVESDF in simulated subjects.



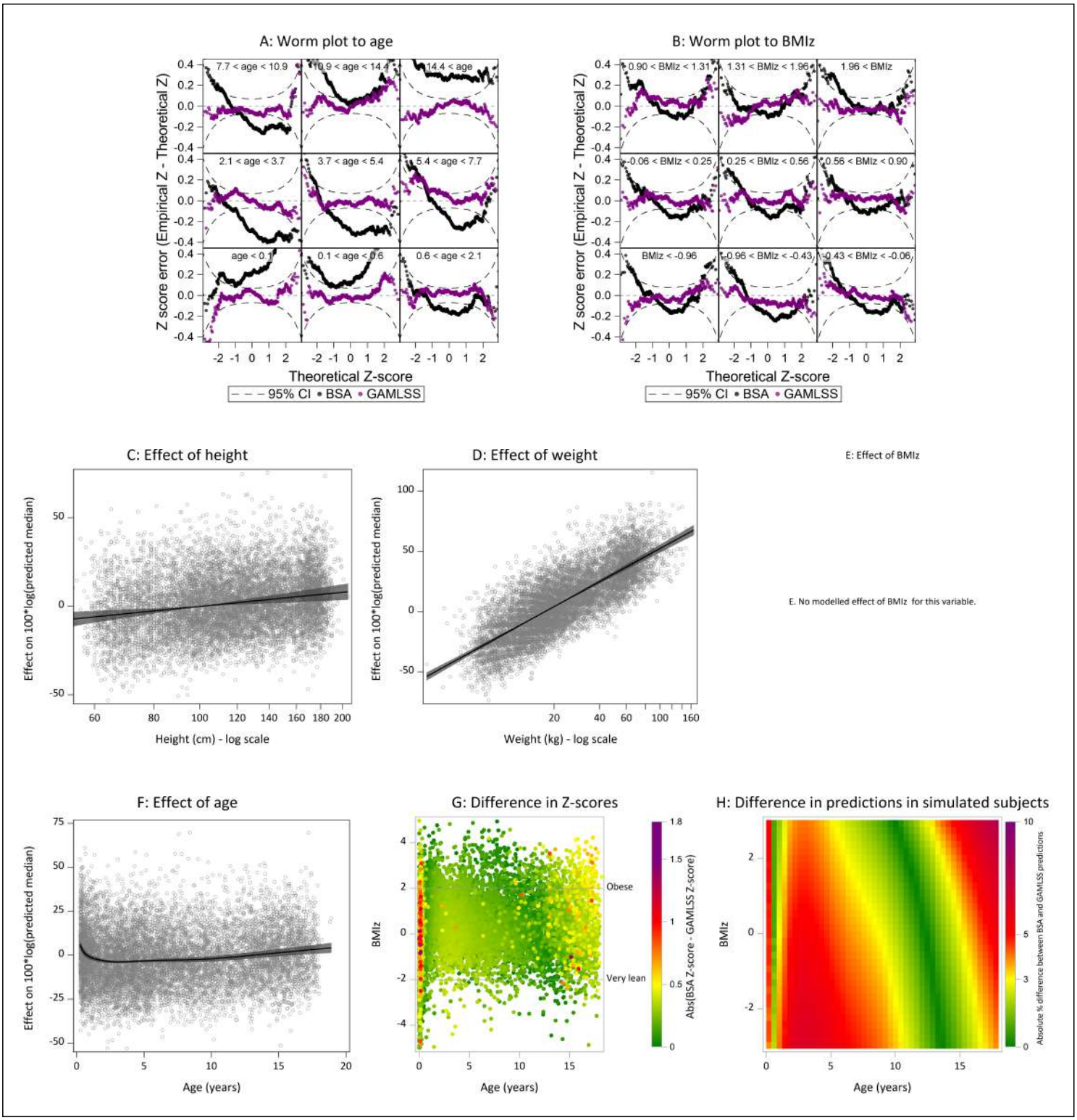
Supplementary figures S4 A-G: Left-ventricular end-systolic diameter in males (LVESDM)

A: Worm plot by age of the Z-scores of the GAMLSS model in comparison to the BSA-allometric model for LVESDM. B: Worm plot by BMIz of the Z-scores of the GAMLSS model in comparison to the BSA-allometric model for LVESDM. C: Effect of height on the log of the predicted median of the LVESDM. D: Effect of weight on the log of the predicted median of LVESDM. E: Effect of BMIz on the log of the predicted median of LVESDM. F: Effect of age on the log of the predicted median of LVESDM. G: Difference between Z-scores of the GAMLSS model and the BSA-allometric model for LVESDM. H: Difference between predicted median of the GAMLSS model and the BSA-allometric model for LVESDM in simulated subjects.



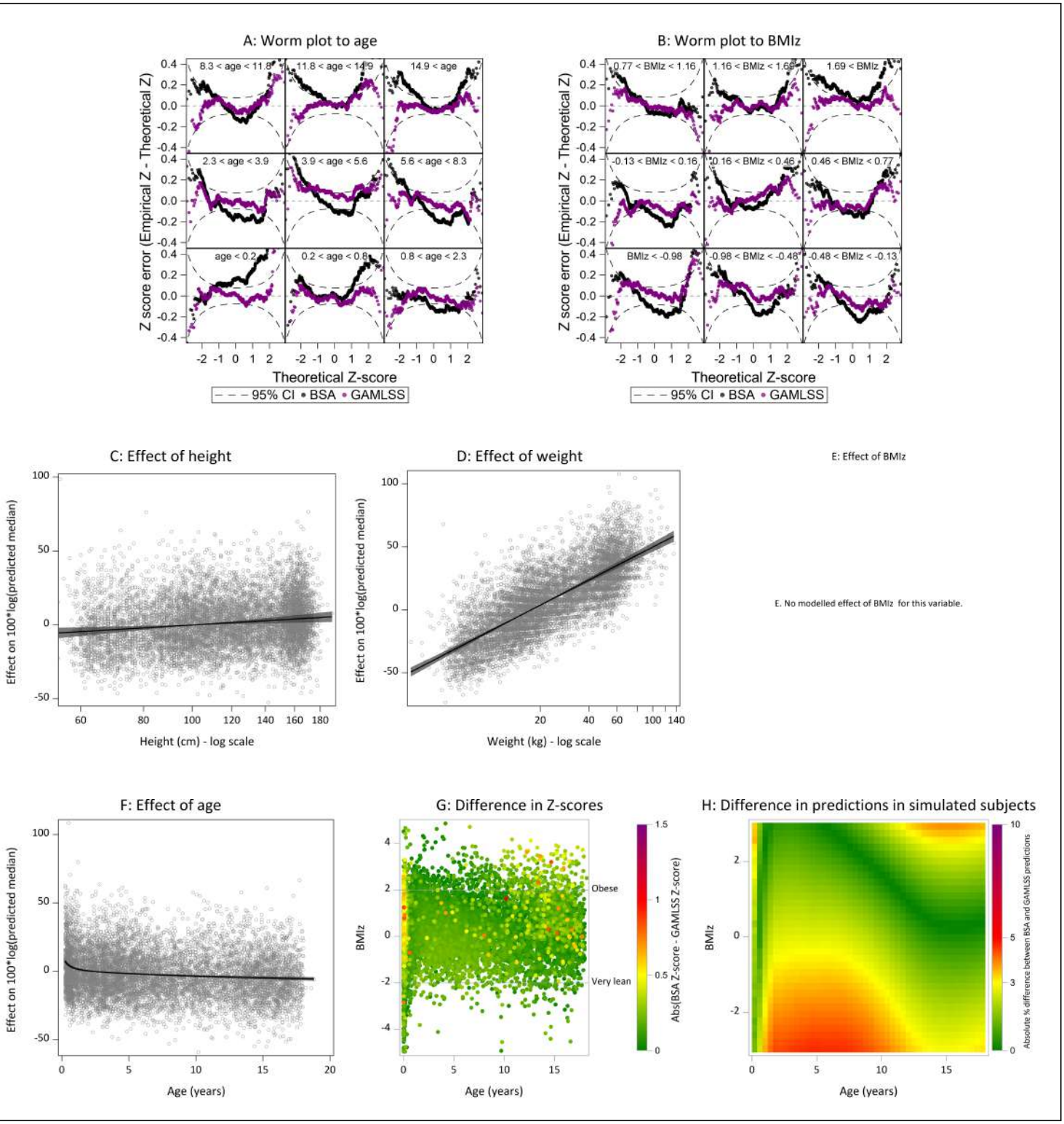
Supplementary figures S5 A-G: Left-ventricular end-diastolic posterior wall thickness in females (LVEDPWTF)

A: Worm plot by age of the Z-scores of the GAMLSS model in comparison to the BSA-allometric model for LVEDPWTF. B: Worm plot by BMIz of the Z-scores of the GAMLSS model in comparison to the BSA-allometric model for LVEDPWTF. C: Effect of height on the log of the predicted median of the LVEDPWTF. D: Effect of weight on the log of the predicted median of LVEDPWTF. E: Effect of BMIz on the log of the predicted median of LVEDPWTF. F: Effect of age on the log of the predicted median of LVEDPWTF. G: Difference between Z-scores of the GAMLSS model and the BSA-allometric model for LVEDPWTF. H: Difference between predicted median of the GAMLSS model and the BSA-allometric model for LVEDPWTF in simulated subjects.



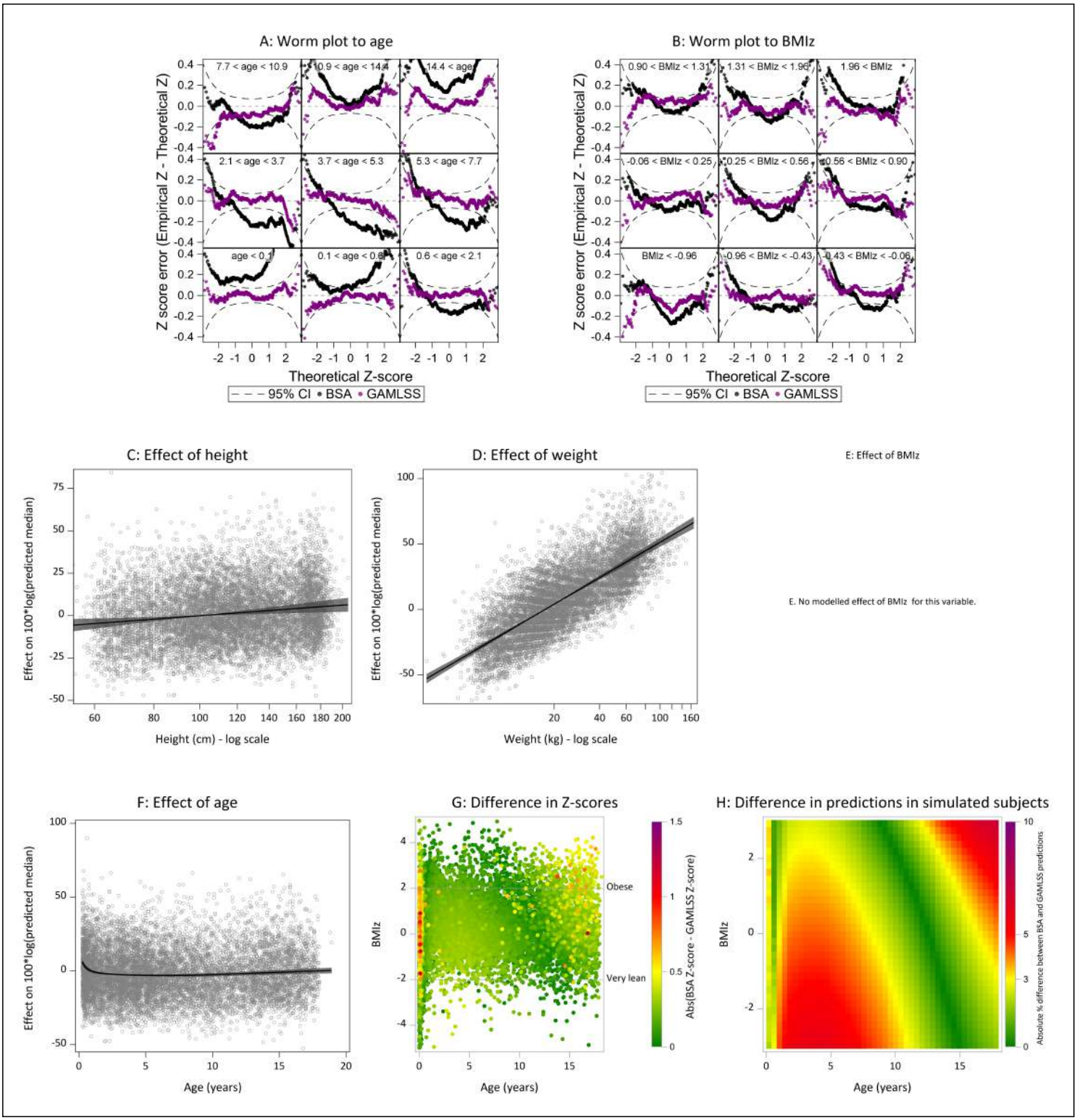
Supplementary figures S6 A-G: Left-ventricular end-diastolic posterior wall thickness in males (LVEDPWTM)

A: Worm plot by age of the Z-scores of the GAMLSS model in comparison to the BSA-allometric model for LVEDPWTM. B: Worm plot by BMIz of the Z-scores of the GAMLSS model in comparison to the BSA-allometric model for LVEDPWTM. C: Effect of height on the log of the predicted median of the LVEDPWTM. D: Effect of weight on the log of the predicted median of LVEDPWTM. E: Effect of BMIz on the log of the predicted median of LVEDPWTM. F: Effect of age on the log of the predicted median of LVEDPWTM. G: Difference between Z-scores of the GAMLSS model and the BSA-allometric model for LVEDPWTM. H: Difference between predicted median of the GAMLSS model and the BSA-allometric model for LVEDPWTM in simulated subjects.



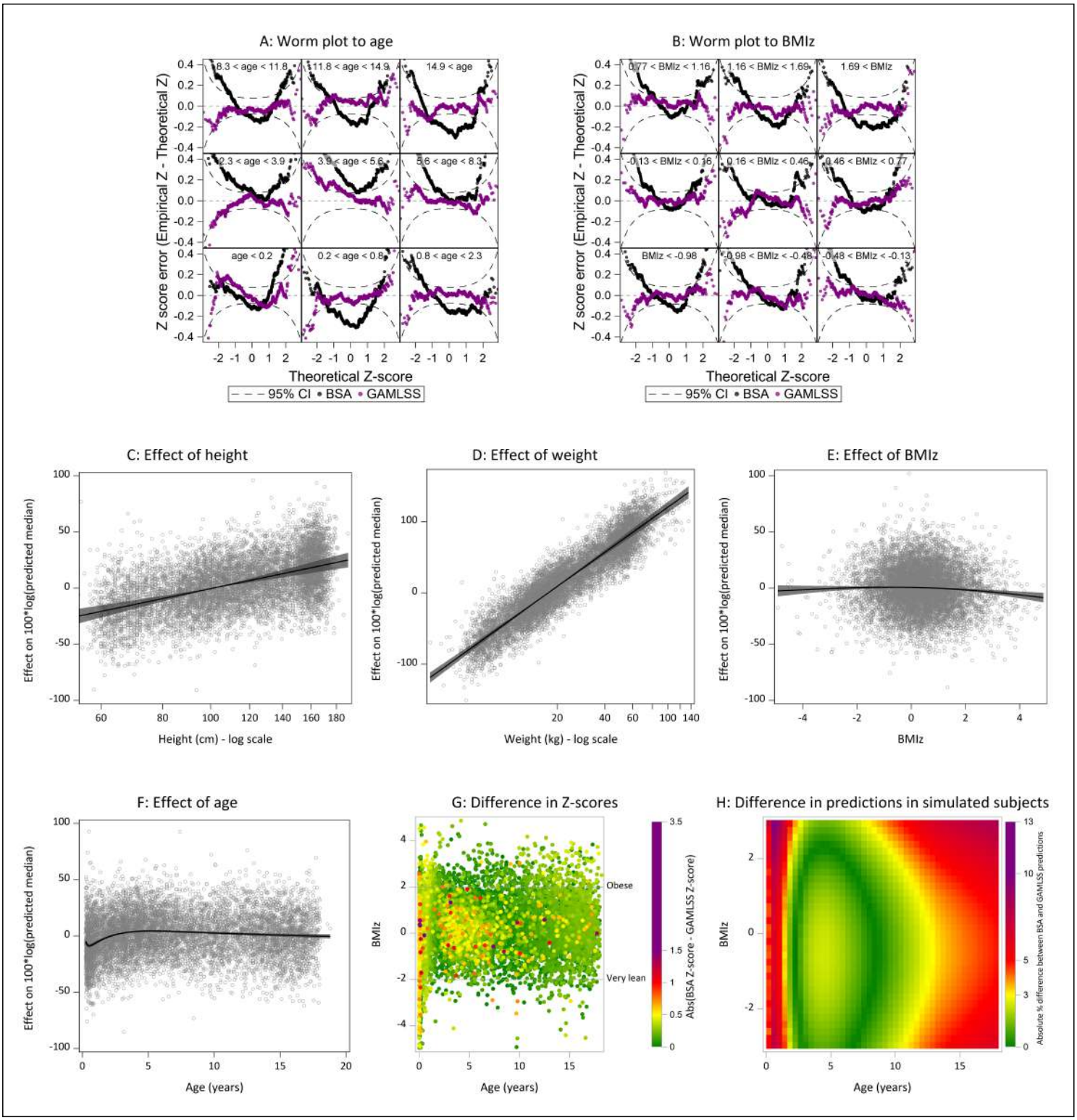
Supplementary figures S7 A-G: Left-ventricular end-diastolic septal wall thickness in females (LVEDSWTF)

A: Worm plot by age of the Z-scores of the GAMLSS model in comparison to the BSA-allometric model for LVEDSWTF. B: Worm plot by BMIz of the Z-scores of the GAMLSS model in comparison to the BSA-allometric model for LVEDSWTF. C: Effect of height on the log of the predicted median of the LVEDSWTF. D: Effect of weight on the log of the predicted median of LVEDSWTF. E: Effect of BMIz on the log of the predicted median of LVEDSWTF. F: Effect of age on the log of the predicted median of LVEDSWTF. G: Difference between Z-scores of the GAMLSS model and the BSA-allometric model for LVEDSWTF. H: Difference between predicted median of the GAMLSS model and the BSA-allometric model for LVEDSWTF in simulated subjects.



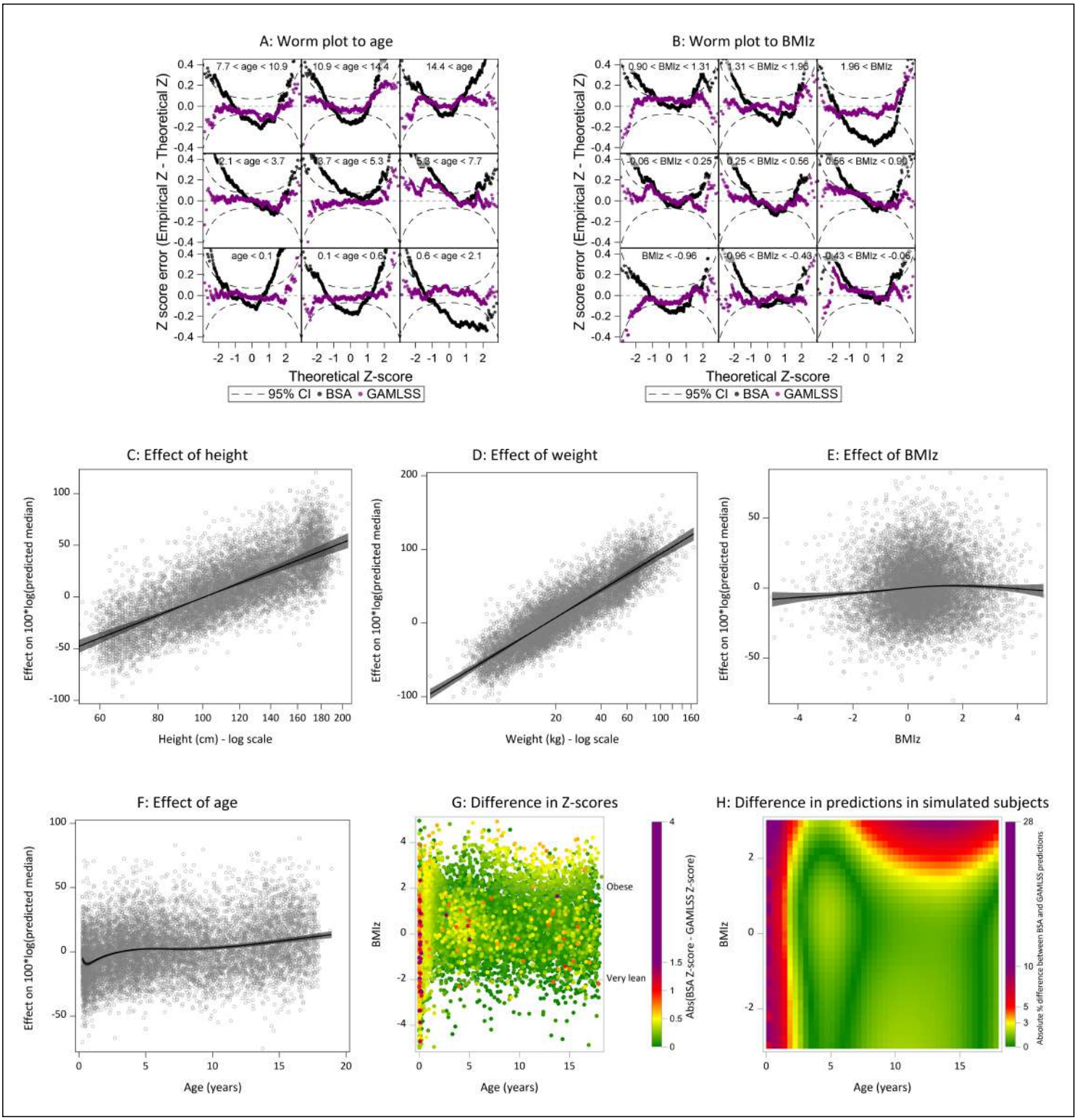
Supplementary figures S8 A-G: Left-ventricular end-diastolic septal wall thickness in males (LVEDSWTM)

A: Worm plot by age of the Z-scores of the GAMLSS model in comparison to the BSA-allometric model for LVEDSWTM. B: Worm plot by BMIz of the Z-scores of the GAMLSS model in comparison to the BSA-allometric model for LVEDSWTM. C: Effect of height on the log of the predicted median of the LVEDSWTM. D: Effect of weight on the log of the predicted median of LVEDSWTM. E: Effect of BMIz on the log of the predicted median of LVEDSWTM. F: Effect of age on the log of the predicted median of LVEDSWTM. G: Difference between Z-scores of the GAMLSS model and the BSA-allometric model for LVEDSWTM. H: Difference between predicted median of the GAMLSS model and the BSA-allometric model for LVEDSWTM in simulated subjects.



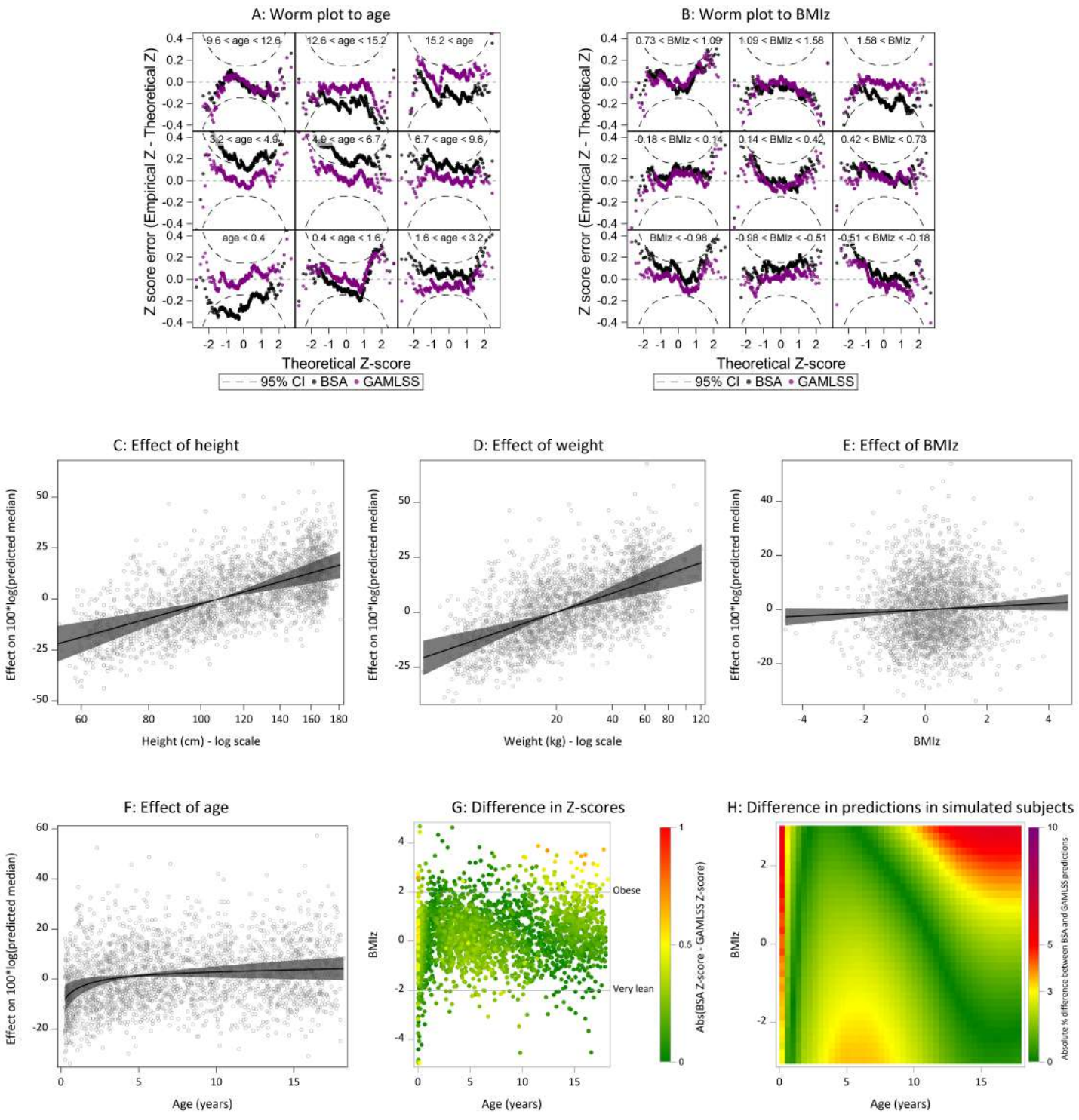
Supplementary figures S9 A-G: Left-ventricular mass in females (LVMF)

A: Worm plot by age of the Z-scores of the GAMLSS model in comparison to the BSA-allometric model for LVMF. B: Worm plot by BMIz of the Z-scores of the GAMLSS model in comparison to the BSA-allometric model for LVMF. C: Effect of height on the log of the predicted median of the LVMF. D: Effect of weight on the log of the predicted median of LVMF. E: Effect of BMIz on the log of the predicted median of LVMF. F: Effect of age on the log of the predicted median of LVMF. G: Difference between Z-scores of the GAMLSS model and the BSA-allometric model for LVMF. H: Difference between predicted median of the GAMLSS model and the BSA-allometric model for LVMF in simulated subjects.



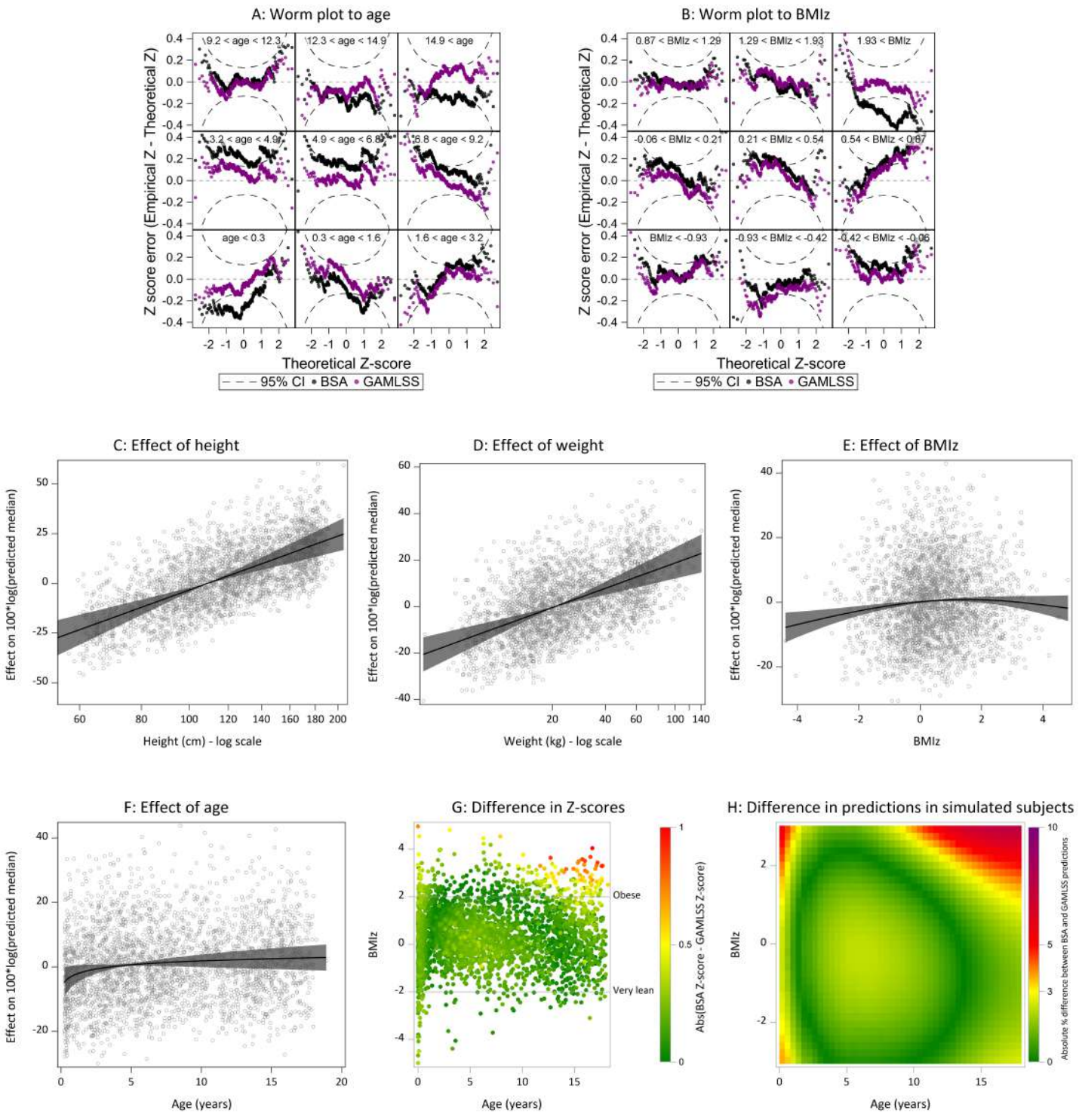
Supplementary figures S10 A-G: Left-ventricular mass in males (LVMM)

A: Worm plot by age of the Z-scores of the GAMLSS model in comparison to the BSA-allometric model for LVMM. B: Worm plot by BMIz of the Z-scores of the GAMLSS model in comparison to the BSA-allometric model for LVMM. C: Effect of height on the log of the predicted median of the LVMM. D: Effect of weight on the log of the predicted median of LVMM. E: Effect of BMIz on the log of the predicted median of LVMM. F: Effect of age on the log of the predicted median of LVMM. G: Difference between Z-scores of the GAMLSS model and the BSA-allometric model for LVMM. H: Difference between predicted median of the GAMLSS model and the BSA-allometric model for LVMM in simulated subjects.



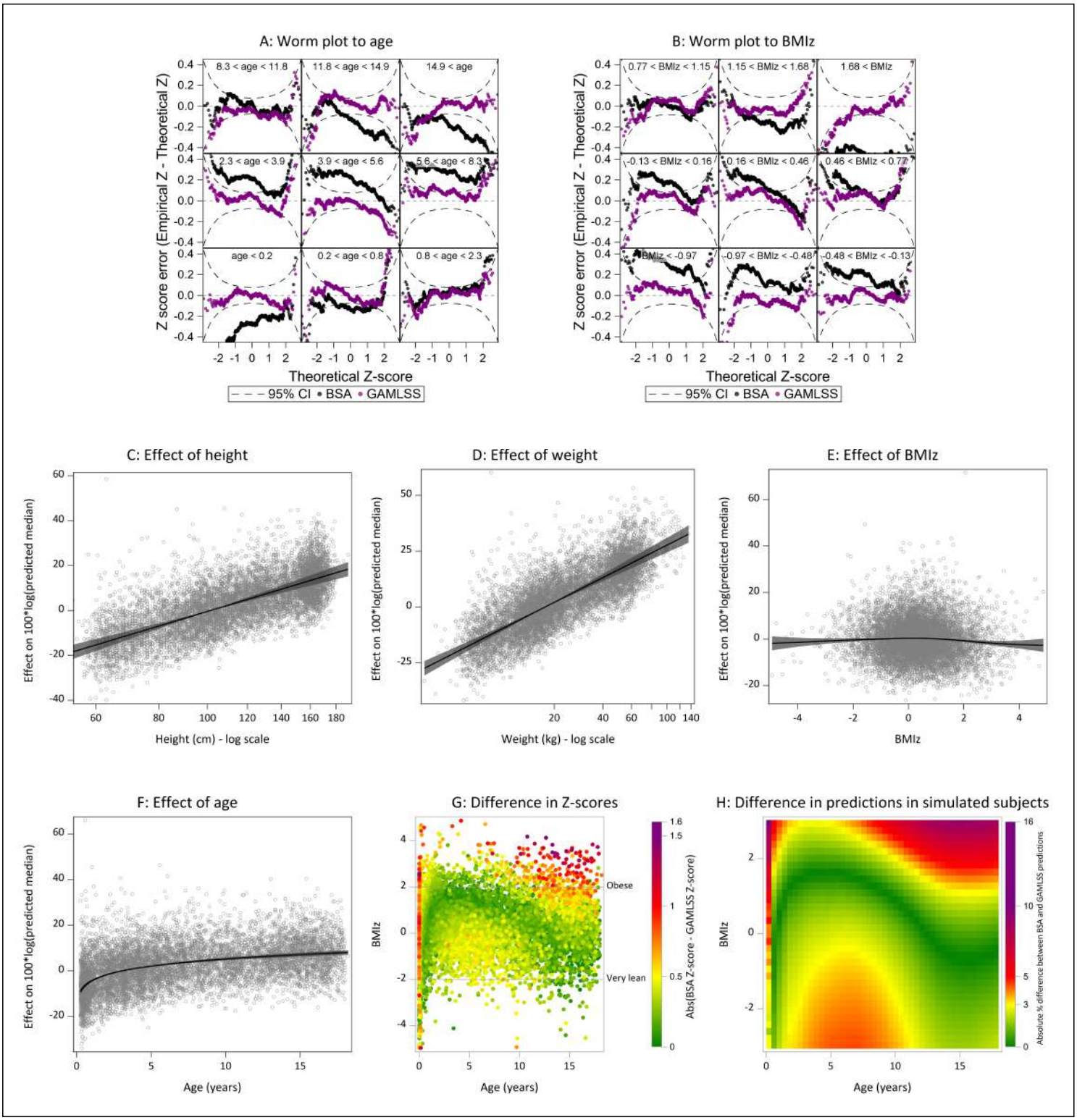
Supplementary figures S11 A-G: Mitral valve diameter in females (MVF)

A: Worm plot by age of the Z-scores of the GAMLSS model in comparison to the BSA-allometric model for MVF. B: Worm plot by BMIz of the Z-scores of the GAMLSS model in comparison to the BSA-allometric model for MVF. C: Effect of height on the log of the predicted median of the MVF. D: Effect of weight on the log of the predicted median of MVF. E: Effect of BMIz on the log of the predicted median of MVF. F: Effect of age on the log of the predicted median of MVF. G: Difference between Z-scores of the GAMLSS model and the BSA-allometric model for MVF. H: Difference between predicted median of the GAMLSS model and the BSA-allometric model for MVF in simulated subjects.



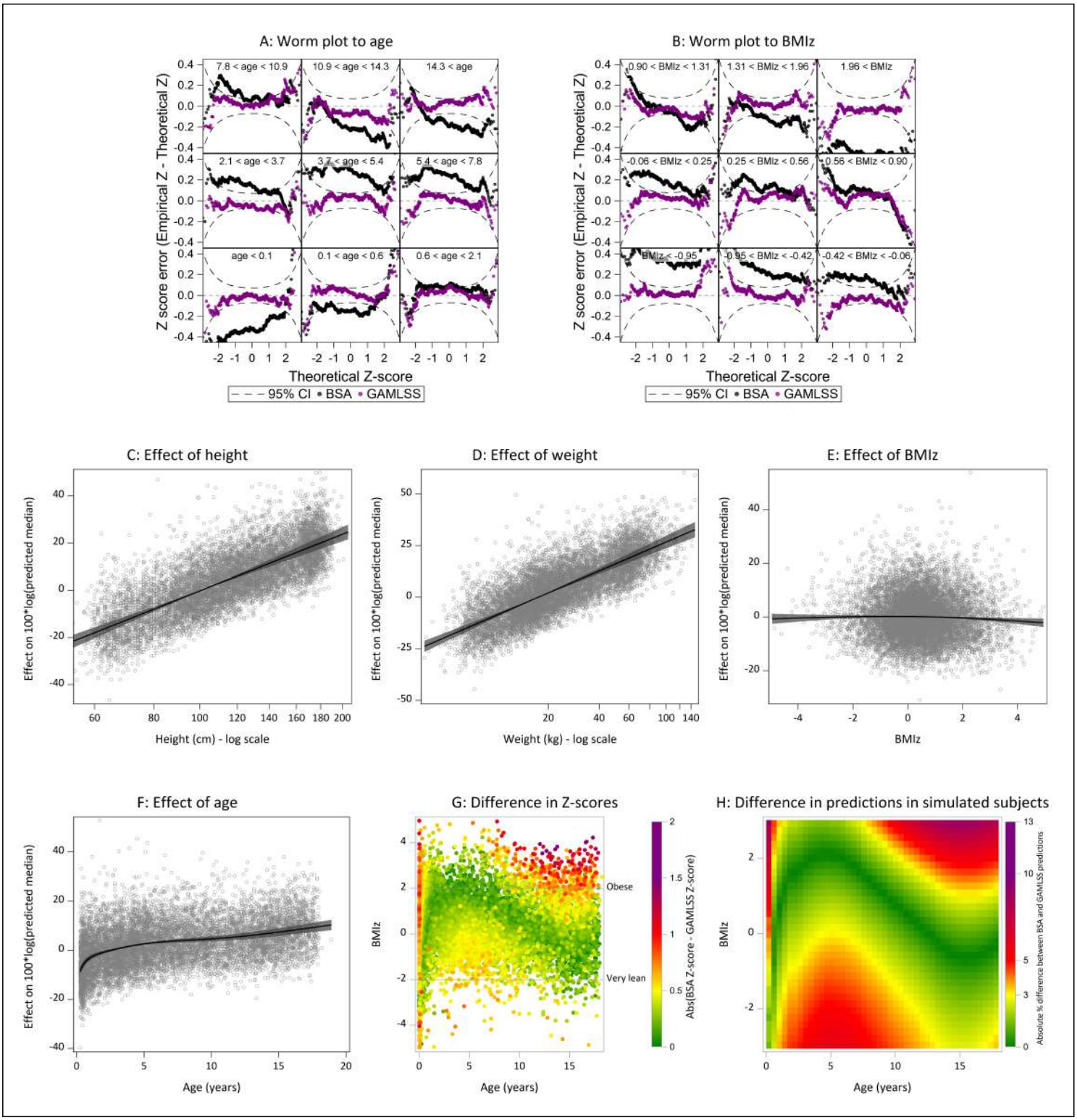
Supplementary figures S12 A-G: Mitral valve diameter in males (MVM)

A: Worm plot by age of the Z-scores of the GAMLSS model in comparison to the BSA-allometric model for MVM. B: Worm plot by BMIz of the Z-scores of the GAMLSS model in comparison to the BSA-allometric model for MVM. C: Effect of height on the log of the predicted median of the MVM. D: Effect of weight on the log of the predicted median of MVM. E: Effect of BMIz on the log of the predicted median of MVM. F: Effect of age on the log of the predicted median of MVM. G: Difference between Z-scores of the GAMLSS model and the BSA-allometric model for MVM. H: Difference between predicted median of the GAMLSS model and the BSA-allometric model for MVM in simulated subjects.



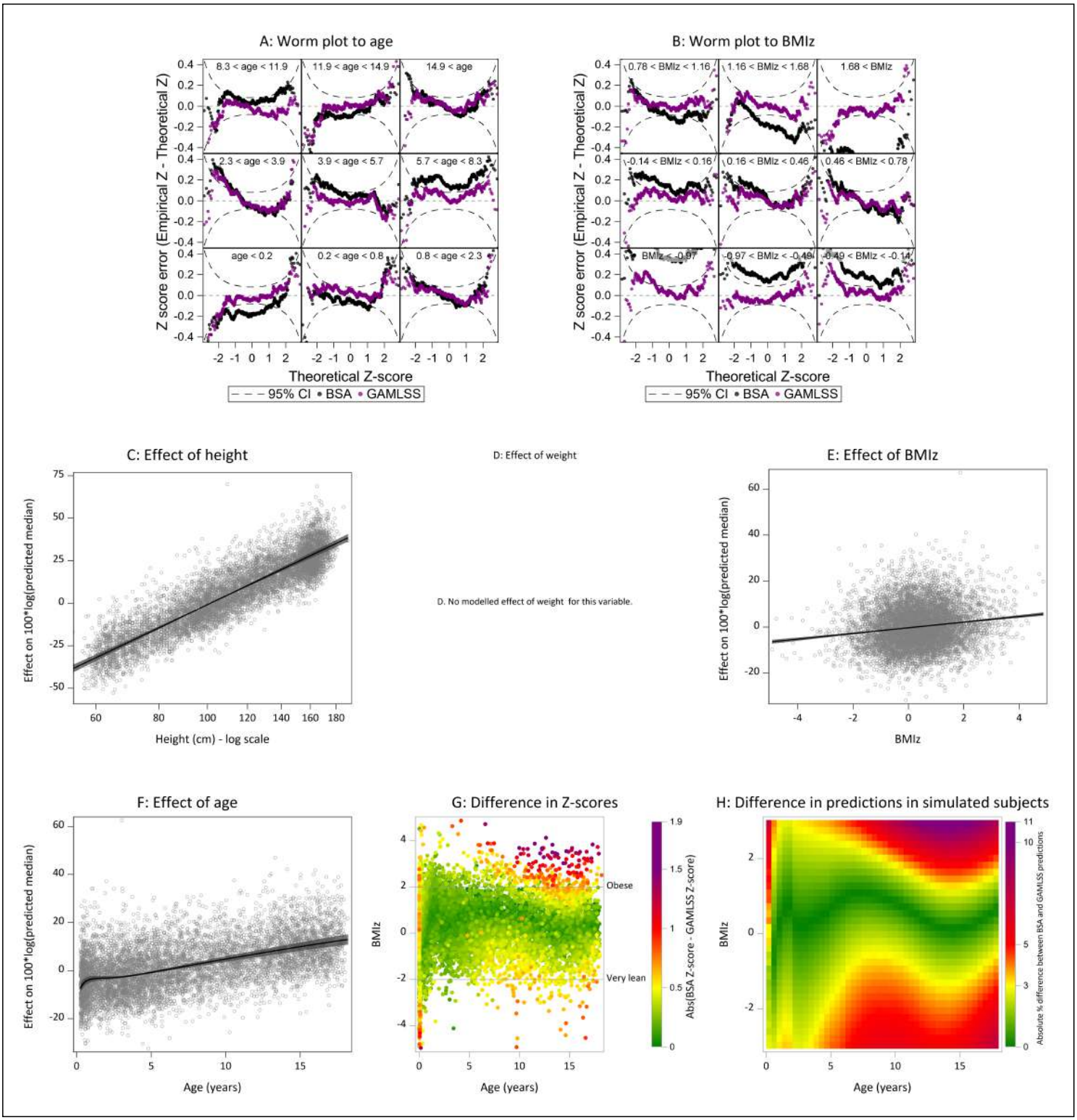
Supplementary figures S13 A-G: Aortic valve diameter in females (AOVF)

A: Worm plot by age of the Z-scores of the GAMLSS model in comparison to the BSA-allometric model for AOVF. B: Worm plot by BMIz of the Z-scores of the GAMLSS model in comparison to the BSA-allometric model for AOVF. C: Effect of height on the log of the predicted median of the AOVF. D: Effect of weight on the log of the predicted median of AOVF. E: Effect of BMIz on the log of the predicted median of AOVF. F: Effect of age on the log of the predicted median of AOVF. G: Difference between Z-scores of the GAMLSS model and the BSA-allometric model for AOVF. H: Difference between predicted median of the GAMLSS model and the BSA-allometric model for AOVF in simulated subjects.



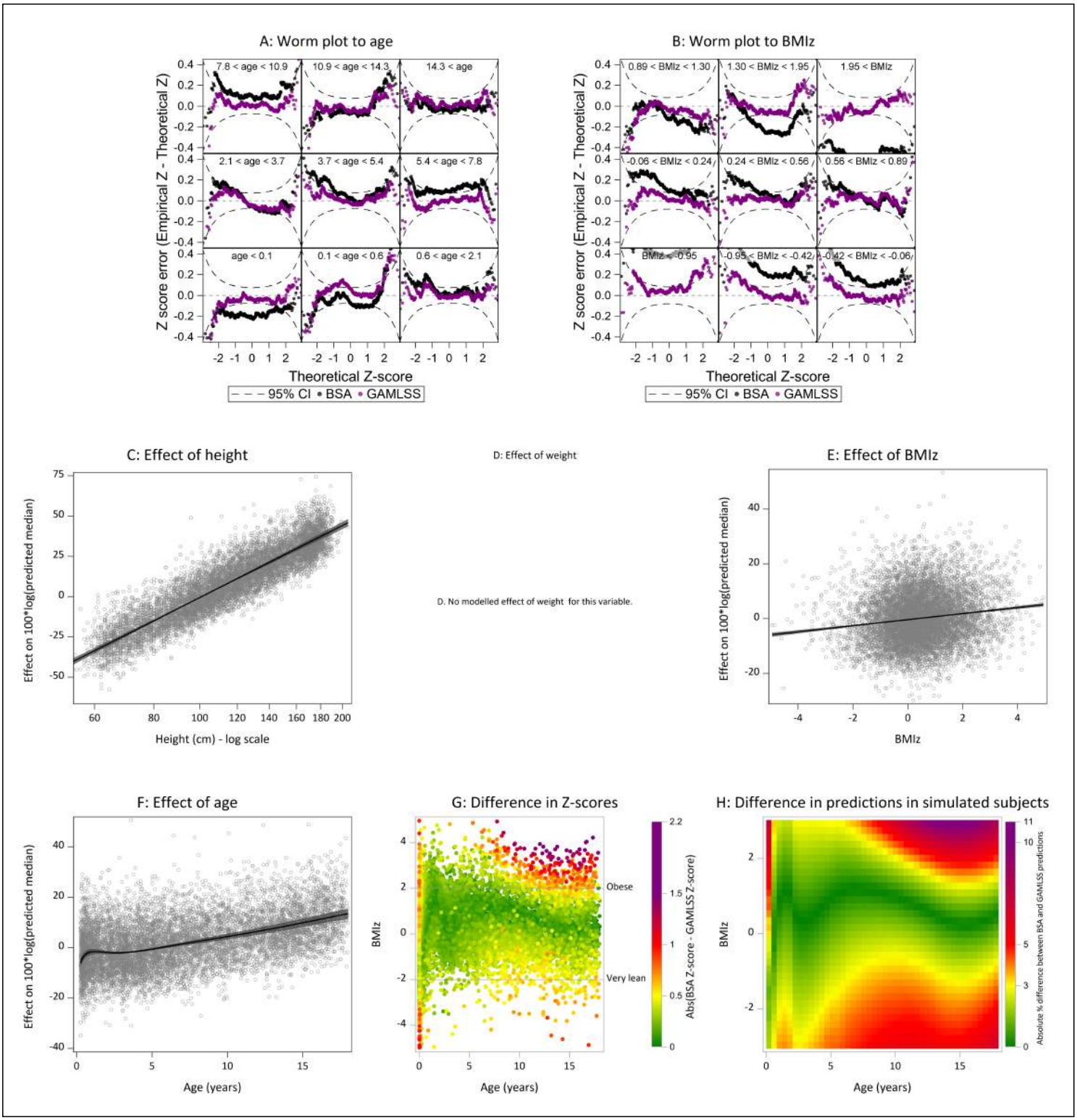
Supplementary figures S14 A-G: Aortic valve diameter in males (AOVM)

A: Worm plot by age of the Z-scores of the GAMLSS model in comparison to the BSA-allometric model for AOVM. B: Worm plot by BMIz of the Z-scores of the GAMLSS model in comparison to the BSA-allometric model for AOVM. C: Effect of height on the log of the predicted median of the AOVM. D: Effect of weight on the log of the predicted median of AOVM. E: Effect of BMIz on the log of the predicted median of AOVM. F: Effect of age on the log of the predicted median of AOVM. G: Difference between Z-scores of the GAMLSS model and the BSA-allometric model for AOVM. H: Difference between predicted median of the GAMLSS model and the BSA-allometric model for AOVM in simulated subjects.



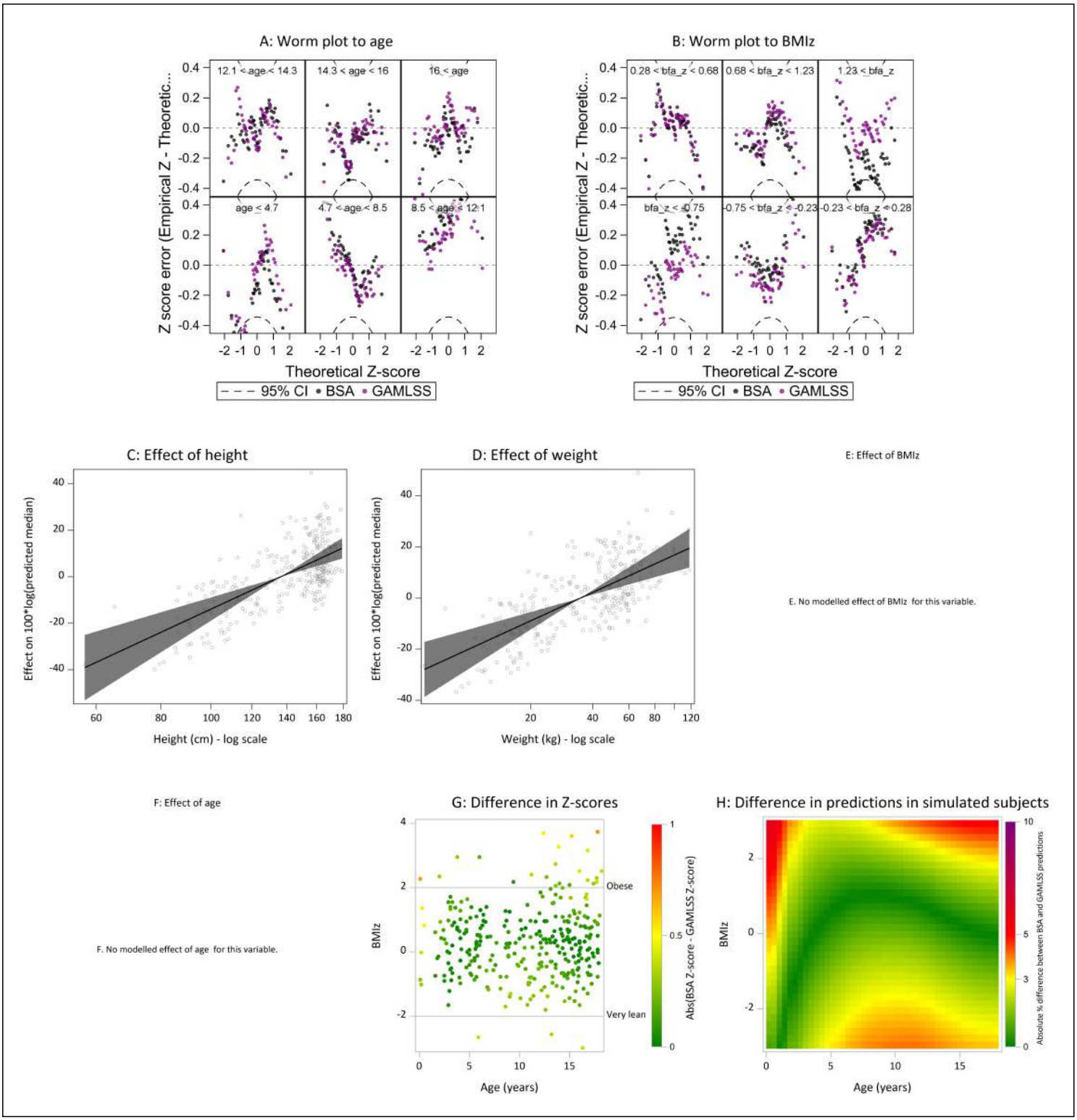
Supplementary figures S15 A-G: Sinus of Valsalva diameter in females (SOVF)

A: Worm plot by age of the Z-scores of the GAMLSS model in comparison to the BSA-allometric model for SOVF. B: Worm plot by BMIz of the Z-scores of the GAMLSS model in comparison to the BSA-allometric model for SOVF. C: Effect of height on the log of the predicted median of the SOVF. D: Effect of weight on the log of the predicted median of SOVF. E: Effect of BMIz on the log of the predicted median of SOVF. F: Effect of age on the log of the predicted median of SOVF. G: Difference between Z-scores of the GAMLSS model and the BSA-allometric model for SOVF. H: Difference between predicted median of the GAMLSS model and the BSA-allometric model for SOVF in simulated subjects.



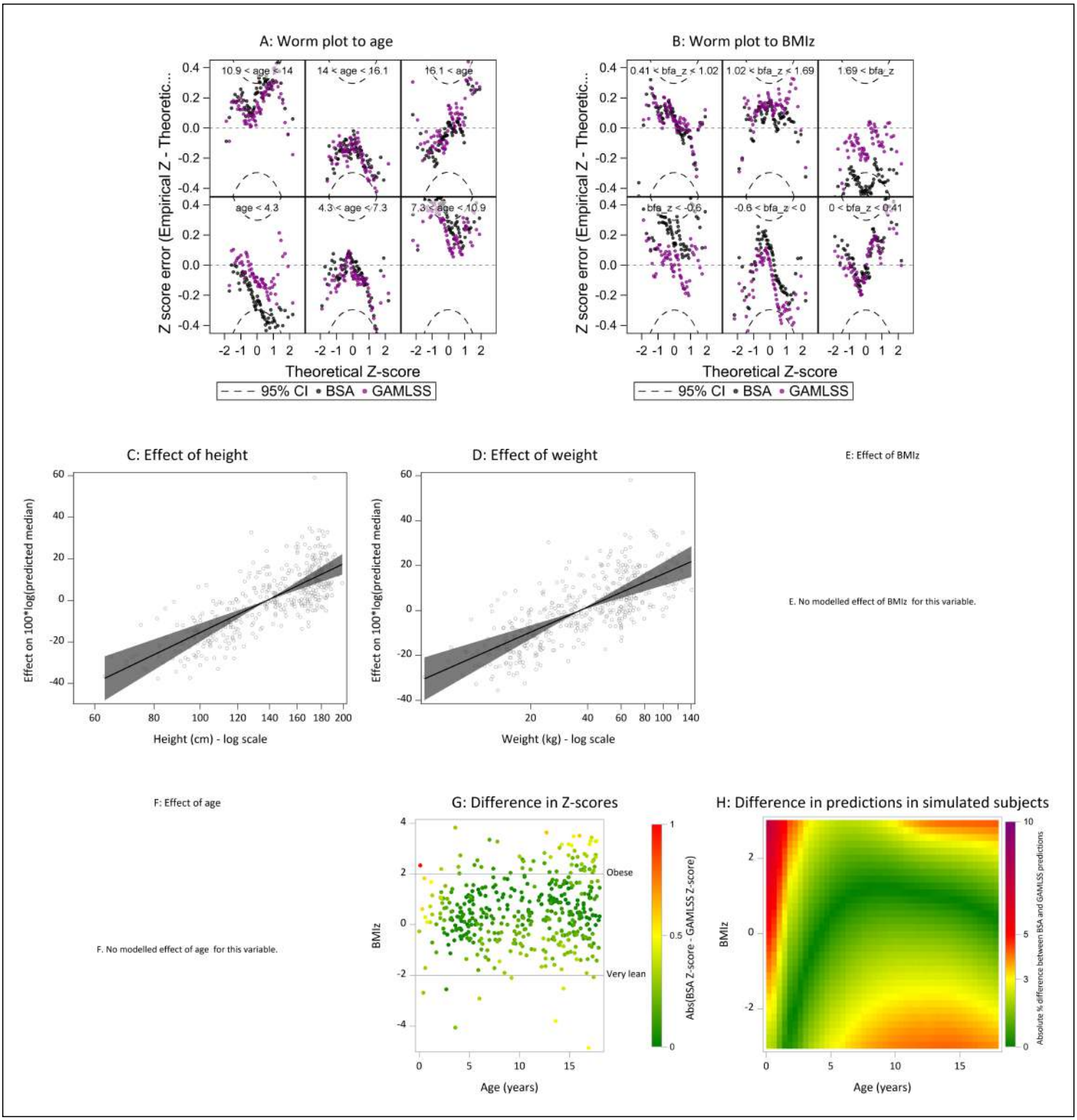
Supplementary figures S16 A-G: Sinus of Valsalva diameter in males (SOVM)

A: Worm plot by age of the Z-scores of the GAMLSS model in comparison to the BSA-allometric model for SOVM. B: Worm plot by BMIz of the Z-scores of the GAMLSS model in comparison to the BSA-allometric model for SOVM. C: Effect of height on the log of the predicted median of the SOVM. D: Effect of weight on the log of the predicted median of SOVM. E: Effect of BMIz on the log of the predicted median of SOVM. F: Effect of age on the log of the predicted median of SOVM. G: Difference between Z-scores of the GAMLSS model and the BSA-allometric model for SOVM. H: Difference between predicted median of the GAMLSS model and the BSA-allometric model for SOVM in simulated subjects.



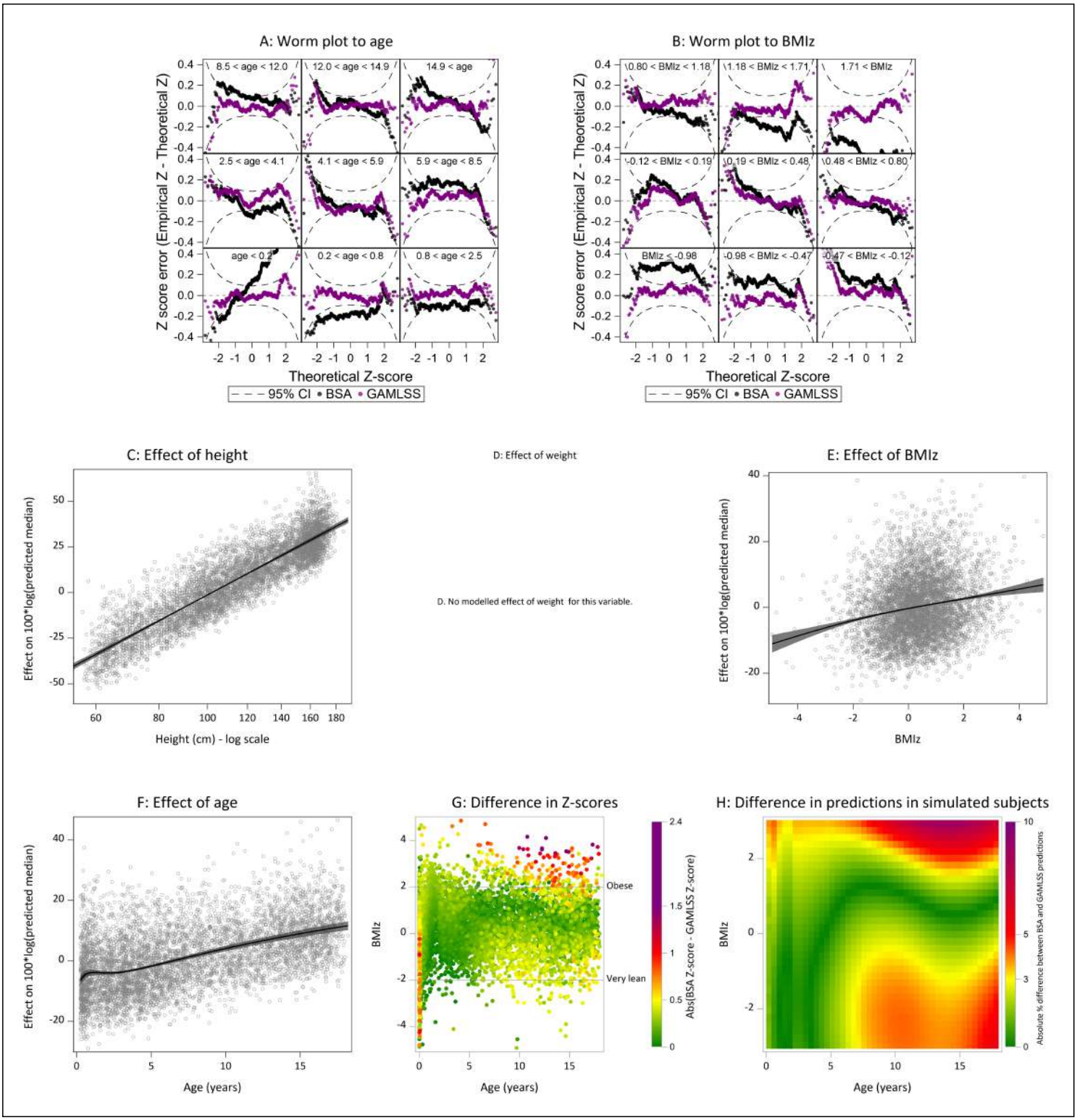
Supplementary figures S17 A-G: Aortic sinotubular junction diameter in females (STJF)

A: Worm plot by age of the Z-scores of the GAMLSS model in comparison to the BSA-allometric model for STJF. B: Worm plot by BMIz of the Z-scores of the GAMLSS model in comparison to the BSA-allometric model for STJF. C: Effect of height on the log of the predicted median of the STJF. D: Effect of weight on the log of the predicted median of STJF. E: Effect of BMIz on the log of the predicted median of STJF. F: Effect of age on the log of the predicted median of STJF. G: Difference between Z-scores of the GAMLSS model and the BSA-allometric model for STJF. H: Difference between predicted median of the GAMLSS model and the BSA-allometric model for STJF in simulated subjects.



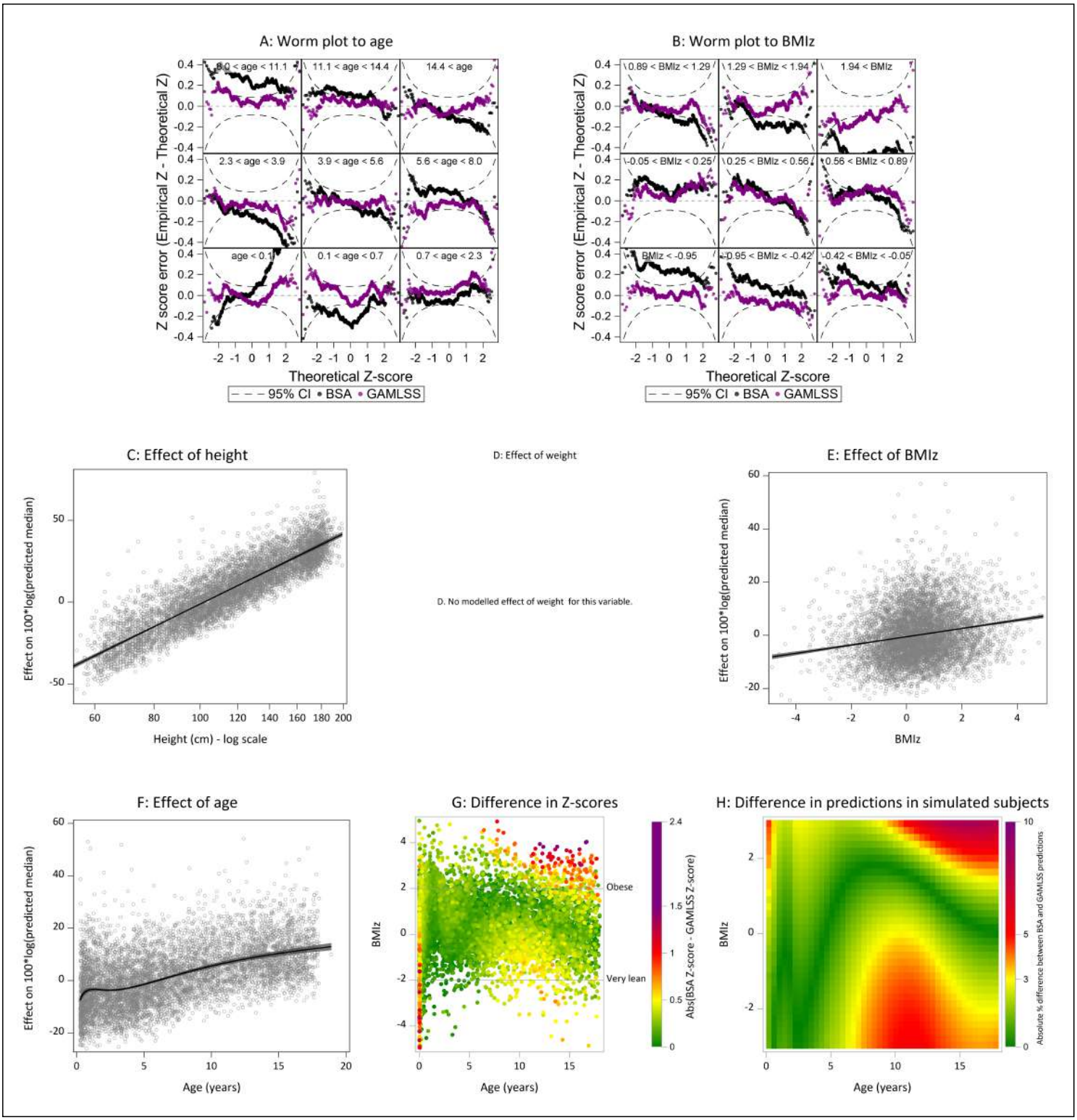
Supplementary figures S18 A-G: Aortic sinotubular junction diameter in males (STJM)

A: Worm plot by age of the Z-scores of the GAMLSS model in comparison to the BSA-allometric model for STJM. B: Worm plot by BMIz of the Z-scores of the GAMLSS model in comparison to the BSA-allometric model for STJM. C: Effect of height on the log of the predicted median of the STJM. D: Effect of weight on the log of the predicted median of STJM. E: Effect of BMIz on the log of the predicted median of STJM. F: Effect of age on the log of the predicted median of STJM. G: Difference between Z-scores of the GAMLSS model and the BSA-allometric model for STJM. H: Difference between predicted median of the GAMLSS model and the BSA-allometric model for STJM in simulated subjects.



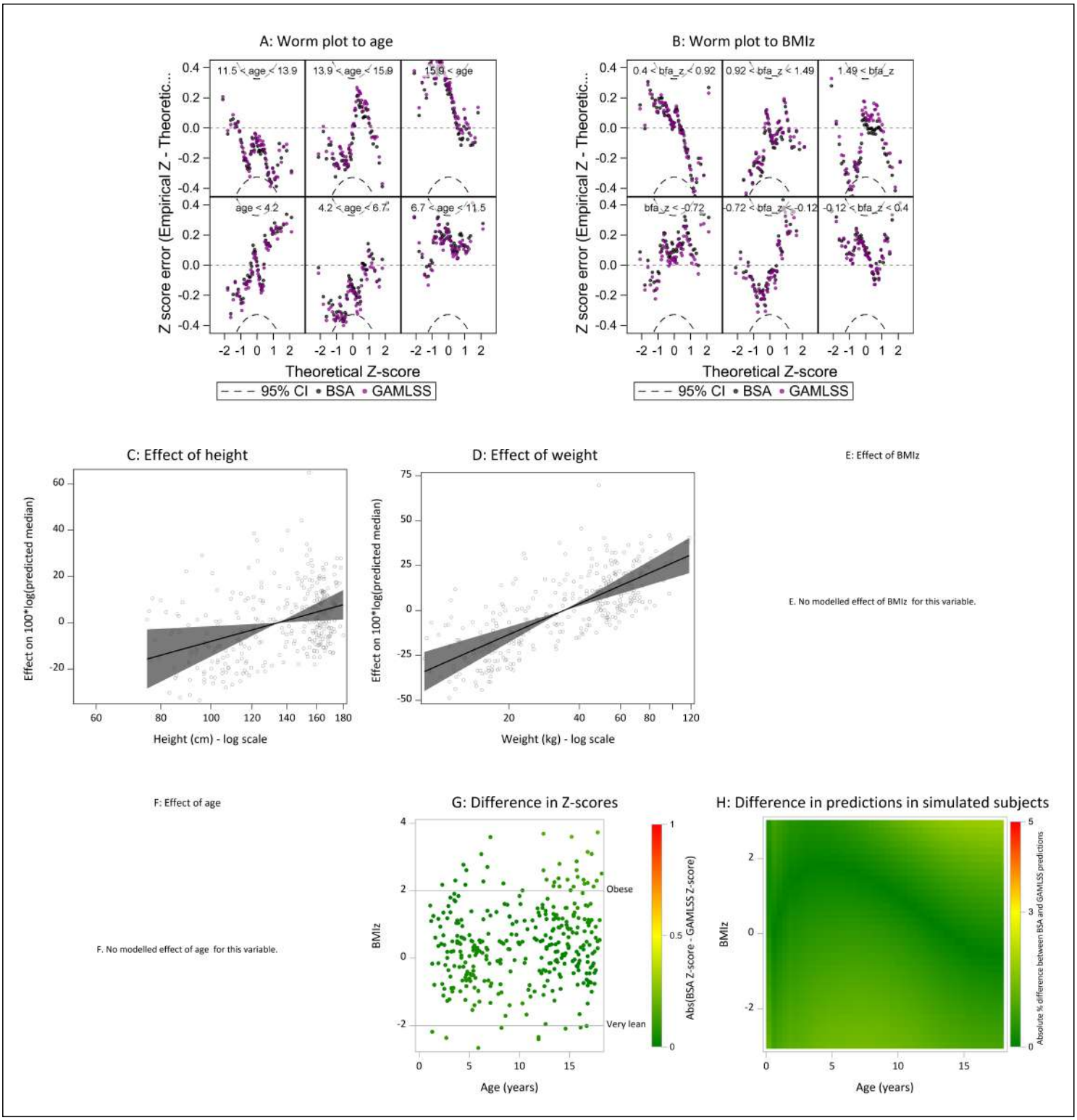
Supplementary figures S19 A-G: Ascending aorta diameter in females (AAOF)

A: Worm plot by age of the Z-scores of the GAMLSS model in comparison to the BSA-allometric model for AAOF. B: Worm plot by BMIz of the Z-scores of the GAMLSS model in comparison to the BSA-allometric model for AAOF. C: Effect of height on the log of the predicted median of the AAOF. D: Effect of weight on the log of the predicted median of AAOF. E: Effect of BMIz on the log of the predicted median of AAOF. F: Effect of age on the log of the predicted median of AAOF. G: Difference between Z-scores of the GAMLSS model and the BSA-allometric model for AAOF. H: Difference between predicted median of the GAMLSS model and the BSA-allometric model for AAOF in simulated subjects.



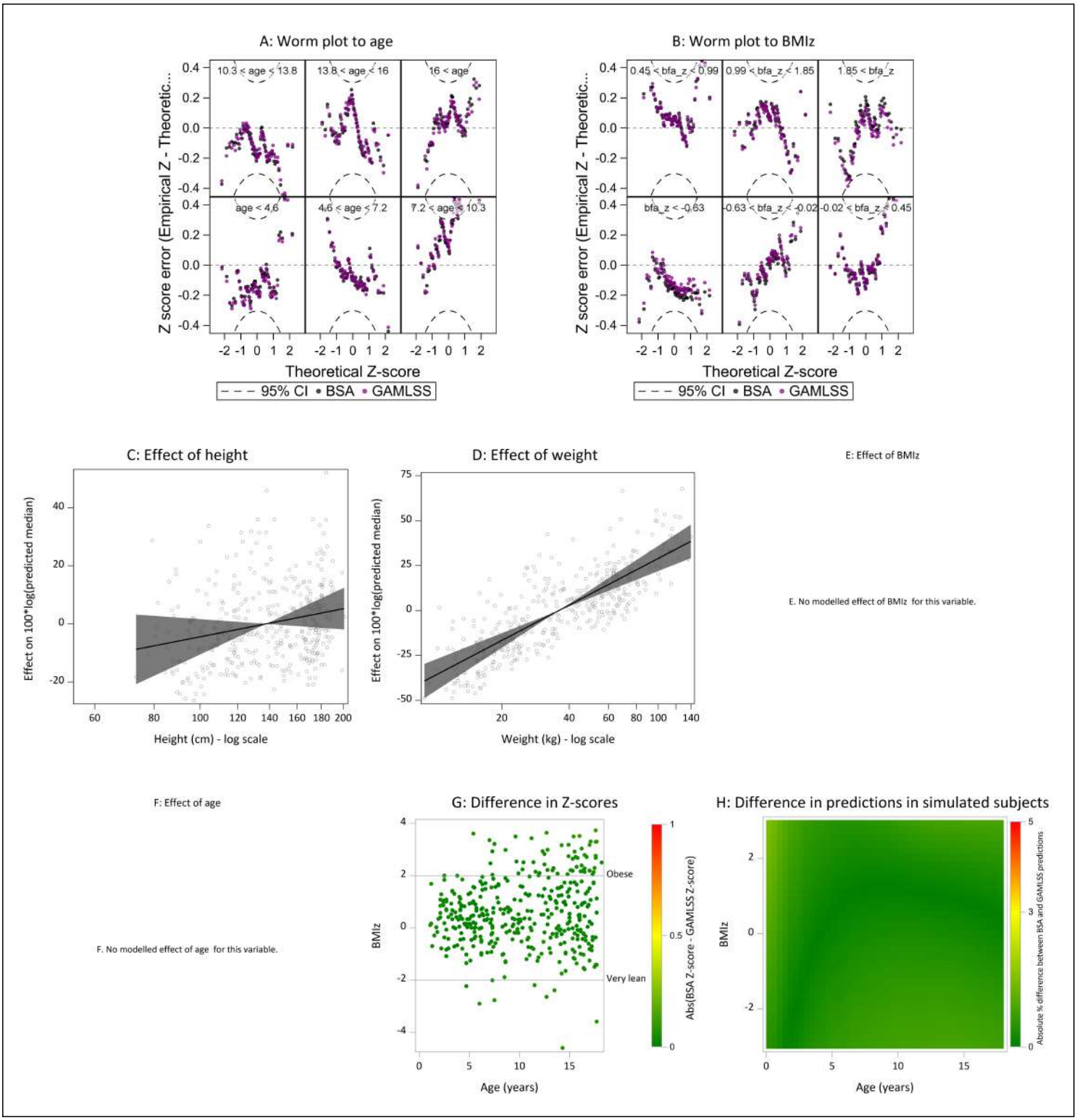
Supplementary figures S20 A-G: Ascending aorta diameter in males (AAOM)

A: Worm plot by age of the Z-scores of the GAMLSS model in comparison to the BSA-allometric model for AAOM. B: Worm plot by BMIz of the Z-scores of the GAMLSS model in comparison to the BSA-allometric model for AAOM. C: Effect of height on the log of the predicted median of the AAOM. D: Effect of weight on the log of the predicted median of AAOM. E: Effect of BMIz on the log of the predicted median of AAOM. F: Effect of age on the log of the predicted median of AAOM. G: Difference between Z-scores of the GAMLSS model and the BSA-allometric model for AAOM. H: Difference between predicted median of the GAMLSS model and the BSA-allometric model for AAOM in simulated subjects.



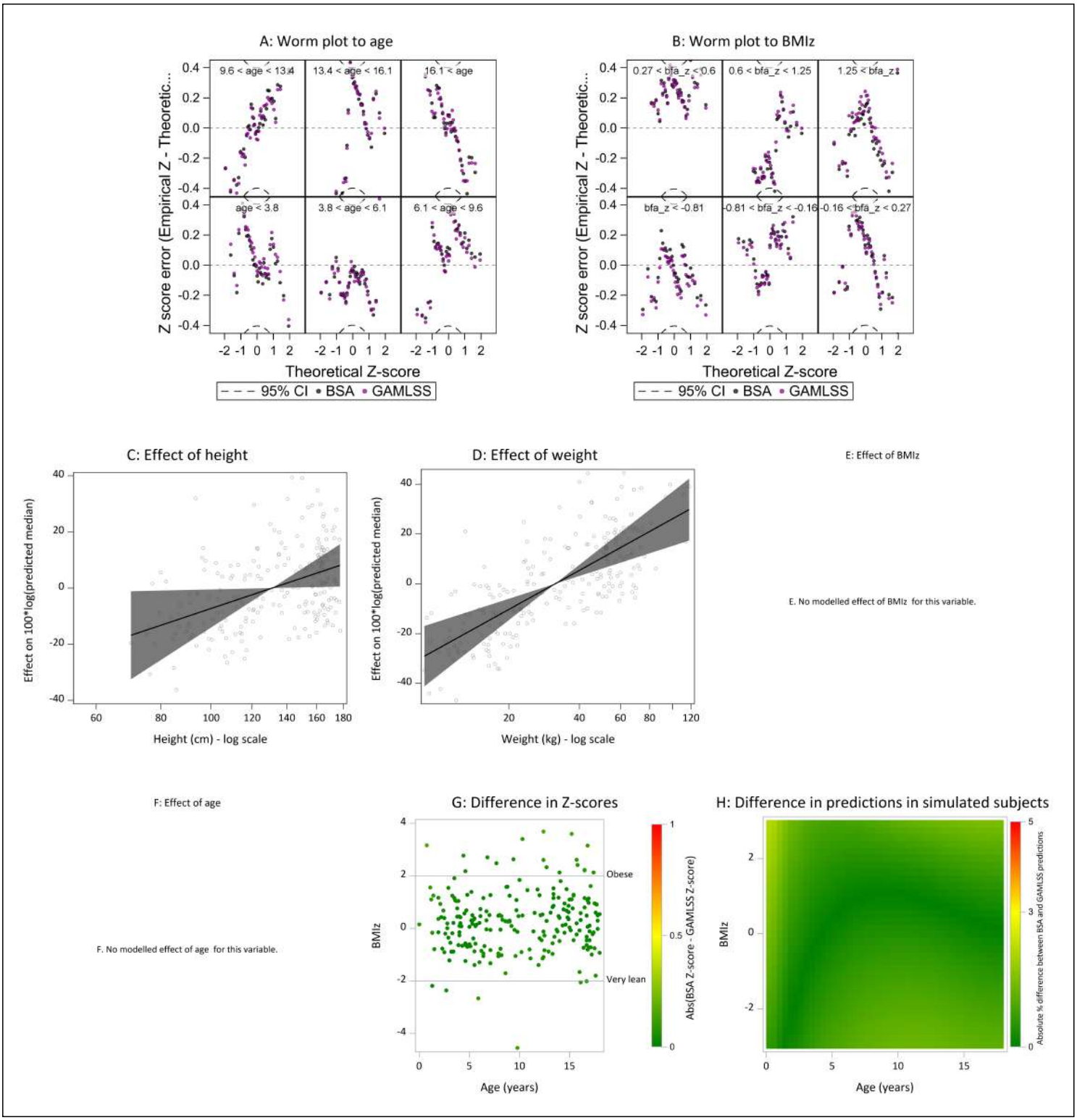
Supplementary figures S21 A-G: Proximal arch diameter in females (PARCF)

A: Worm plot by age of the Z-scores of the GAMLSS model in comparison to the BSA-allometric model for PARCF. B: Worm plot by BMIz of the Z-scores of the GAMLSS model in comparison to the BSA-allometric model for PARCF. C: Effect of height on the log of the predicted median of the PARCF. D: Effect of weight on the log of the predicted median of PARCF. E: Effect of BMIz on the log of the predicted median of PARCF. F: Effect of age on the log of the predicted median of PARCF. G: Difference between Z-scores of the GAMLSS model and the BSA-allometric model for PARCF. H: Difference between predicted median of the GAMLSS model and the BSA-allometric model for PARCF in simulated subjects.



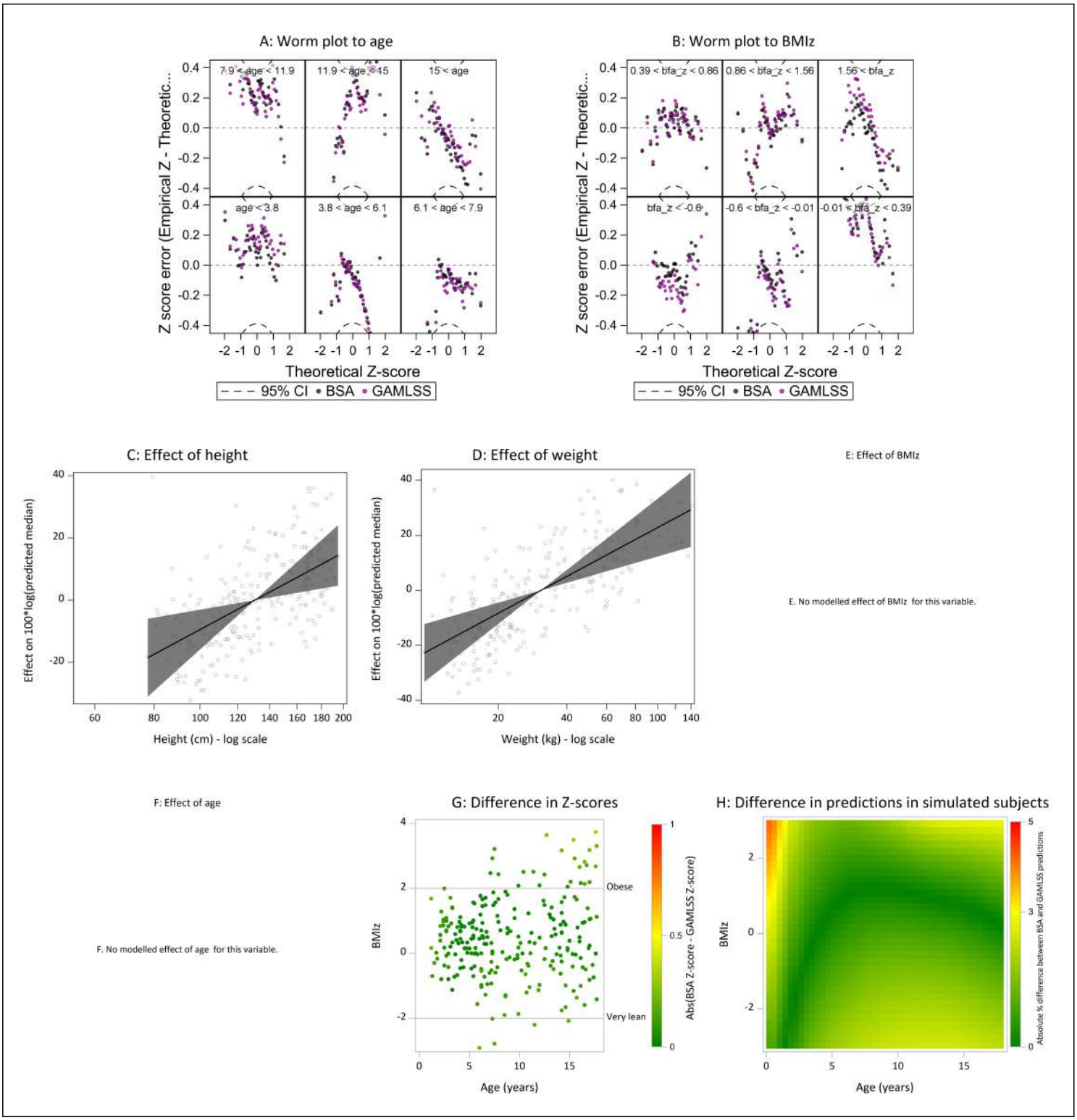
Supplementary figures S22 A-G: Proximal arch diameter in males (PARCM)

A: Worm plot by age of the Z-scores of the GAMLSS model in comparison to the BSA-allometric model for PARCM. B: Worm plot by BMIz of the Z-scores of the GAMLSS model in comparison to the BSA-allometric model for PARCM. C: Effect of height on the log of the predicted median of the PARCM. D: Effect of weight on the log of the predicted median of PARCM. E: Effect of BMIz on the log of the predicted median of PARCM. F: Effect of age on the log of the predicted median of PARCM. G: Difference between Z-scores of the GAMLSS model and the BSA-allometric model for PARCM. H: Difference between predicted median of the GAMLSS model and the BSA-allometric model for PARCM in simulated subjects.



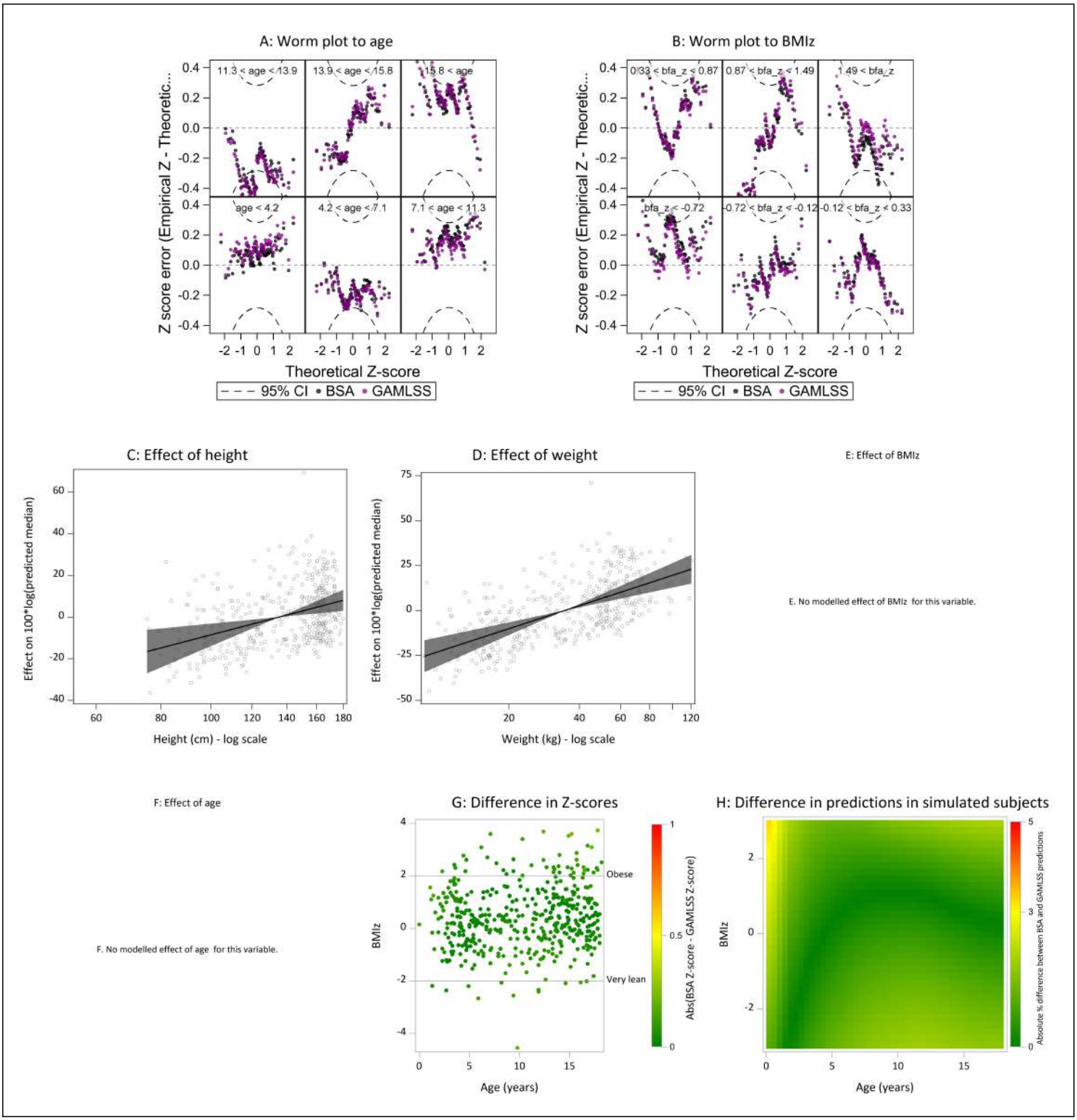
Supplementary figures S23 A-G: Distal arch diameter in females (DARCF)

A: Worm plot by age of the Z-scores of the GAMLSS model in comparison to the BSA-allometric model for DARCF. B: Worm plot by BMIz of the Z-scores of the GAMLSS model in comparison to the BSA-allometric model for DARCF. C: Effect of height on the log of the predicted median of the DARCF. D: Effect of weight on the log of the predicted median of DARCF. E: Effect of BMIz on the log of the predicted median of DARCF. F: Effect of age on the log of the predicted median of DARCF. G: Difference between Z-scores of the GAMLSS model and the BSA-allometric model for DARCF. H: Difference between predicted median of the GAMLSS model and the BSA-allometric model for DARCF in simulated subjects.



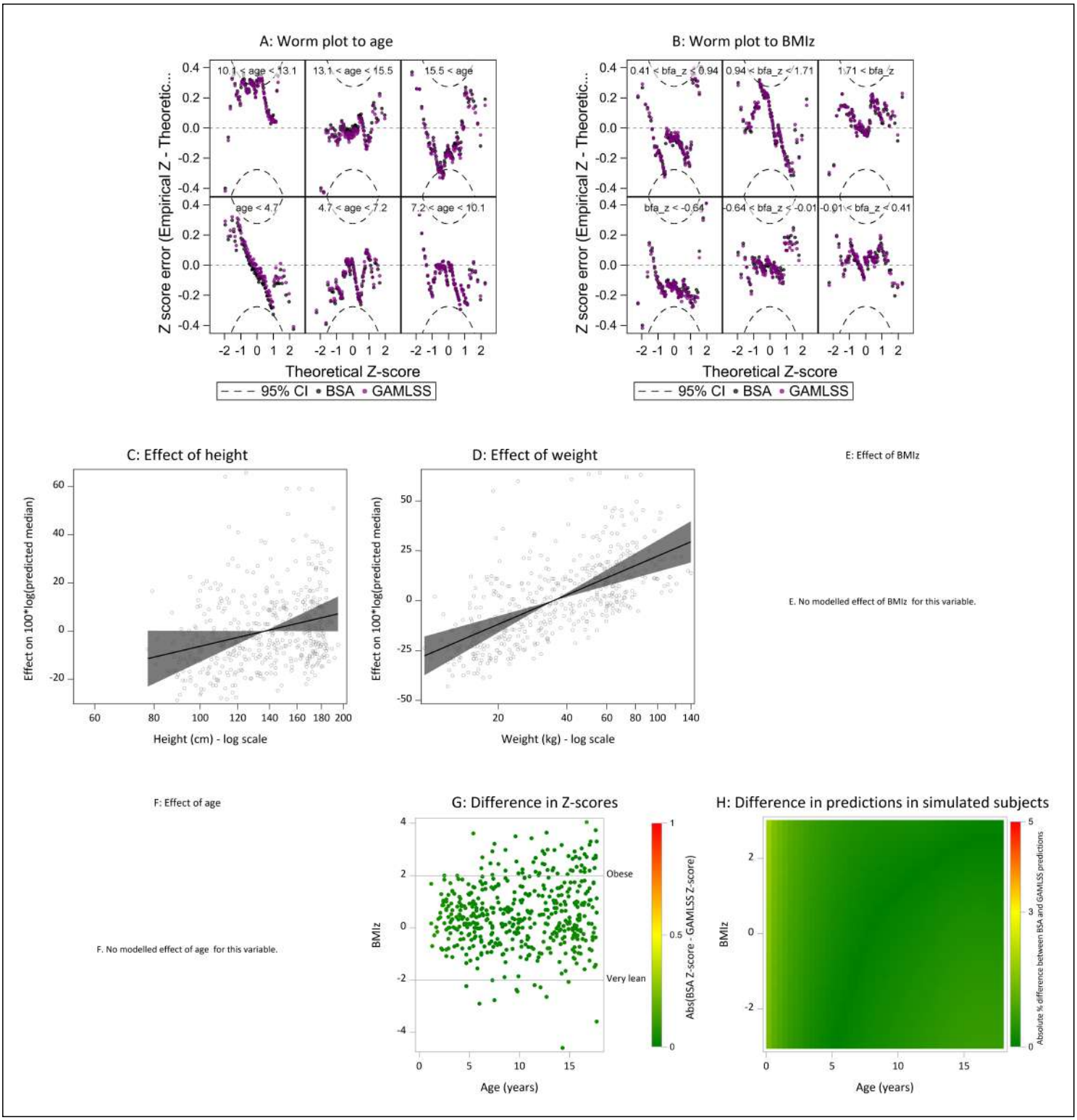
Supplementary figures S24 A-G: Distal arch diameter in males (DARCM)

A: Worm plot by age of the Z-scores of the GAMLSS model in comparison to the BSA-allometric model for DARCM. B: Worm plot by BMIz of the Z-scores of the GAMLSS model in comparison to the BSA-allometric model for DARCM. C: Effect of height on the log of the predicted median of the DARCM. D: Effect of weight on the log of the predicted median of DARCM. E: Effect of BMIz on the log of the predicted median of DARCM. F: Effect of age on the log of the predicted median of DARCM. G: Difference between Z-scores of the GAMLSS model and the BSA-allometric model for DARCM. H: Difference between predicted median of the GAMLSS model and the BSA-allometric model for DARCM in simulated subjects.



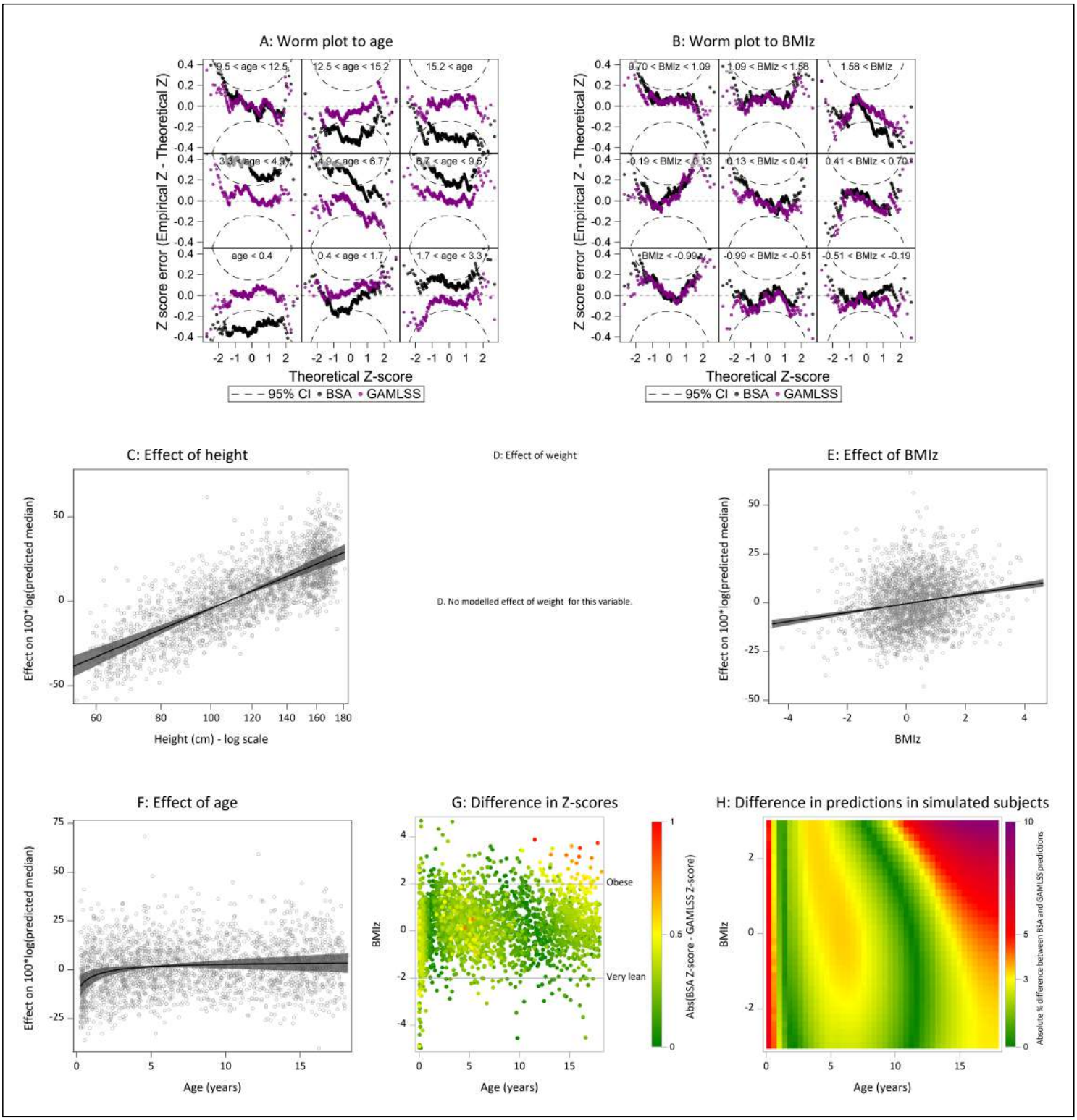
Supplementary figures S25 A-G: Aortic isthm diamter in females (AOIF)

A: Worm plot by age of the Z-scores of the GAMLSS model in comparison to the BSA-allometric model for AOIF. B: Worm plot by BMIz of the Z-scores of the GAMLSS model in comparison to the BSA-allometric model for AOIF. C: Effect of height on the log of the predicted median of the AOIF. D: Effect of weight on the log of the predicted median of AOIF. E: Effect of BMIz on the log of the predicted median of AOIF. F: Effect of age on the log of the predicted median of AOIF. G: Difference between Z-scores of the GAMLSS model and the BSA-allometric model for AOIF. H: Difference between predicted median of the GAMLSS model and the BSA-allometric model for AOIF in simulated subjects.



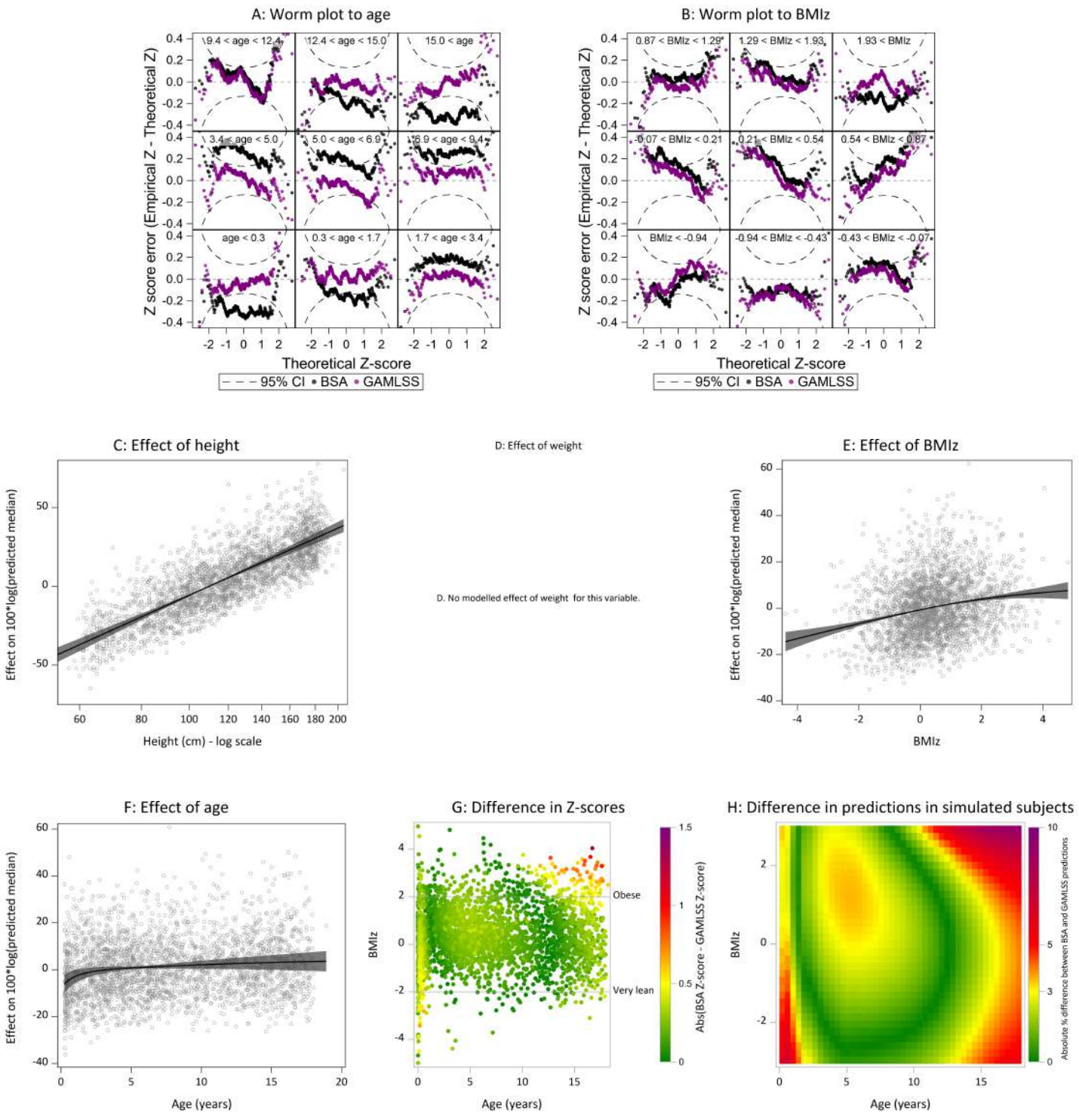
Supplementary figures S26 A-G: Aortic isthm diamter in males (AOIM)

A: Worm plot by age of the Z-scores of the GAMLSS model in comparison to the BSA-allometric model for AOIM. B: Worm plot by BMIz of the Z-scores of the GAMLSS model in comparison to the BSA-allometric model for AOIM. C: Effect of height on the log of the predicted median of the AOIM. D: Effect of weight on the log of the predicted median of AOIM. E: Effect of BMIz on the log of the predicted median of AOIM. F: Effect of age on the log of the predicted median of AOIM. G: Difference between Z-scores of the GAMLSS model and the BSA-allometric model for AOIM. H: Difference between predicted median of the GAMLSS model and the BSA-allometric model for AOIM in simulated subjects.



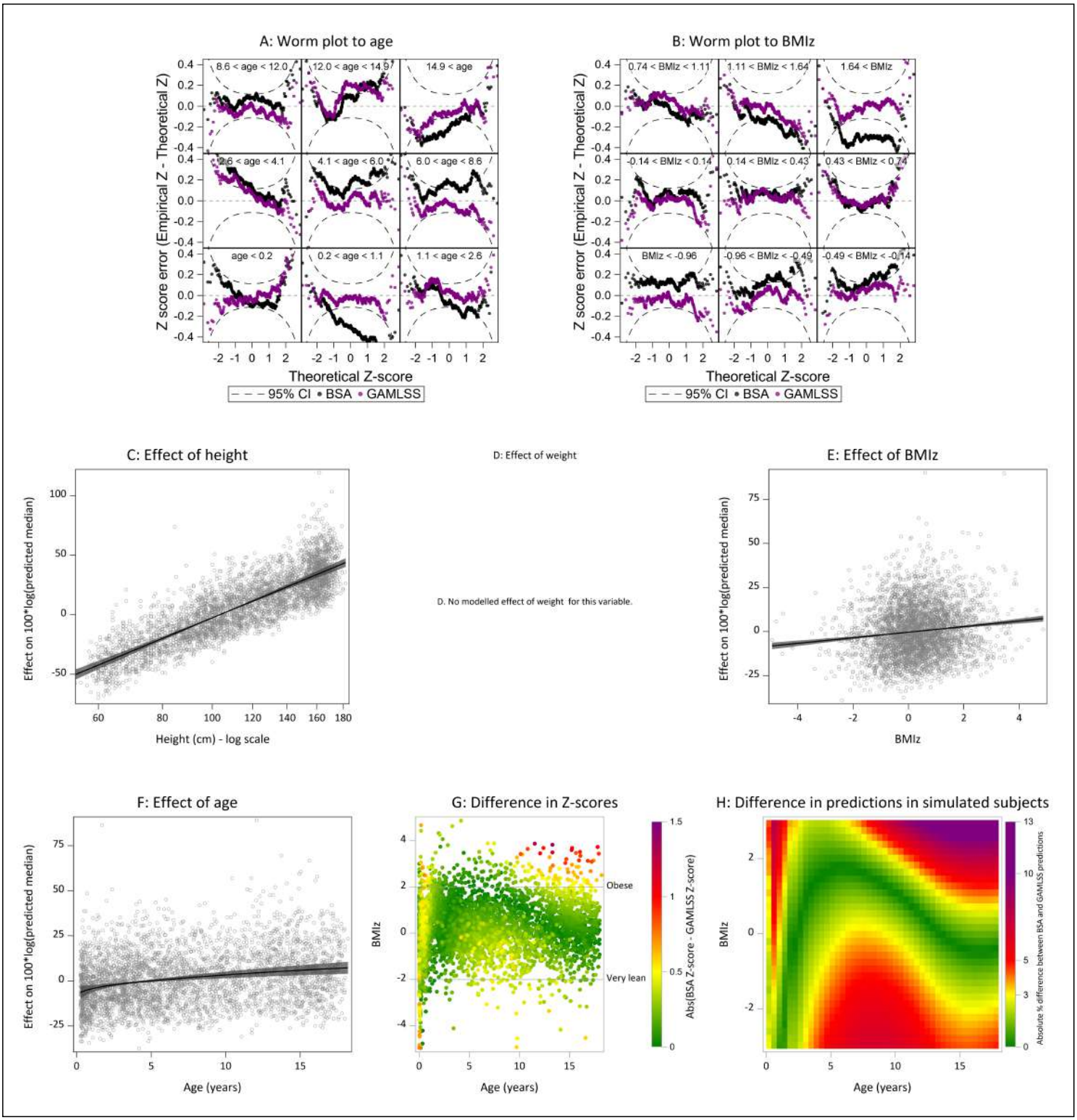
Supplementary figures S27 A-G: Tricuspid valve diameter in females (TVF)

A: Worm plot by age of the Z-scores of the GAMLSS model in comparison to the BSA-allometric model for TVF. B: Worm plot by BMIz of the Z-scores of the GAMLSS model in comparison to the BSA-allometric model for TVF. C: Effect of height on the log of the predicted median of the TVF. D: Effect of weight on the log of the predicted median of TVF. E: Effect of BMIz on the log of the predicted median of TVF. F: Effect of age on the log of the predicted median of TVF. G: Difference between Z-scores of the GAMLSS model and the BSA-allometric model for TVF. H: Difference between predicted median of the GAMLSS model and the BSA-allometric model for TVF in simulated subjects.



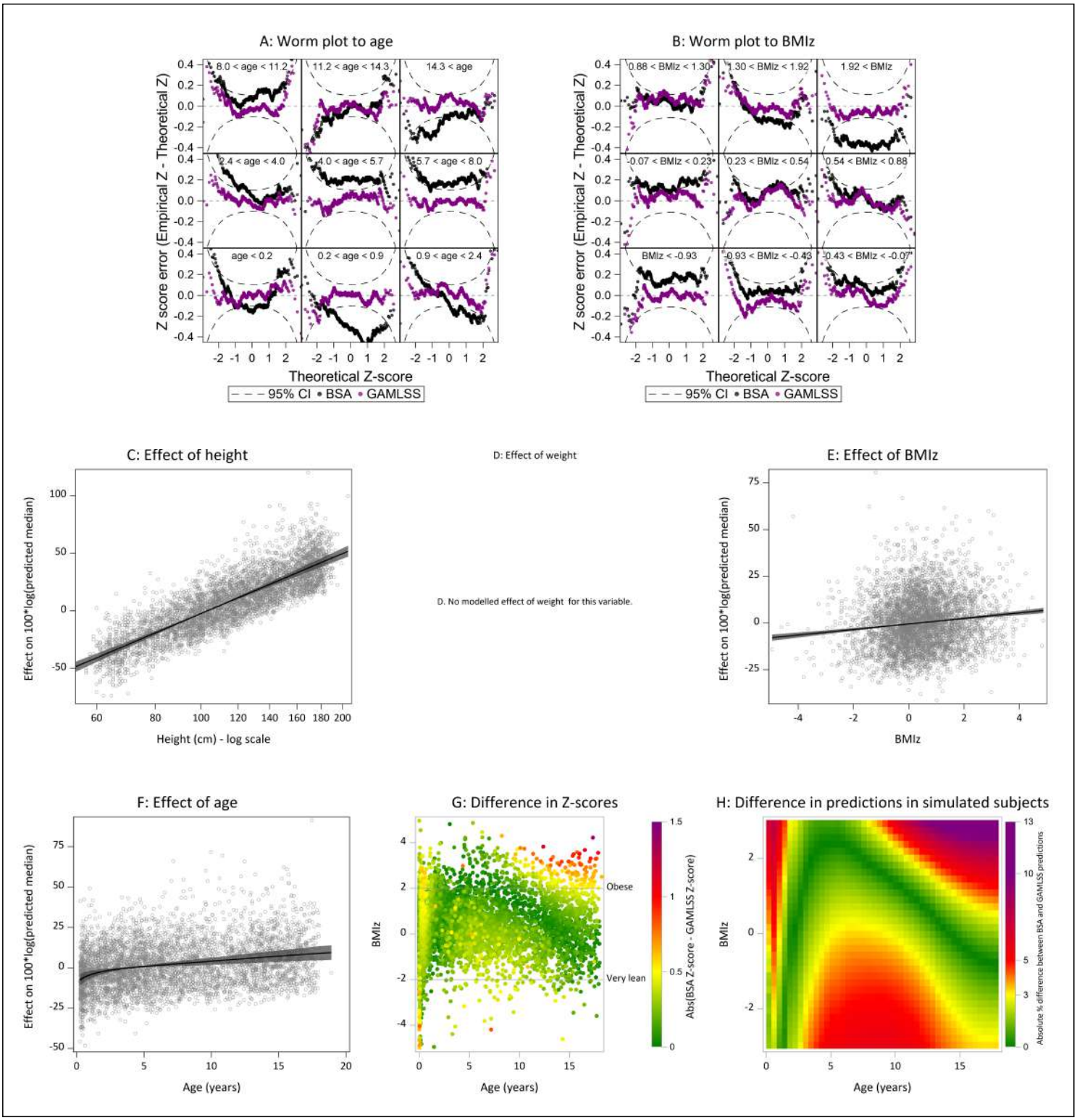
Supplementary figures S28 A-G: Tricuspid valve diameter in males (TVM)

A: Worm plot by age of the Z-scores of the GAMLSS model in comparison to the BSA-allometric model for TVM. B: Worm plot by BMIz of the Z-scores of the GAMLSS model in comparison to the BSA-allometric model for TVM. C: Effect of height on the log of the predicted median of the TVM. D: Effect of weight on the log of the predicted median of TVM. E: Effect of BMIz on the log of the predicted median of TVM. F: Effect of age on the log of the predicted median of TVM. G: Difference between Z-scores of the GAMLSS model and the BSA-allometric model for TVM. H: Difference between predicted median of the GAMLSS model and the BSA-allometric model for TVM in simulated subjects.



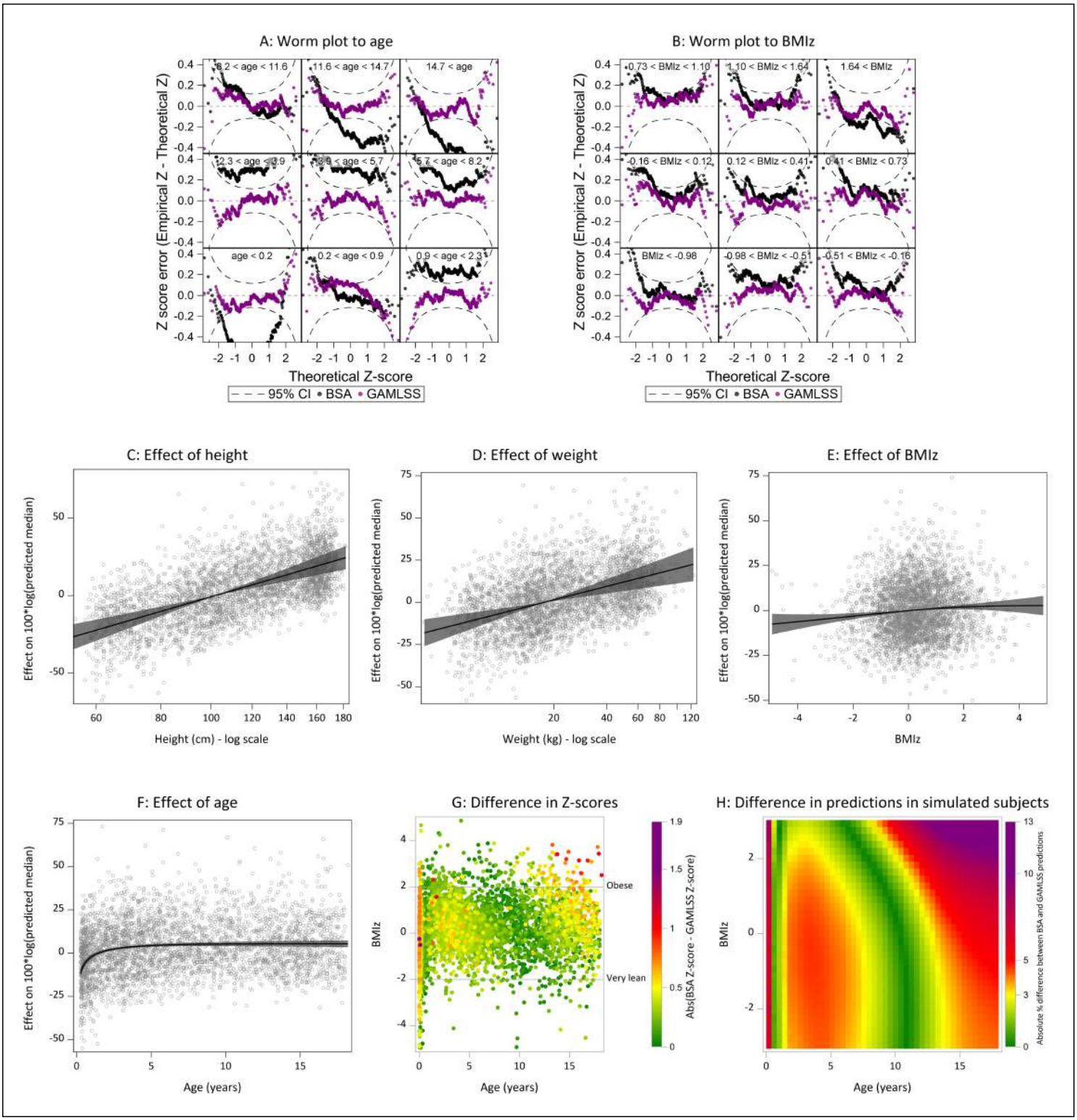
Supplementary figures S29 A-G: Pulmonary valve diameter in females (PVF)

A: Worm plot by age of the Z-scores of the GAMLSS model in comparison to the BSA-allometric model for PVF. B: Worm plot by BMIz of the Z-scores of the GAMLSS model in comparison to the BSA-allometric model for PVF. C: Effect of height on the log of the predicted median of the PVF. D: Effect of weight on the log of the predicted median of PVF. E: Effect of BMIz on the log of the predicted median of PVF. F: Effect of age on the log of the predicted median of PVF. G: Difference between Z-scores of the GAMLSS model and the BSA-allometric model for PVF. H: Difference between predicted median of the GAMLSS model and the BSA-allometric model for PVF in simulated subjects.



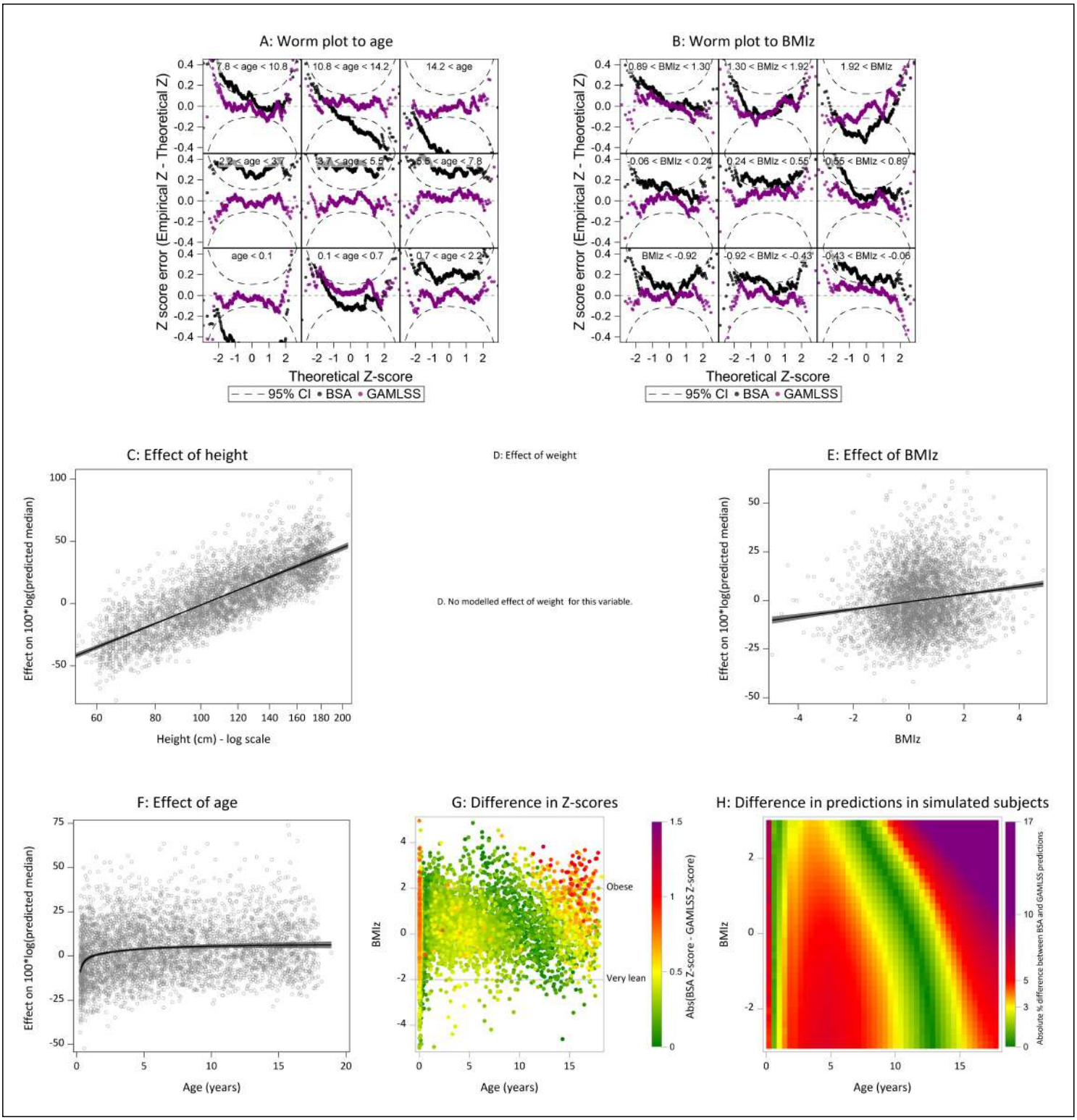
Supplementary figures S30 A-G: Pulmonary valve diameter in males (PVM)

A: Worm plot by age of the Z-scores of the GAMLSS model in comparison to the BSA-allometric model for PVM. B: Worm plot by BMIz of the Z-scores of the GAMLSS model in comparison to the BSA-allometric model for PVM. C: Effect of height on the log of the predicted median of the PVM. D: Effect of weight on the log of the predicted median of PVM. E: Effect of BMIz on the log of the predicted median of PVM. F: Effect of age on the log of the predicted median of PVM. G: Difference between Z-scores of the GAMLSS model and the BSA-allometric model for PVM. H: Difference between predicted median of the GAMLSS model and the BSA-allometric model for PVM in simulated subjects.



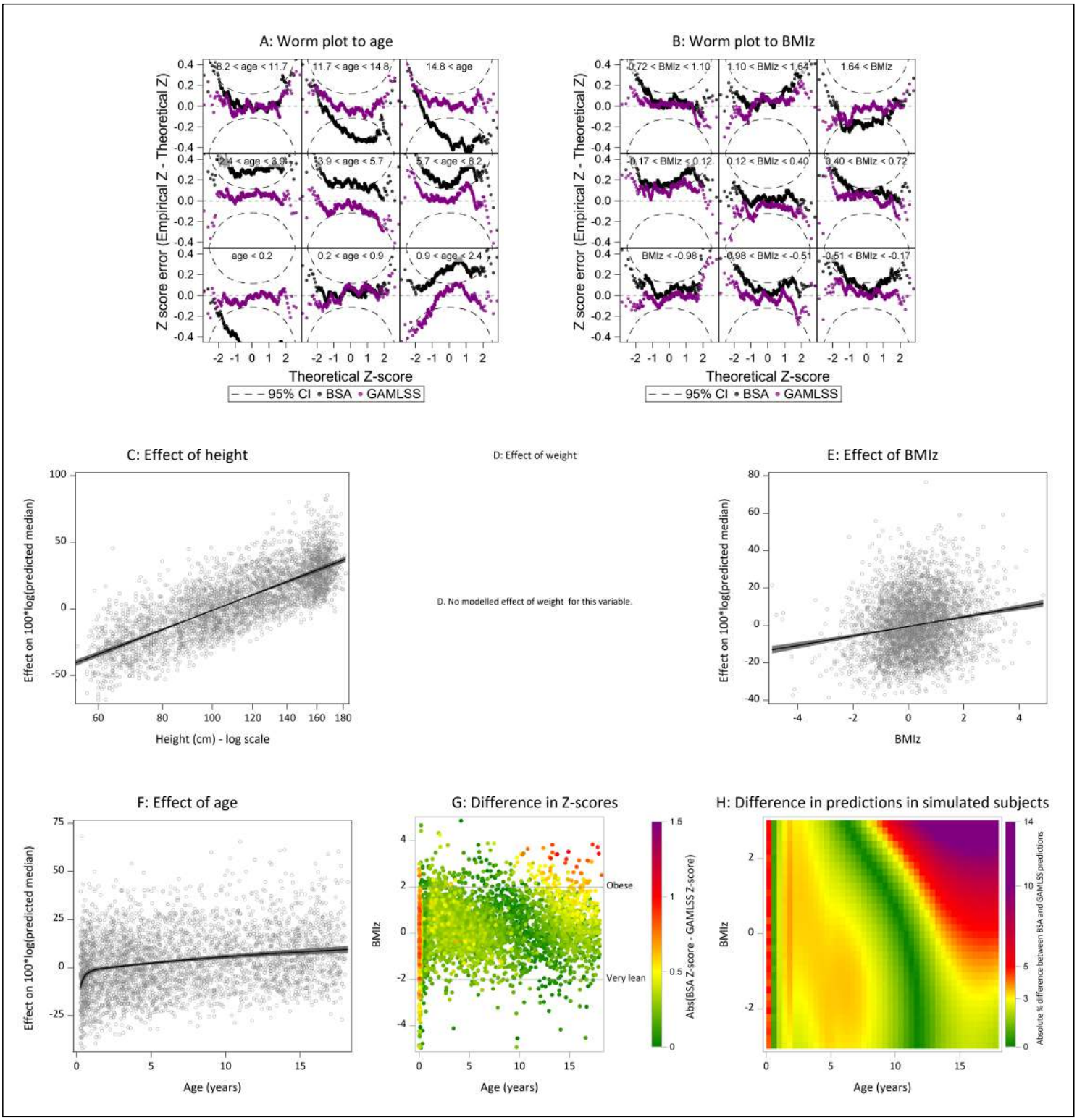
Supplementary figures S31 A-G: Left pulmonary artery diameter in females (LPAF)

A: Worm plot by age of the Z-scores of the GAMLSS model in comparison to the BSA-allometric model for LPAF. B: Worm plot by BMIz of the Z-scores of the GAMLSS model in comparison to the BSA-allometric model for LPAF. C: Effect of height on the log of the predicted median of the LPAF. D: Effect of weight on the log of the predicted median of LPAF. E: Effect of BMIz on the log of the predicted median of LPAF. F: Effect of age on the log of the predicted median of LPAF. G: Difference between Z-scores of the GAMLSS model and the BSA-allometric model for LPAF. H: Difference between predicted median of the GAMLSS model and the BSA-allometric model for LPAF in simulated subjects.



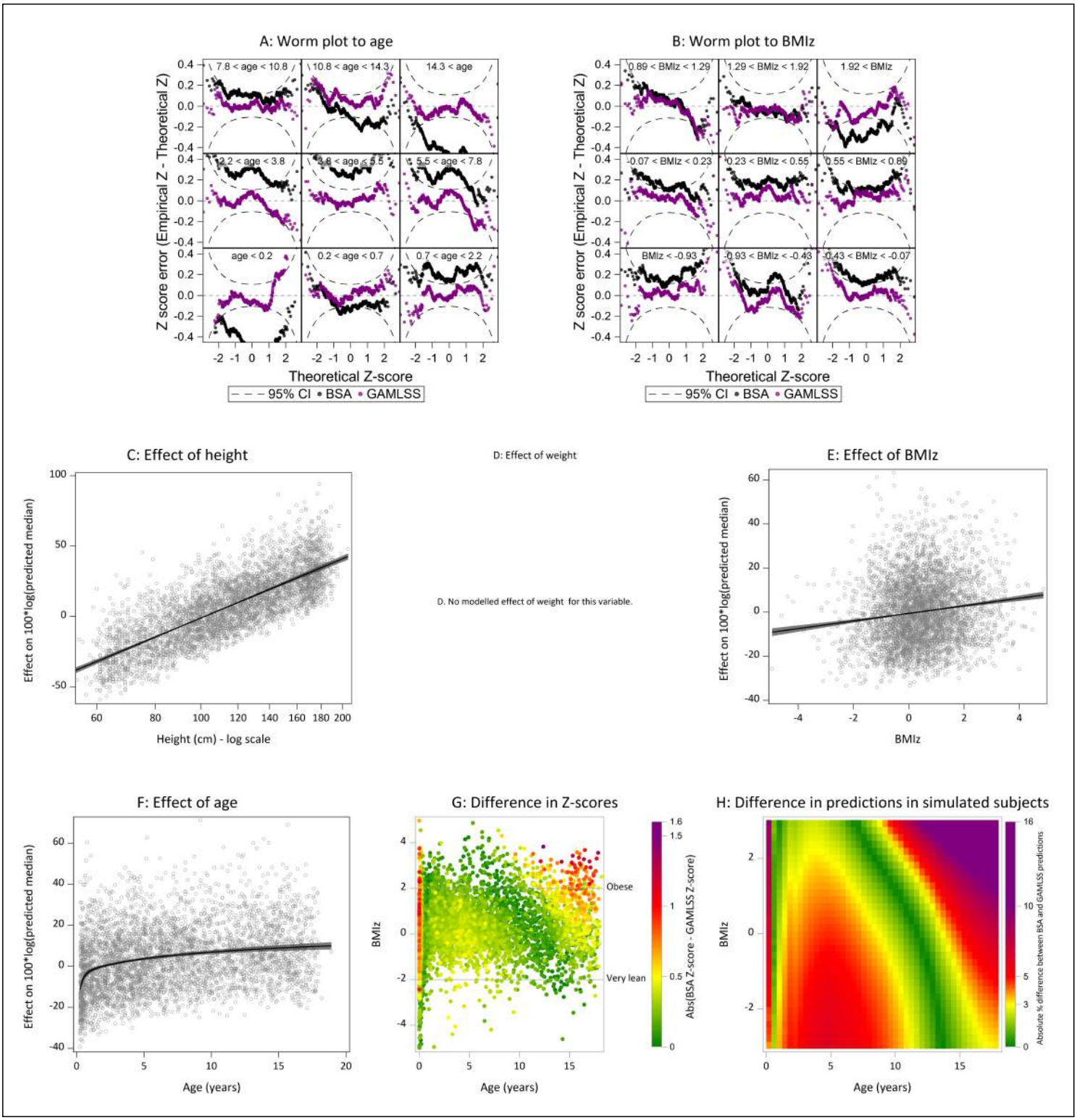
Supplementary figures S32 A-G: Left pulmonary artery diameter in males (LPAM)

A: Worm plot by age of the Z-scores of the GAMLSS model in comparison to the BSA-allometric model for LPAM. B: Worm plot by BMIz of the Z-scores of the GAMLSS model in comparison to the BSA-allometric model for LPAM. C: Effect of height on the log of the predicted median of the LPAM. D: Effect of weight on the log of the predicted median of LPAM. E: Effect of BMIz on the log of the predicted median of LPAM. F: Effect of age on the log of the predicted median of LPAM. G: Difference between Z-scores of the GAMLSS model and the BSA-allometric model for LPAM. H: Difference between predicted median of the GAMLSS model and the BSA-allometric model for LPAM in simulated subjects.



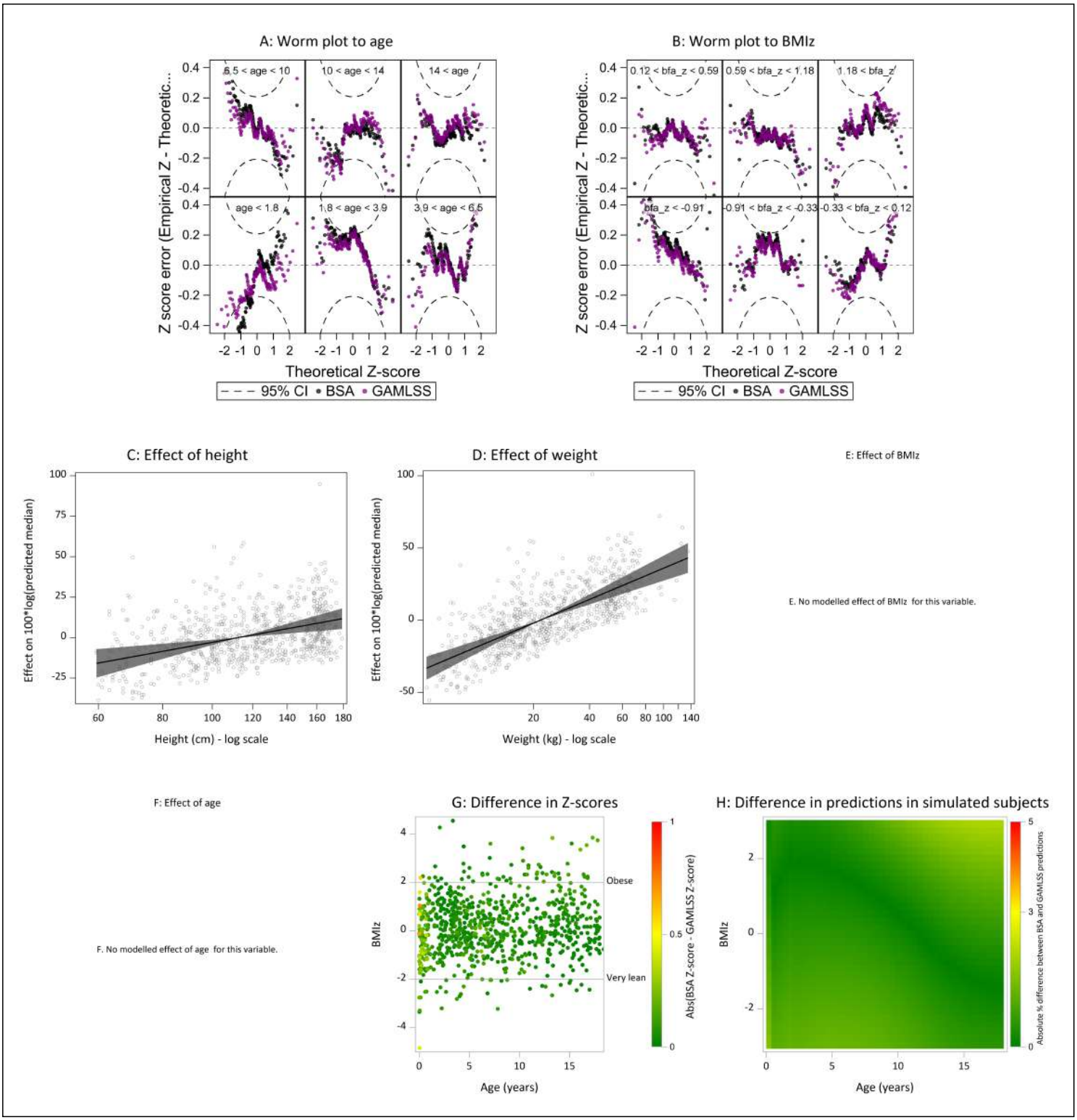
Supplementary figures S33 A-G: Right pulmonary artery diameter in females (RPAF)

A: Worm plot by age of the Z-scores of the GAMLSS model in comparison to the BSA-allometric model for RPAF. B: Worm plot by BMIz of the Z-scores of the GAMLSS model in comparison to the BSA-allometric model for RPAF. C: Effect of height on the log of the predicted median of the RPAF. D: Effect of weight on the log of the predicted median of RPAF. E: Effect of BMIz on the log of the predicted median of RPAF. F: Effect of age on the log of the predicted median of RPAF. G: Difference between Z-scores of the GAMLSS model and the BSA-allometric model for RPAF. H: Difference between predicted median of the GAMLSS model and the BSA-allometric model for RPAF in simulated subjects.



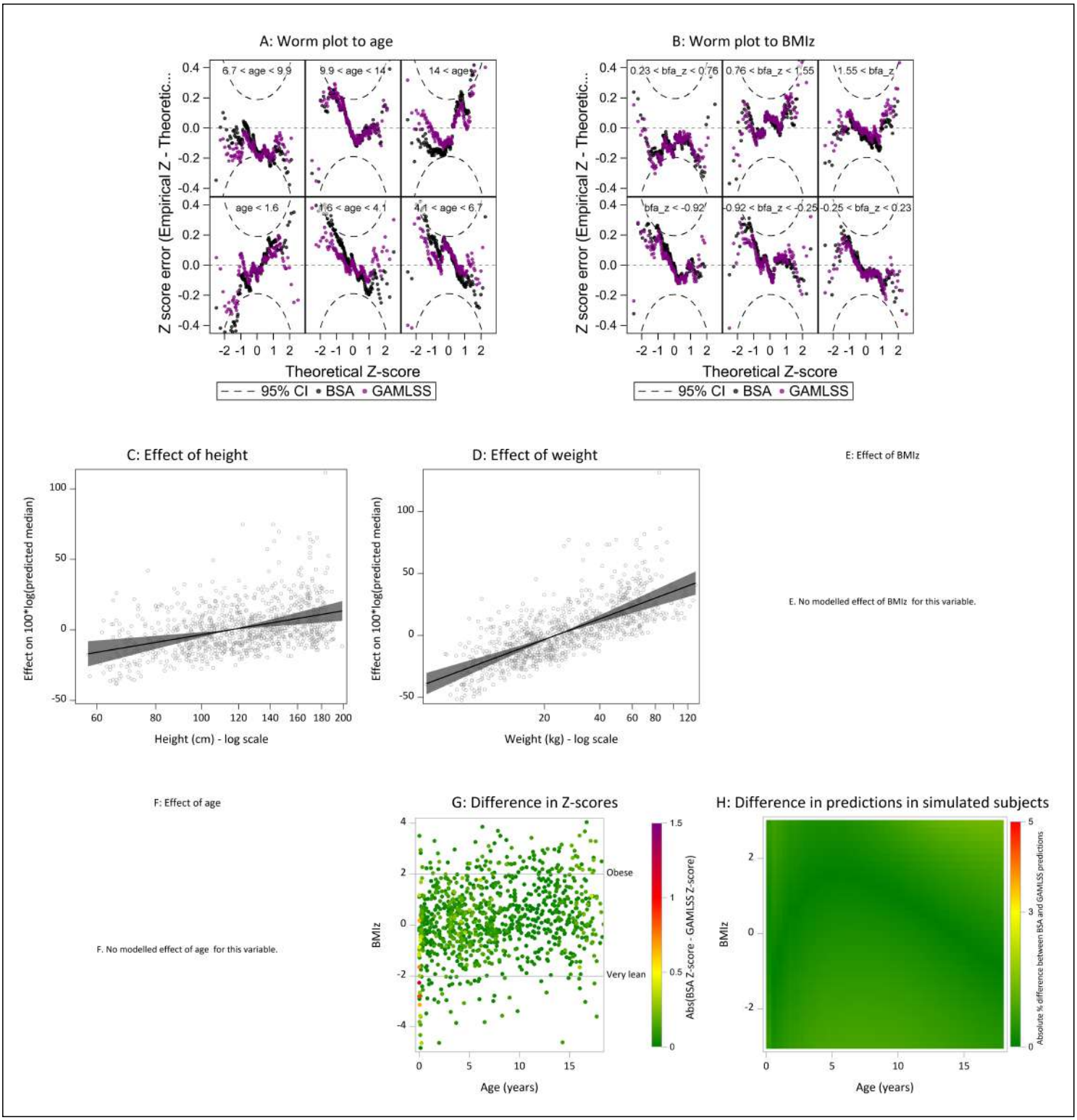
Supplementary figures S34 A-G: Right pulmonary artery diameter in males (RPAM)

A: Worm plot by age of the Z-scores of the GAMLSS model in comparison to the BSA-allometric model for RPAM. B: Worm plot by BMIz of the Z-scores of the GAMLSS model in comparison to the BSA-allometric model for RPAM. C: Effect of height on the log of the predicted median of the RPAM. D: Effect of weight on the log of the predicted median of RPAM. E: Effect of BMIz on the log of the predicted median of RPAM. F: Effect of age on the log of the predicted median of RPAM. G: Difference between Z-scores of the GAMLSS model and the BSA-allometric model for RPAM. H: Difference between predicted median of the GAMLSS model and the BSA-allometric model for RPAM in simulated subjects.



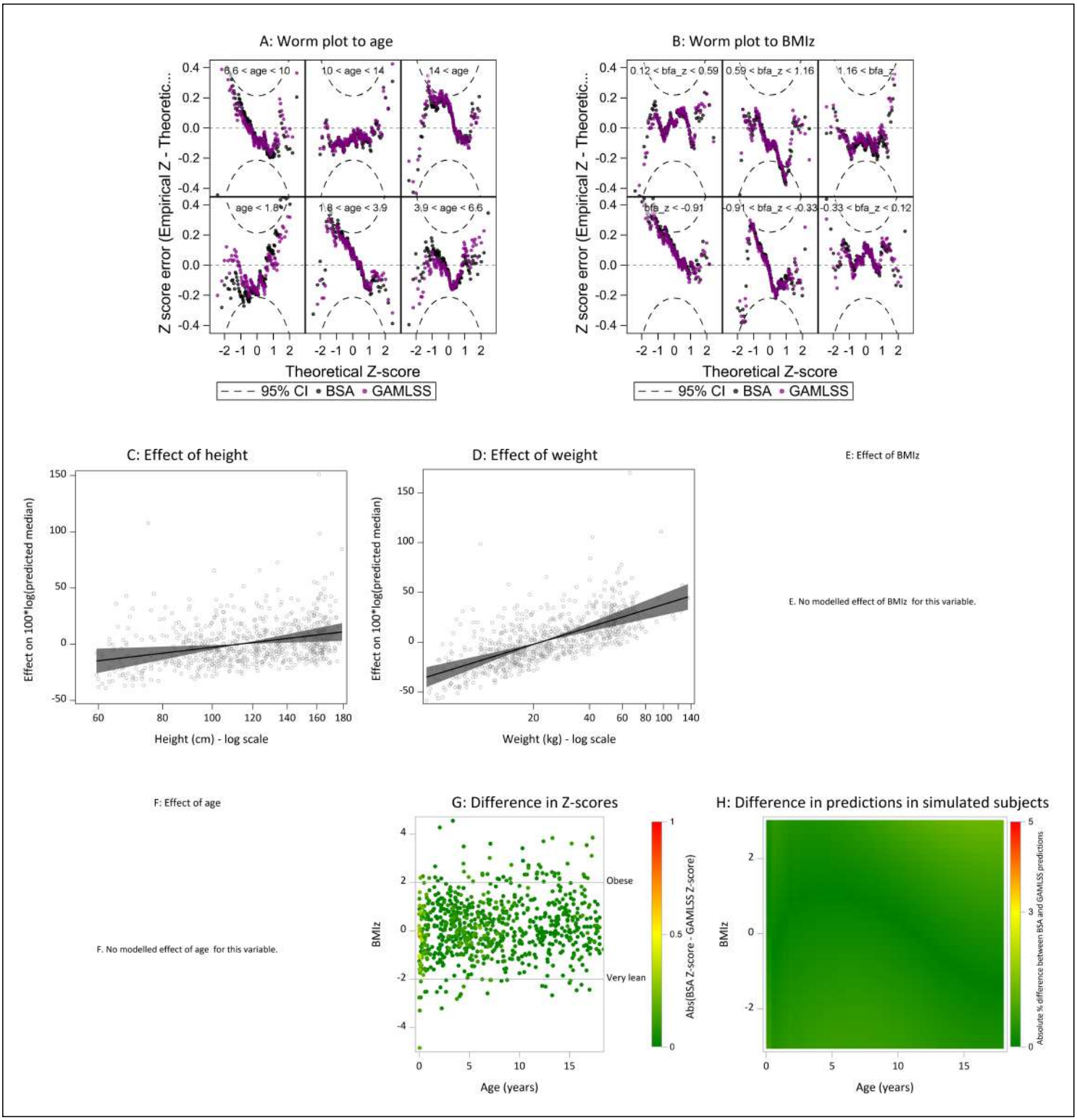
Supplementary figures S35 A-G: Left main coronary artery diameter in females (LMCAF)

A: Worm plot by age of the Z-scores of the GAMLSS model in comparison to the BSA-allometric model for LMCAF. B: Worm plot by BMIz of the Z-scores of the GAMLSS model in comparison to the BSA-allometric model for LMCAF. C: Effect of height on the log of the predicted median of the LMCAF. D: Effect of weight on the log of the predicted median of LMCAF. E: Effect of BMIz on the log of the predicted median of LMCAF. F: Effect of age on the log of the predicted median of LMCAF. G: Difference between Z-scores of the GAMLSS model and the BSA-allometric model for LMCAF. H: Difference between predicted median of the GAMLSS model and the BSA-allometric model for LMCAF in simulated subjects.



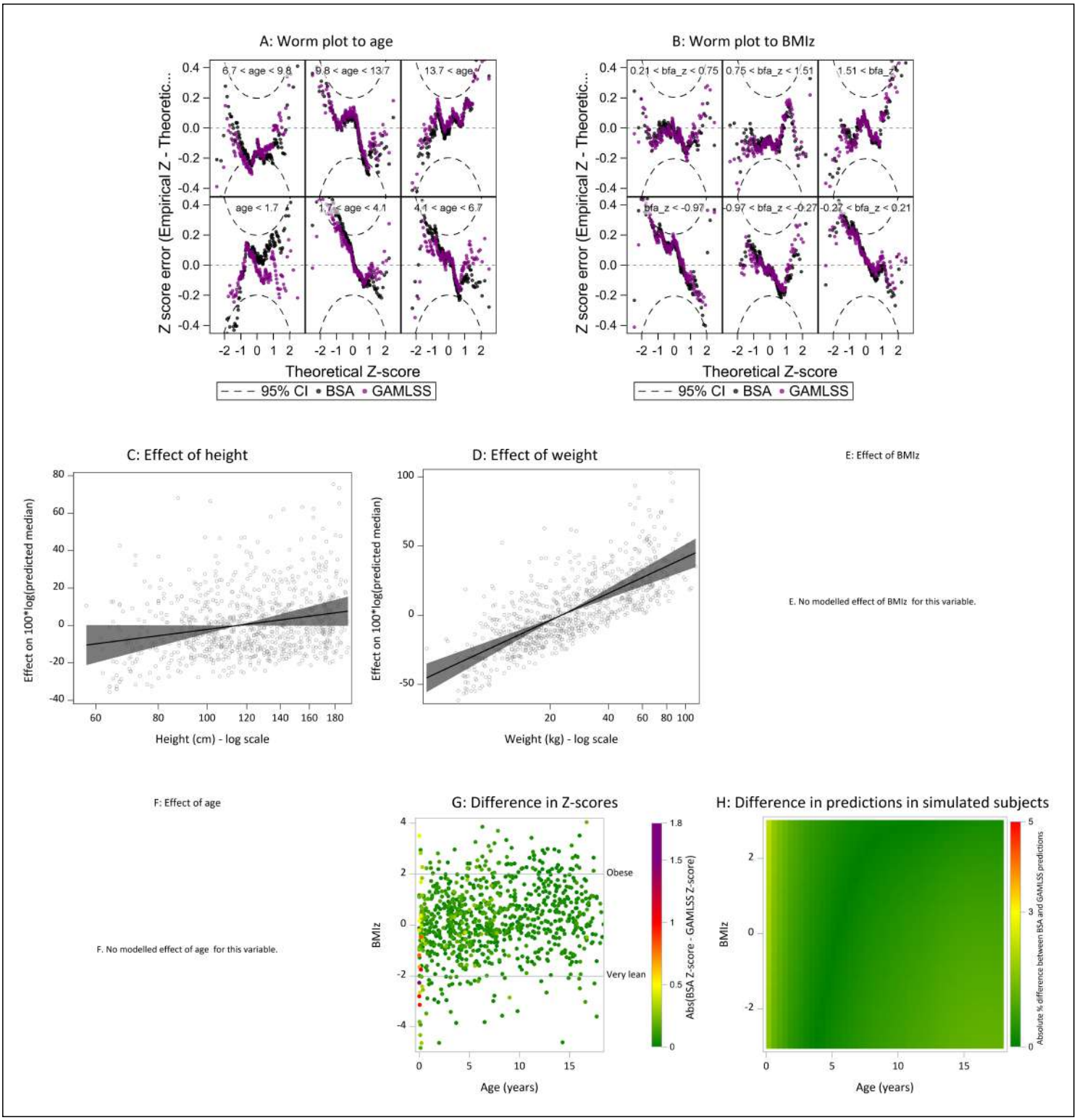
Supplementary figures S36 A-G: Left main coronary artery diameter in males (LMCAM)

A: Worm plot by age of the Z-scores of the GAMLSS model in comparison to the BSA-allometric model for LMCAM. B: Worm plot by BMIz of the Z-scores of the GAMLSS model in comparison to the BSA-allometric model for LMCAM. C: Effect of height on the log of the predicted median of the LMCAM. D: Effect of weight on the log of the predicted median of LMCAM. E: Effect of BMIz on the log of the predicted median of LMCAM. F: Effect of age on the log of the predicted median of LMCAM. G: Difference between Z-scores of the GAMLSS model and the BSA-allometric model for LMCAM. H: Difference between predicted median of the GAMLSS model and the BSA-allometric model for LMCAM in simulated subjects.



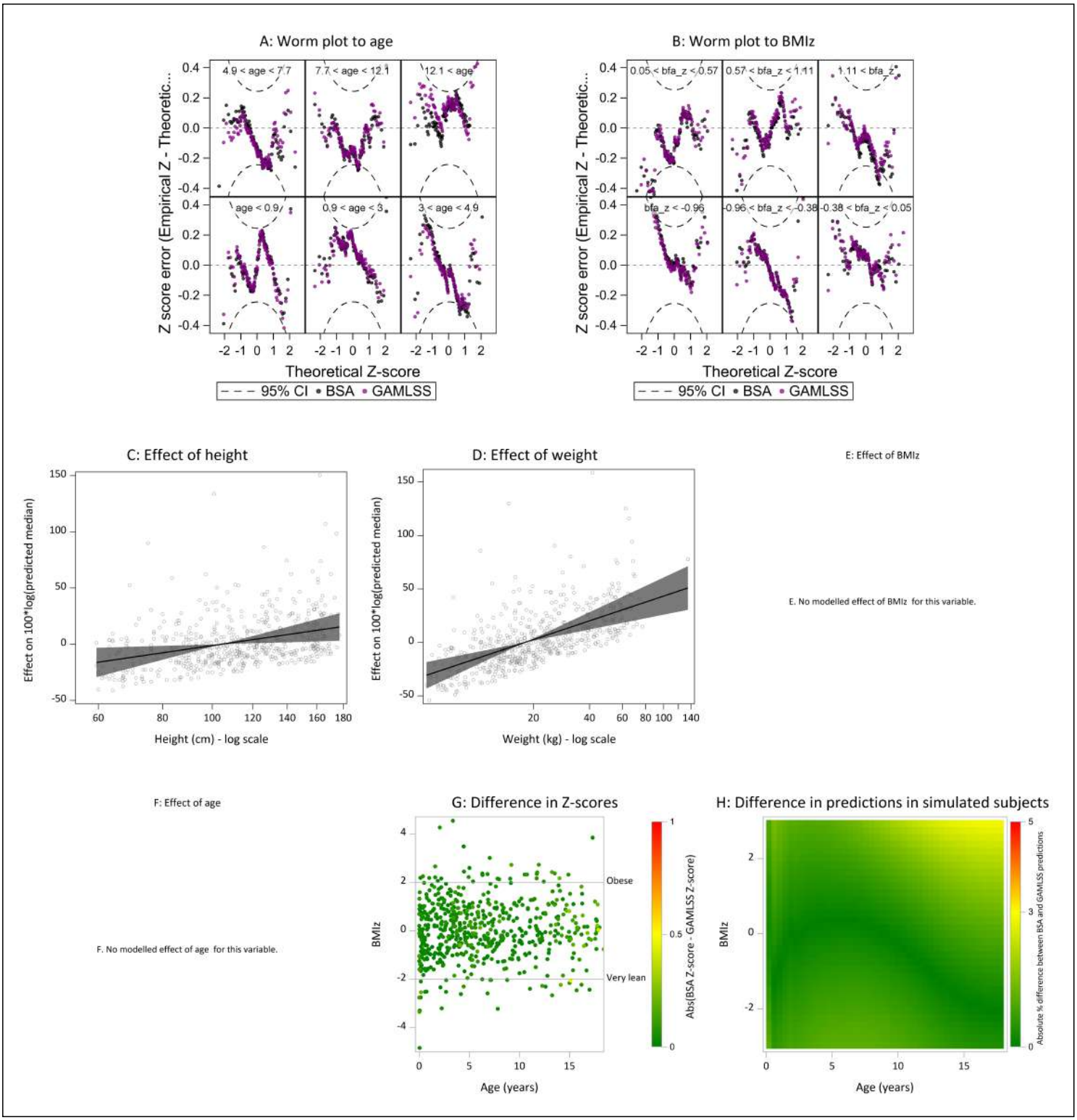
Supplementary figures S37 A-G: Left anterior descending artery diameter in females (LADF)

A: Worm plot by age of the Z-scores of the GAMLSS model in comparison to the BSA-allometric model for LADF. B: Worm plot by BMIz of the Z-scores of the GAMLSS model in comparison to the BSA-allometric model for LADF. C: Effect of height on the log of the predicted median of the LADF. D: Effect of weight on the log of the predicted median of LADF. E: Effect of BMIz on the log of the predicted median of LADF. F: Effect of age on the log of the predicted median of LADF. G: Difference between Z-scores of the GAMLSS model and the BSA-allometric model for LADF. H: Difference between predicted median of the GAMLSS model and the BSA-allometric model for LADF in simulated subjects.



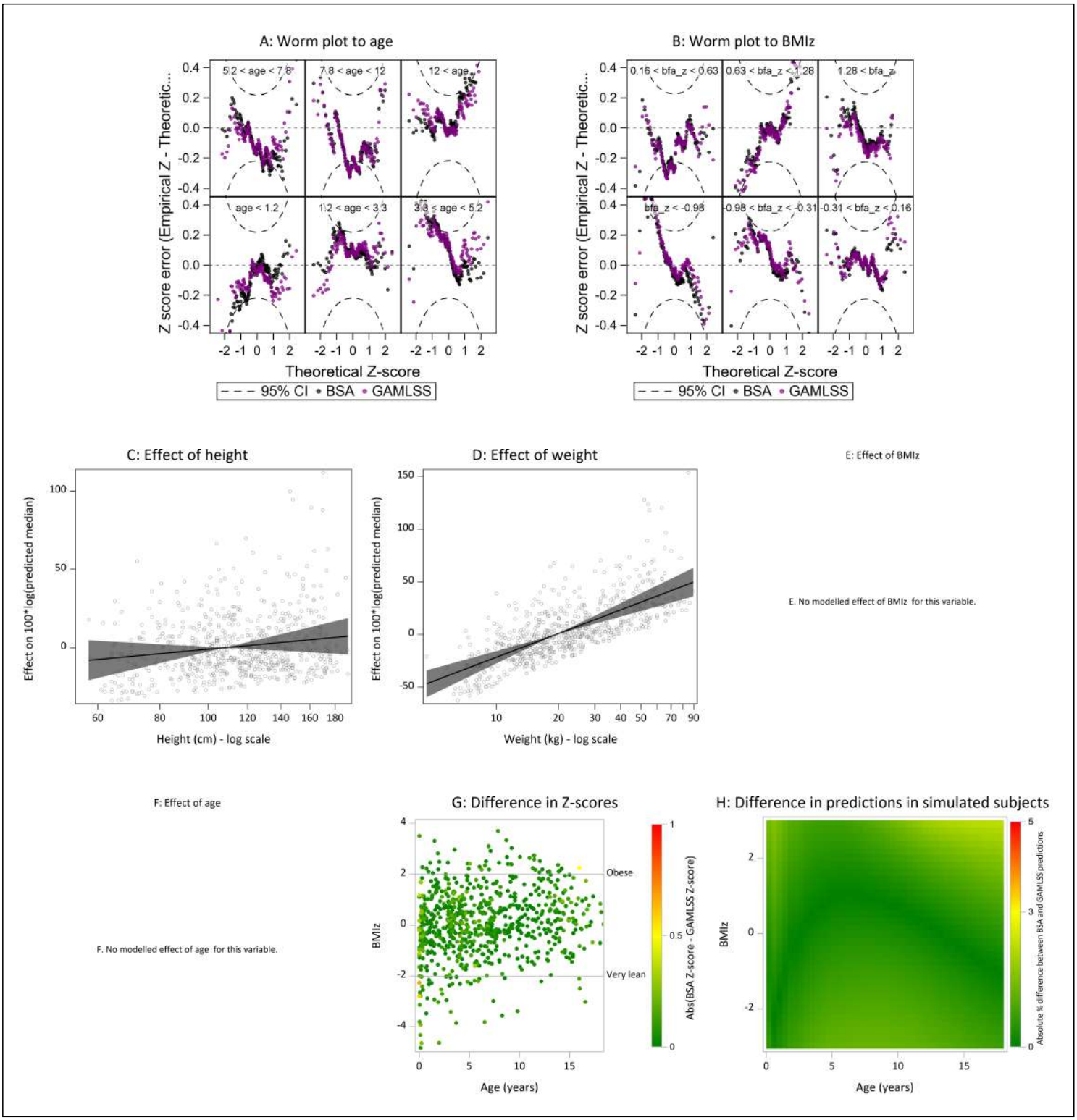
Supplementary figures S38 A-G: Left anterior descending artery diameter in males (LADM)

A: Worm plot by age of the Z-scores of the GAMLSS model in comparison to the BSA-allometric model for LADM. B: Worm plot by BMIz of the Z-scores of the GAMLSS model in comparison to the BSA-allometric model for LADM. C: Effect of height on the log of the predicted median of the LADM. D: Effect of weight on the log of the predicted median of LADM. E: Effect of BMIz on the log of the predicted median of LADM. F: Effect of age on the log of the predicted median of LADM. G: Difference between Z-scores of the GAMLSS model and the BSA-allometric model for LADM. H: Difference between predicted median of the GAMLSS model and the BSA-allometric model for LADM in simulated subjects.



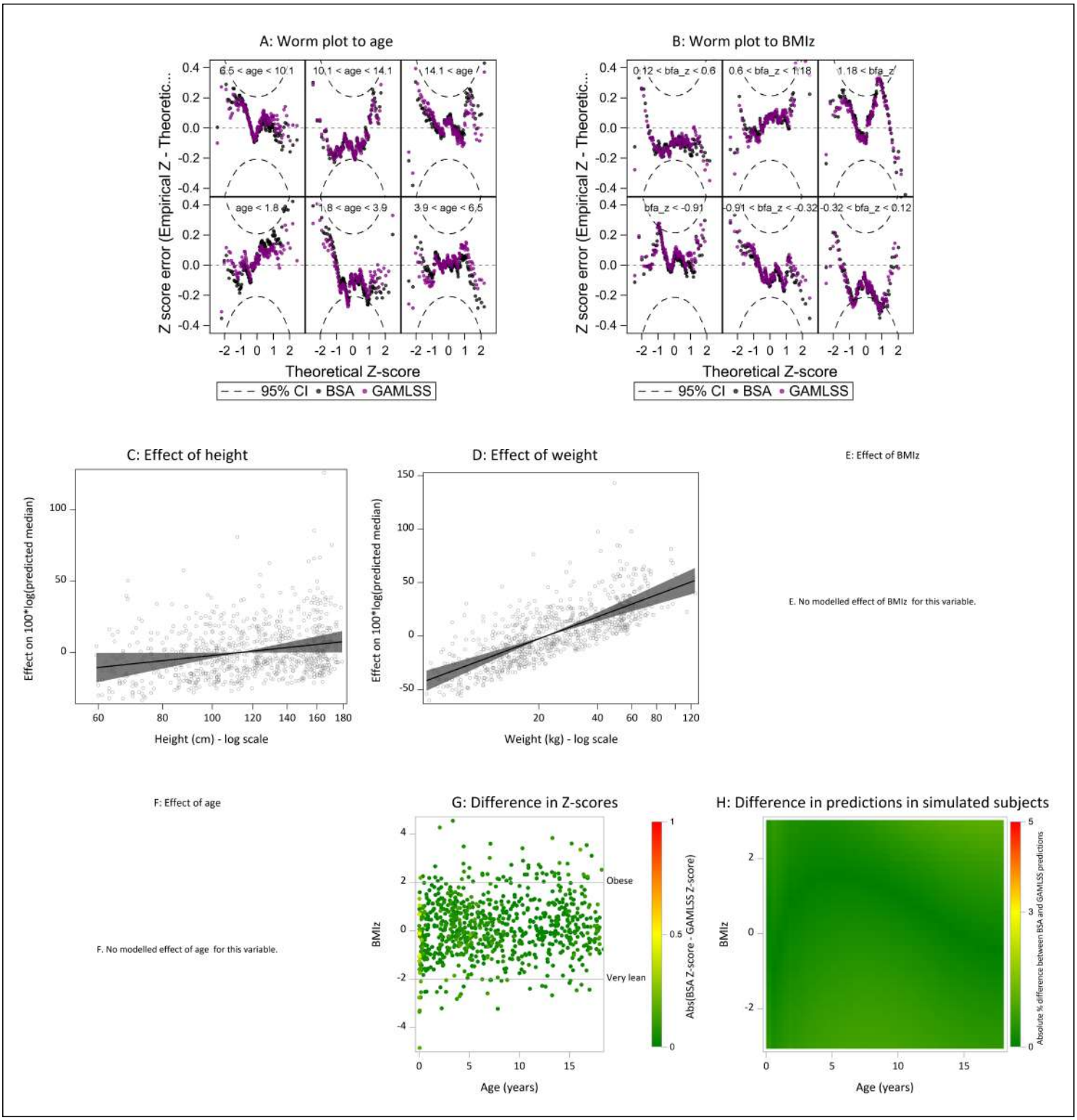
Supplementary figures S39 A-G: Left circumflex artery diameter in females (LCXF)

A: Worm plot by age of the Z-scores of the GAMLSS model in comparison to the BSA-allometric model for LCXF. B: Worm plot by BMIz of the Z-scores of the GAMLSS model in comparison to the BSA-allometric model for LCXF. C: Effect of height on the log of the predicted median of the LCXF. D: Effect of weight on the log of the predicted median of LCXF. E: Effect of BMIz on the log of the predicted median of LCXF. F: Effect of age on the log of the predicted median of LCXF. G: Difference between Z-scores of the GAMLSS model and the BSA-allometric model for LCXF. H: Difference between predicted median of the GAMLSS model and the BSA-allometric model for LCXF in simulated subjects.



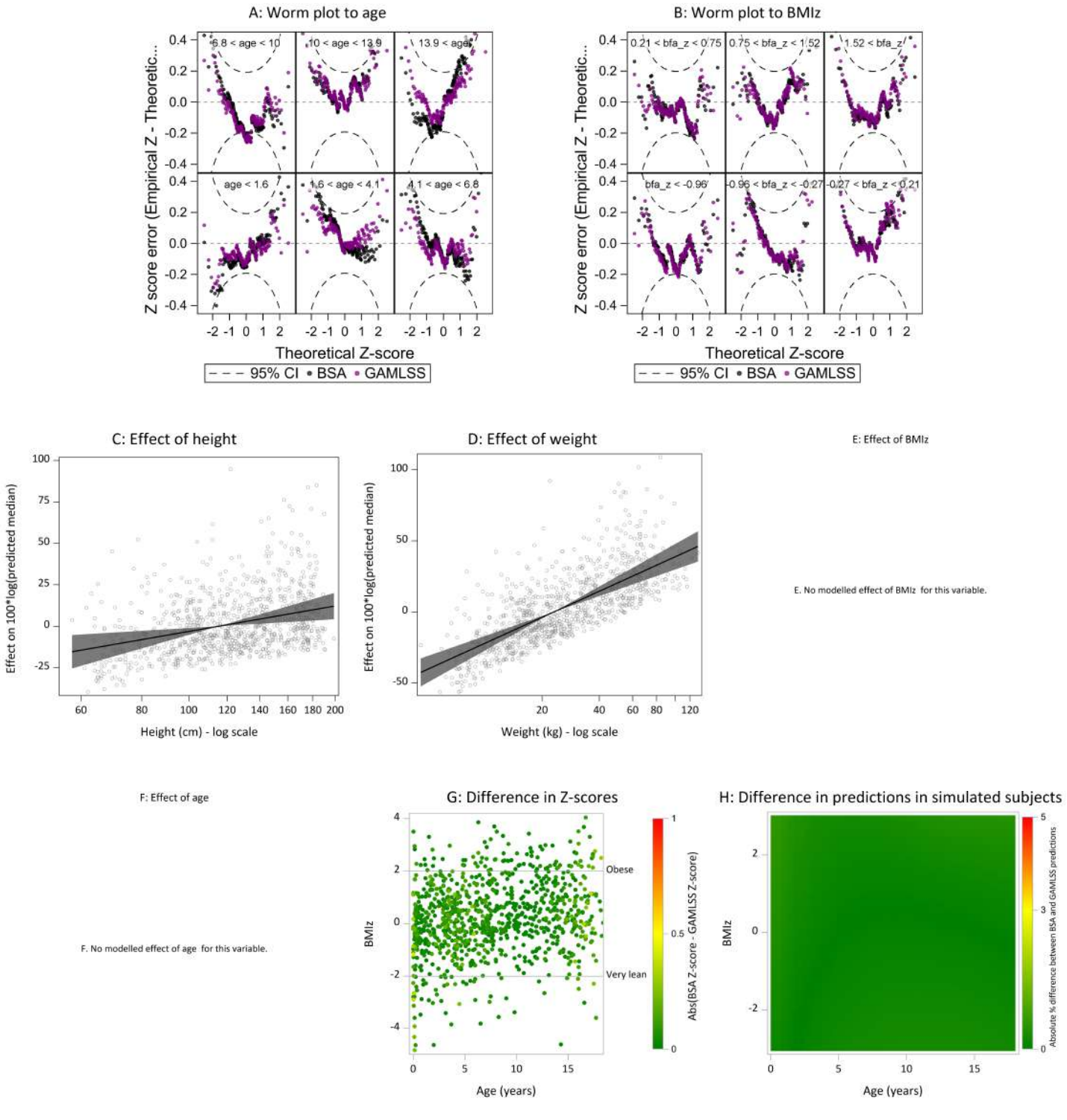
Supplementary figures S40 A-G: Left circumflex artery diameter in males (LCXM)

A: Worm plot by age of the Z-scores of the GAMLSS model in comparison to the BSA-allometric model for LCXM. B: Worm plot by BMIz of the Z-scores of the GAMLSS model in comparison to the BSA-allometric model for LCXM. C: Effect of height on the log of the predicted median of the LCXM. D: Effect of weight on the log of the predicted median of LCXM. E: Effect of BMIz on the log of the predicted median of LCXM. F: Effect of age on the log of the predicted median of LCXM. G: Difference between Z-scores of the GAMLSS model and the BSA-allometric model for LCXM. H: Difference between predicted median of the GAMLSS model and the BSA-allometric model for LCXM in simulated subjects.



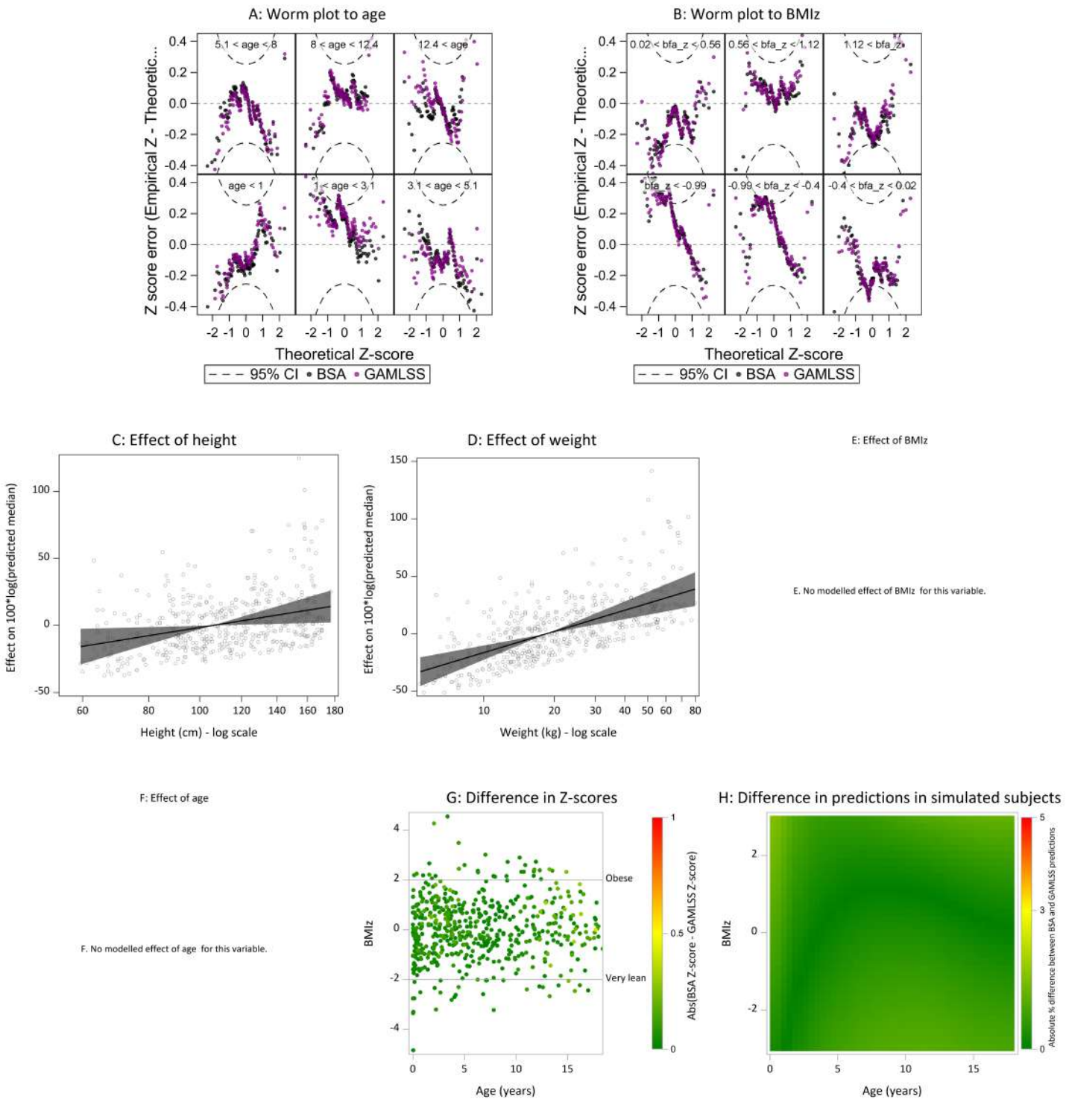
Supplementary figures S41 A-G: Proximal right coronary artery diameter in females (RCAPF)

A: Worm plot by age of the Z-scores of the GAMLSS model in comparison to the BSA-allometric model for RCAPF. B: Worm plot by BMIz of the Z-scores of the GAMLSS model in comparison to the BSA-allometric model for RCAPF. C: Effect of height on the log of the predicted median of the RCAPF. D: Effect of weight on the log of the predicted median of RCAPF. E: Effect of BMIz on the log of the predicted median of RCAPF. F: Effect of age on the log of the predicted median of RCAPF. G: Difference between Z-scores of the GAMLSS model and the BSA-allometric model for RCAPF. H: Difference between predicted median of the GAMLSS model and the BSA-allometric model for RCAPF in simulated subjects.



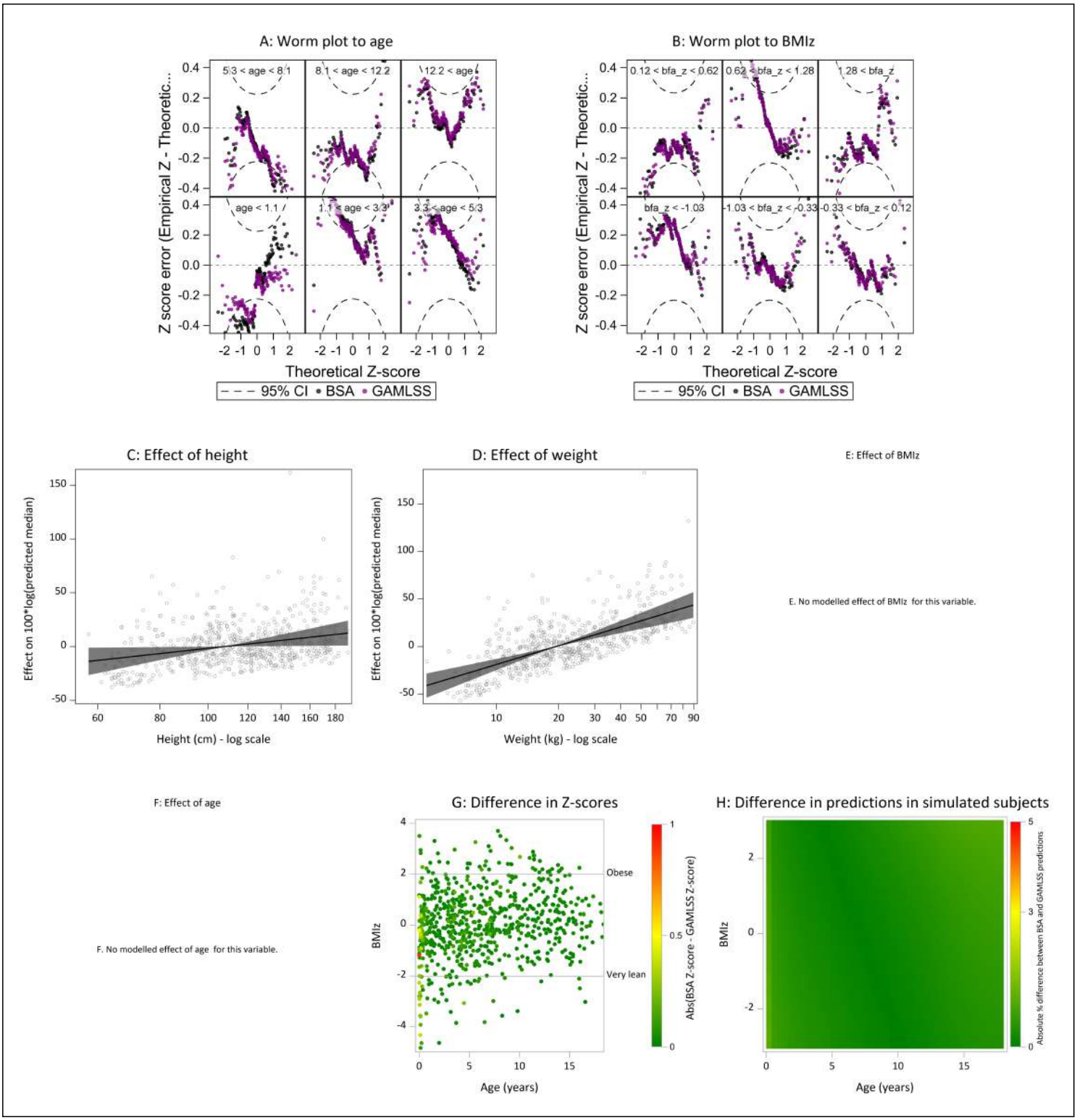
Supplementary figures S42 A-G: Proximal right coronary artery diameter in males (RCAPM)

A: Worm plot by age of the Z-scores of the GAMLSS model in comparison to the BSA-allometric model for RCAPM. B: Worm plot by BMIz of the Z-scores of the GAMLSS model in comparison to the BSA-allometric model for RCAPM. C: Effect of height on the log of the predicted median of the RCAPM. D: Effect of weight on the log of the predicted median of RCAPM. E: Effect of BMIz on the log of the predicted median of RCAPM. F: Effect of age on the log of the predicted median of RCAPM. G: Difference between Z-scores of the GAMLSS model and the BSA-allometric model for RCAPM. H: Difference between predicted median of the GAMLSS model and the BSA-allometric model for RCAPM in simulated subjects.



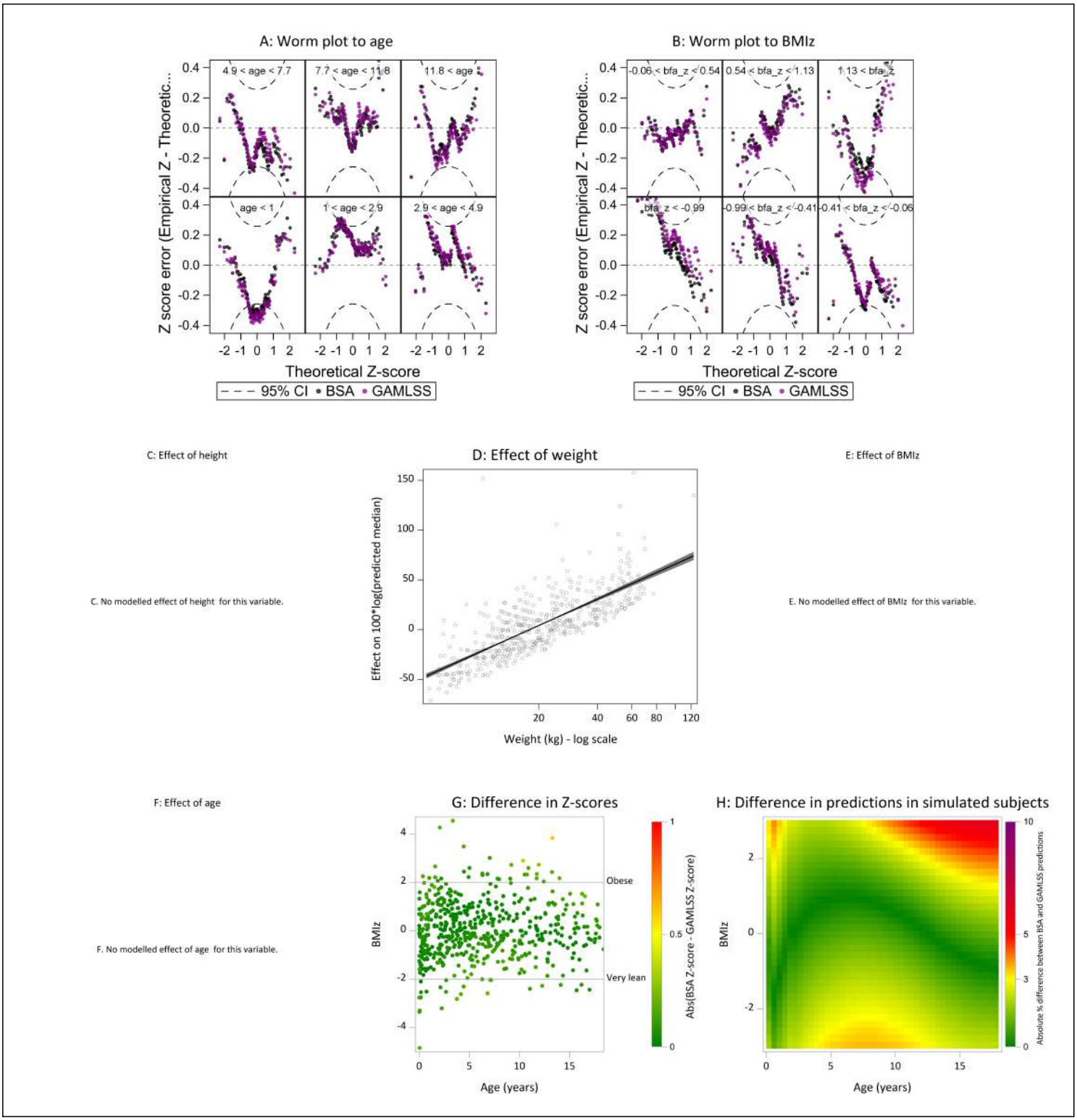
Supplementary figures S43 A-G: Medium right coronary artery diameter in females (RCAMF)

A: Worm plot by age of the Z-scores of the GAMLSS model in comparison to the BSA-allometric model for RCAMF. B: Worm plot by BMIz of the Z-scores of the GAMLSS model in comparison to the BSA-allometric model for RCAMF. C: Effect of height on the log of the predicted median of the RCAMF. D: Effect of weight on the log of the predicted median of RCAMF. E: Effect of BMIz on the log of the predicted median of RCAMF. F: Effect of age on the log of the predicted median of RCAMF. G: Difference between Z-scores of the GAMLSS model and the BSA-allometric model for RCAMF. H: Difference between predicted median of the GAMLSS model and the BSA-allometric model for RCAMF in simulated subjects.



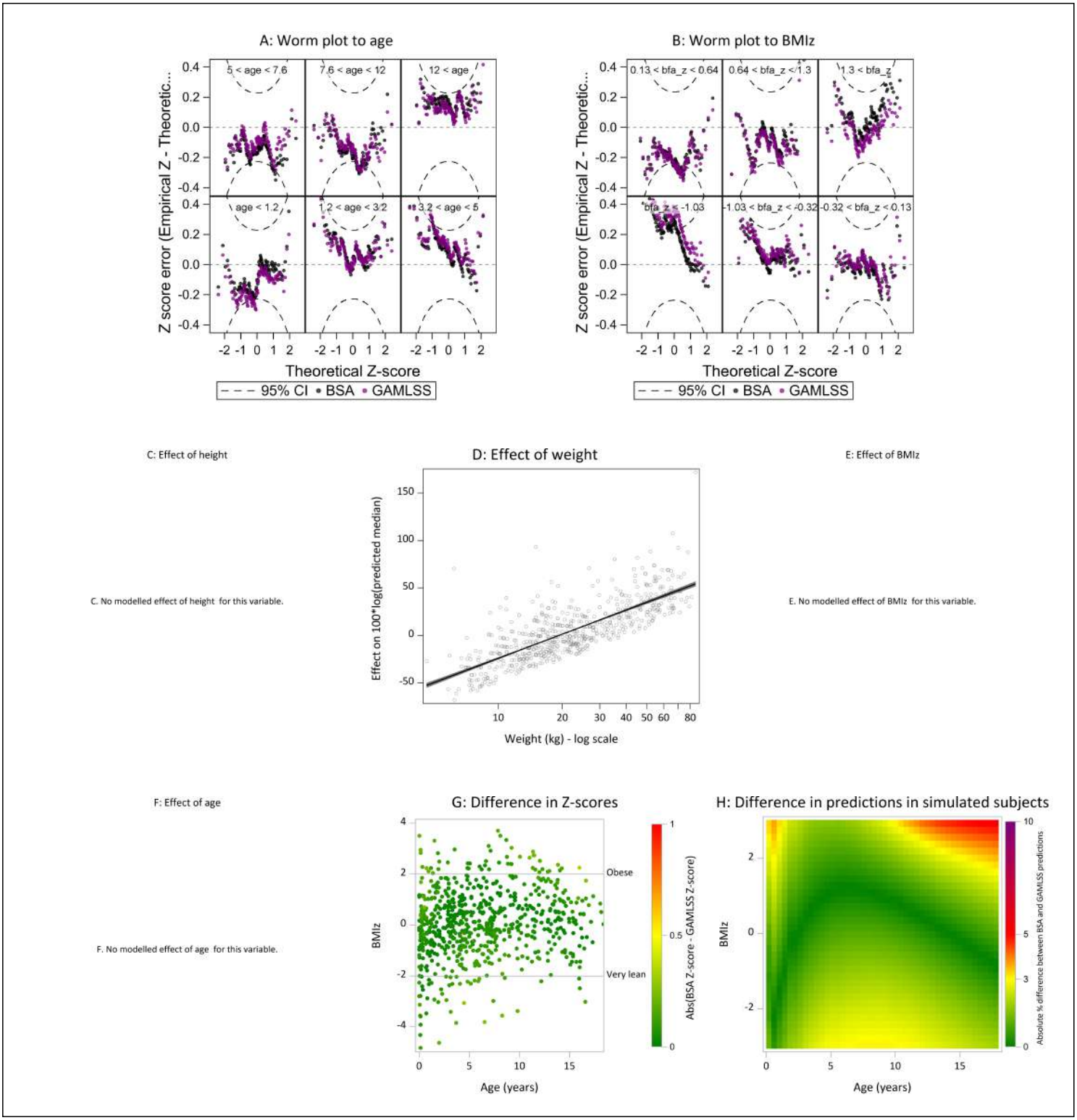
Supplementary figures S44 A-G: Medium right coronary artery diameter in males (RCAMM)

A: Worm plot by age of the Z-scores of the GAMLSS model in comparison to the BSA-allometric model for RCAMM. B: Worm plot by BMIz of the Z-scores of the GAMLSS model in comparison to the BSA-allometric model for RCAMM. C: Effect of height on the log of the predicted median of the RCAMM. D: Effect of weight on the log of the predicted median of RCAMM. E: Effect of BMIz on the log of the predicted median of RCAMM. F: Effect of age on the log of the predicted median of RCAMM. G: Difference between Z-scores of the GAMLSS model and the BSA-allometric model for RCAMM. H: Difference between predicted median of the GAMLSS model and the BSA-allometric model for RCAMM in simulated subjects.



Supplementary figures S45 A-G: Distal right coronary artery diameter in females (RCADF)

A: Worm plot by age of the Z-scores of the GAMLSS model in comparison to the BSA-allometric model for RCADF. B: Worm plot by BMIz of the Z-scores of the GAMLSS model in comparison to the BSA-allometric model for RCADF. C: Effect of height on the log of the predicted median of the RCADF. D: Effect of weight on the log of the predicted median of RCADF. E: Effect of BMIz on the log of the predicted median of RCADF. F: Effect of age on the log of the predicted median of RCADF. G: Difference between Z-scores of the GAMLSS model and the BSA-allometric model for RCADF. H: Difference between predicted median of the GAMLSS model and the BSA-allometric model for RCADF in simulated subjects.



Supplementary figures S46 A-G: Distal right coronary artery diameter in males (RCADM)

A: Worm plot by age of the Z-scores of the GAMLSS model in comparison to the BSA-allometric model for RCADM. B: Worm plot by BMIz of the Z-scores of the GAMLSS model in comparison to the BSA-allometric model for RCADM. C: Effect of height on the log of the predicted median of the RCADM. D: Effect of weight on the log of the predicted median of RCADM. E: Effect of BMIz on the log of the predicted median of RCADM. F: Effect of age on the log of the predicted median of RCADM. G: Difference between Z-scores of the GAMLSS model and the BSA-allometric model for RCADM. H: Difference between predicted median of the GAMLSS model and the BSA-allometric model for RCADM in simulated subjects.

Methods for Figures S47 and S48.

To further evaluate the model fit while considering the risk of overfitting, we evaluated the mean Z-scores in different strata of age and BMIz in a cross validation setting. This is virtually the same analysis as the heatmaps that are presented in the main manuscript, but under cross-validation. For each variable, the study population was randomly split in a training subsample (70%) and a validation subsample (the remaining 30%). The training subsample was used for model regression with the chosen hyperparameters. The mean Z-score in different strata was then calculated on the validation subsample, identically to the heatmaps presented in the main manuscript. The confidence intervals are calculated using usual inference methods, however the sample size is smaller because only 30% of the sample is used. The results are similar to those presented in the main manuscript. Some estimations of the mean Z-scores could suggest errors as large as 1 Z-score, however the confidence intervals are wide in these cases. We note that calculating many statistics increases the risk of finding extreme estimates simply by chance.

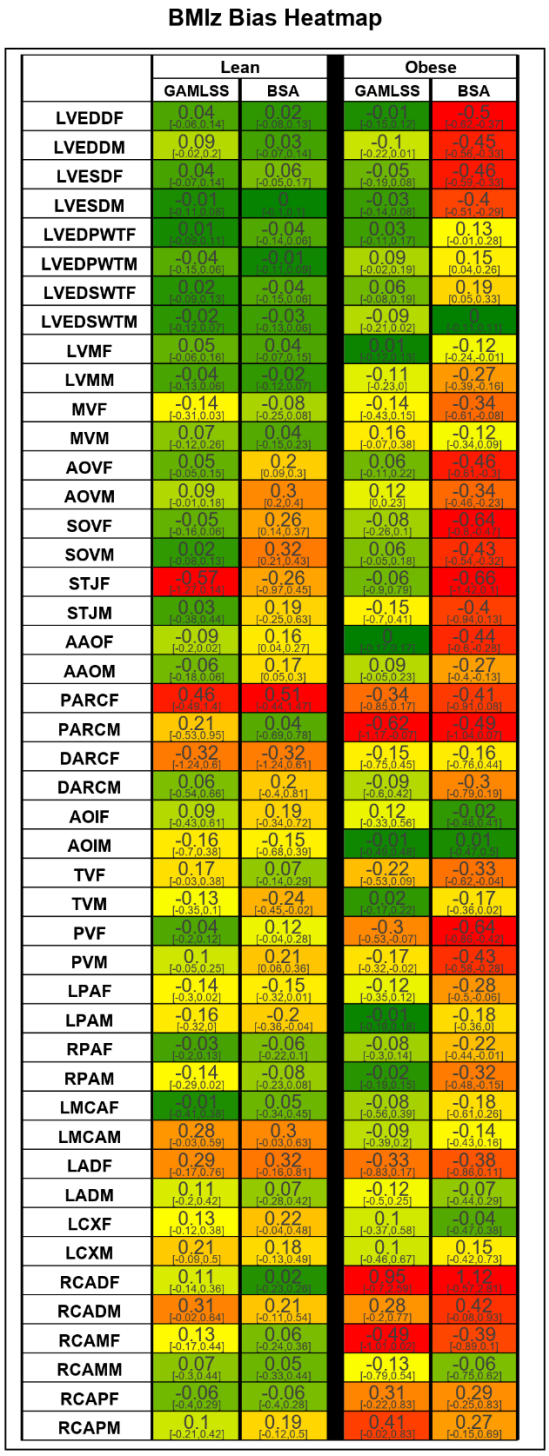


Figure S47. Heatmap of the mean Z-score in lean and obese patients in the GAMLSS model and the BSA-allometric model under cross validation. Each cell provides the mean Z-score

[95% CI]. Expected mean in all strata is 0, deviations from 0 suggest systematic error. Colors are calculated using the absolute value of the mean. Lean: BMIz < -1. Obese: BMIz > 2. GAMLSS: Generalized Additive Model for Location, Scale and Shape. BSA: allometric model with body surface area. LVEDDF: left-ventricular end-diastolic diameter in females; LVEDDM: left-ventricular end-diastolic diameter in males; LVESDF: left-ventricular end-systolic diameter in females; LVESDM: left-ventricular end-systolic diameter in males; LVEDPWTF: left-ventricular posterior wall thickness in females; LVEDPWTM: left-ventricular posterior wall thickness in males; LVEDSWTF: left-ventricular septal wall thickness in females; LVEDSWTM: left-ventricular septal wall thickness in males; LVMF: left-ventricular mass in females; LVMM: left-ventricular mass in males; MVF: mitral valve diameter in apical view in females; MVM: mitral valve diameter in apical view in males; AOVF: aortic valve diameter in females; AOVM: aortic valve diameter in males; SOVF: Sinus of Valsalva diameter in females; SOVM: Sinus of Valsalva diameter in males; STJF: sinotubular junction diameter in females; STJM: sinotubular junction diameter in males; AAOF: ascending aorta diameter in females; AAOM: ascending aorta diameter in males; PARCF: proximal arch diameter of aorta in females; PARCM: proximal arch diameter of aorta in males; DARCF: distal arch diameter of aorta in females; DARCM: distal arch diameter of aorta in males; AOIF: aortic isthmus diameter in females; AOIM: aortic isthmus diameter in males; TVF: tricuspid valve diameter in apical view in females; TVM: tricuspid valve diameter in apical view in males; PVF: pulmonary valve diameter in females; PVM: pulmonary valve diameter in males; LPAF: left pulmonary artery diameter in females; LPAM: left pulmonary artery diameter in males; RPAF: right pulmonary artery diameter in females; RPAM: right pulmonary

artery diameter in males; LMCAF: left main coronary artery diameter in females; LMCAM: left main coronary artery diameter in males; LADF: left anterior descending artery diameter in females; LADM: left anterior descending artery diameter in males; LCXF: left circumflex artery diameter in females; LCXM: left circumflex artery diameter in males; RCADF: right coronary artery in distal segment in females; RCADM: right coronary artery in distal segment in males; RCAMF: right coronary artery in medium segment in females; RCAMM: right coronary artery in medium segment in males; RCAPF: right coronary artery diameter in proximal segment in females; RCAPM: right coronary artery diameter in proximal segment in males

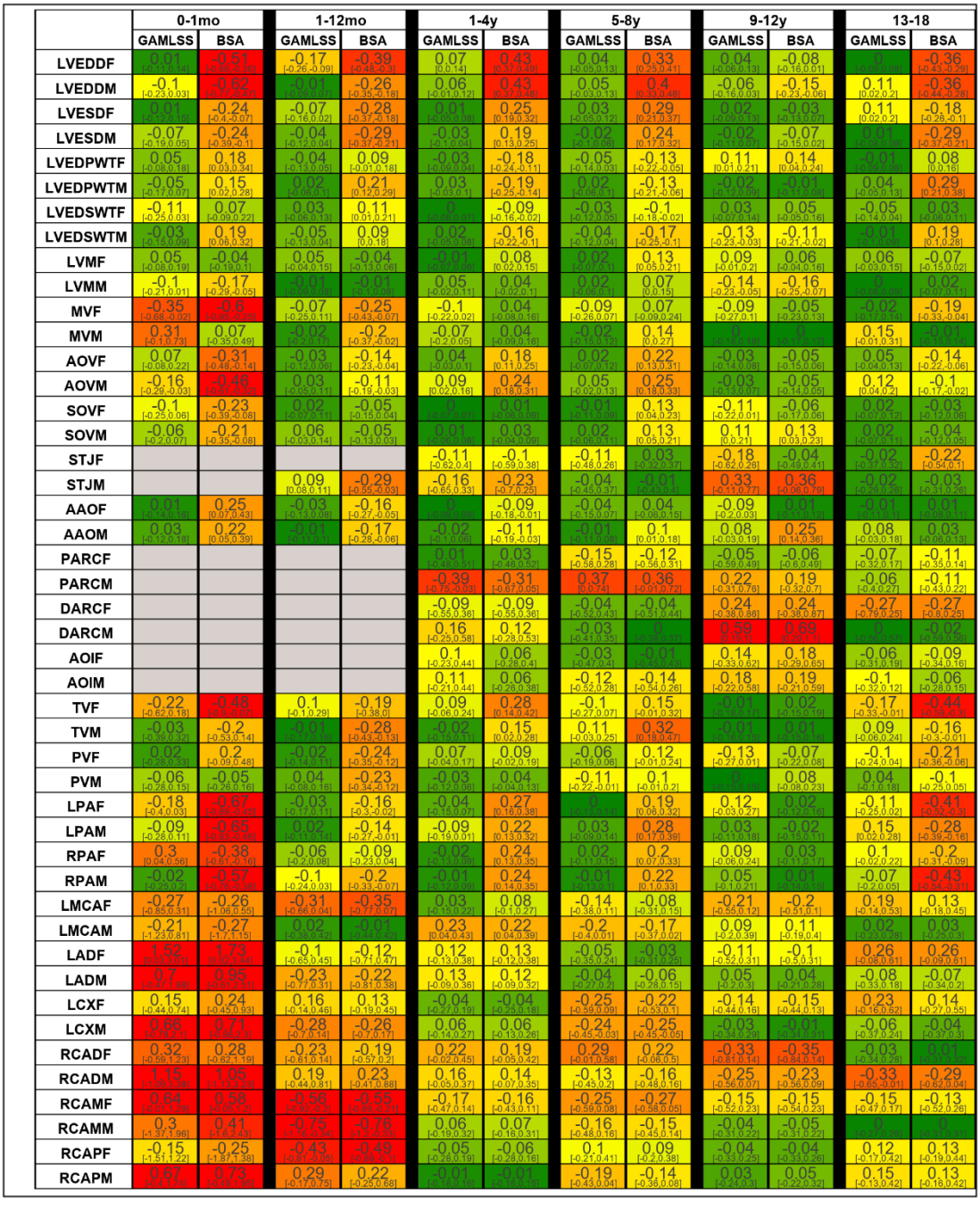


Figure S48. Heatmap of the mean Z-score in different strata of age in the GAMLSS model and the BSA-allometric model under cross validation. Each cell provides the mean Z-score [95% CI]. Expected mean in all strata is 0, deviations from 0 suggest systematic error.

Colors are calculated using the absolute value of the mean. Lean: BMIz < -1. Obese: BMIz > 2. GAMLSS: Generalized Additive Model for Location, Scale and Shape. BSA: allometric model with body surface area. LVEDDF: left-ventricular end-diastolic diameter in females; LVEDDM: left-ventricular end-diastolic diameter in males; LVESDF: left-ventricular end-systolic diameter in females; LVESDM: left-ventricular end-systolic diameter in males; LVEDPWTF: left-ventricular posterior wall thickness in females; LVEDPWTM: left-ventricular posterior wall thickness in males; LVEDSWTF: left-ventricular septal wall thickness in females; LVEDSWTM: left-ventricular septal wall thickness in males; LVMF: left-ventricular mass in females; LVMM: left-ventricular mass in males; MVF: mitral valve diameter in apical view in females; MVM: mitral valve diameter in apical view in males; AOVF: aortic valve diameter in females; AOVM: aortic valve diameter in males; SOVF: Sinus of Valsalva diameter in females; SOVM: Sinus of Valsalva diameter in males; STJF: sinotubular junction diameter in females; STJM: sinotubular junction diameter in males; AAOF: ascending aorta diameter in females; AAOM: ascending aorta diameter in males; PARCF: proximal arch diameter of aorta in females; PARCM: proximal arch diameter of aorta in males; DARCF: distal arch diameter of aorta in females; DARCM: distal arch diameter of aorta in males; AOIF: aortic isthmus diameter in females; AOIM: aortic isthmus diameter in males; TVF: tricuspid valve diameter in apical view in females; TVM: tricuspid valve diameter in apical view in males; PVF: pulmonary valve diameter in females; PVM: pulmonary valve diameter in males; LPAF: left pulmonary artery diameter in females; LPAM: left pulmonary artery diameter in males; RPAF: right pulmonary artery diameter in females; RPAM: right pulmonary artery diameter in males; LMCAF: left main coronary artery diameter in females;

LMCAM: left main coronary artery diameter in males; LADF: left anterior descending artery diameter in females; LADM: left anterior descending artery diameter in males; LCXF: left circumflex artery diameter in females; LCXM: left circumflex artery diameter in males; RCADF: right coronary artery in distal segment in females; RCADM: right coronary artery in distal segment in males; RCAMF: right coronary artery in medium segment in females; RCAMM: right coronary artery in medium segment in males; RCAPF: right coronary artery diameter in proximal segment in females; RCAPM: right coronary artery diameter in proximal segment in males